Electromagnetic Boundary Layer Control

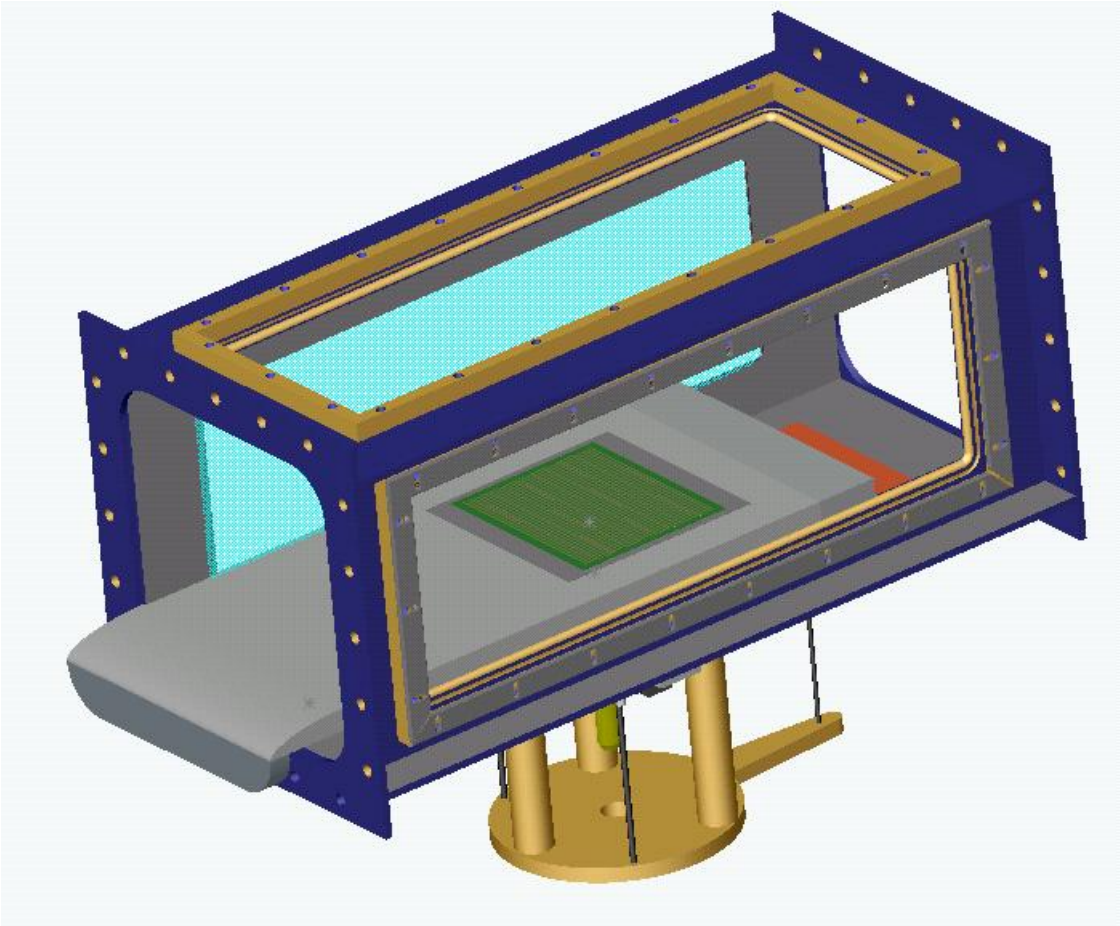

Daniel Sura

EMBC Report - Table of Contents

1.0 Introduction

Over the past several years, experimental work has been conducted in pursuit of validating predicted drag reduction from numerical simulations developed by engineers and scientists working in the hydrodynamics field. Some techniques developed in the past few years have demonstrated drag reduction and have validated some of the theories and simulations of drag behavior in fluid flow over a surface. Drag reduction technologies such as the injection of micro-bubbles into the boundary layer, the use of riblets, and electromagnetic forces to alter the boundary layer characteristics over a surface are prime examples of research experiments conducted in recent years at various institutions.

Professor Karniadakis of Brown University's Center for Fluid Mechanics and visiting professor in the department of Ocean Engineering at Massachusetts Institute of Technology has developed numerical simulations that predict drag reduction by implementing a Lorentz force crosswise to the flow of fluid thereby altering the flow behavior of near wall turbulent structures. The consequence of altering the characteristics of the near wall turbulent structures, at an optimum predicted crosswise forcing magnitude and frequency of oscillation, is drag reduction on the order of 30% predicted by numerical simulations.

The impact of drag reduction technology capable of reducing drag that amount would be tremendous to the ocean technology field. Shipping industries would certainly be one of the first to take advantage of this type of technology. Any reduction in drag is directly associated with a reduction in fuel consumption as well as the ability for a ship or marine vessel to travel at higher speeds. In its current development of higher speed surface and underwater marine vessels, the Navy is another institution that would greatly benefit from the usage of this type of drag reduction technology.

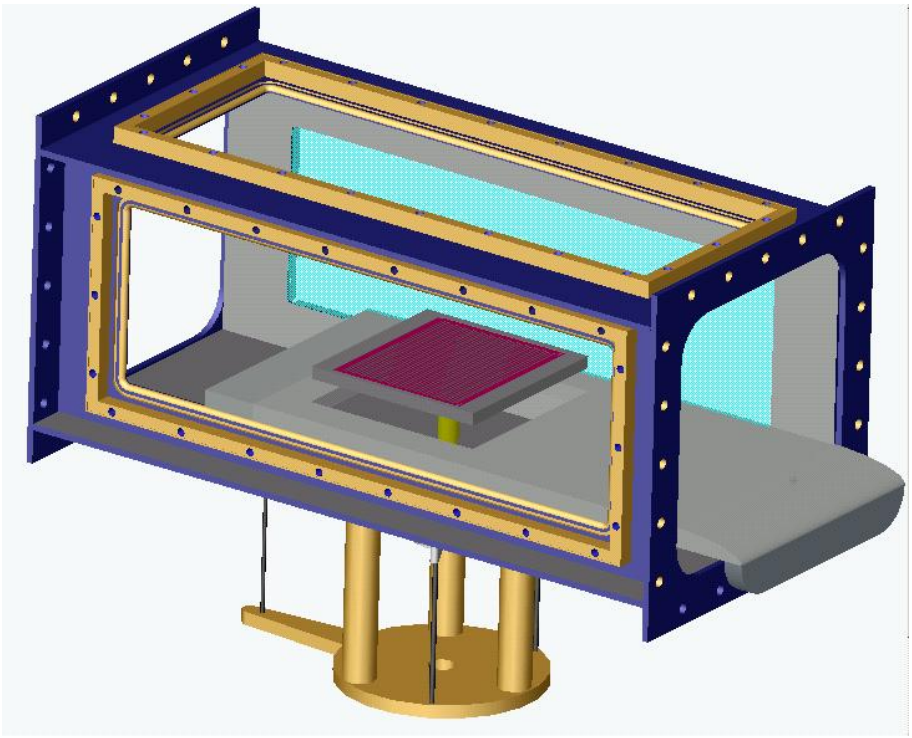

Figure 1.1 3d Solid Model of the baseplate and
cassette installed in the water tunnel test section

The experimental validation of numerical simulations of drag reduction due to Lorentz force excitation was performed in the Marine Hydrodynamics Laboratory at Massachusetts Institute of Technology. A flat plate made of white delrin plastic with an elliptical nose shape was designed and built to be tested in a water tunnel test section. Figure 1.1 shows a 3d solid model assembly of the flat plate in the test section. Notice a square cassette with an integrated electrode board, which upon proper installation sits flush with the delrin cassette and base plate. In the cassette are rows of integrated magnets underneath the electrode board.

A Lorentz force is generated by the crossing of an electric field by current being pumped through the electrodes of the electrode board, with a magnetic field produced by magnets sitting in the cassette underneath the electrode board and in between the electrodes. The design and setup of the hardware and electronics for this experiment, as well as numerical simulation work, and results from experimental work performed at the Marine Hydrodynamics Laboratory, will be discussed in greater detail throughout the following sections of this report.

2.0 Background

2.1 Theoretical

Brown University's Center for Fluid Mechanics has developed numerical simulations that predict drag reduction due to the effect of altering near wall turbulent structures by generation of a Lorentz force. To discuss the effects of the Lorentz forcing in the flow of fluid over a flat plate, it is first necessary to understand the principles of how Lorentz forces are generated in a fluid. A Lorentz force is a direct result of electric and magnetic fields crossing each other and creating a force which is perpendicular to both of the fields where they intersect.

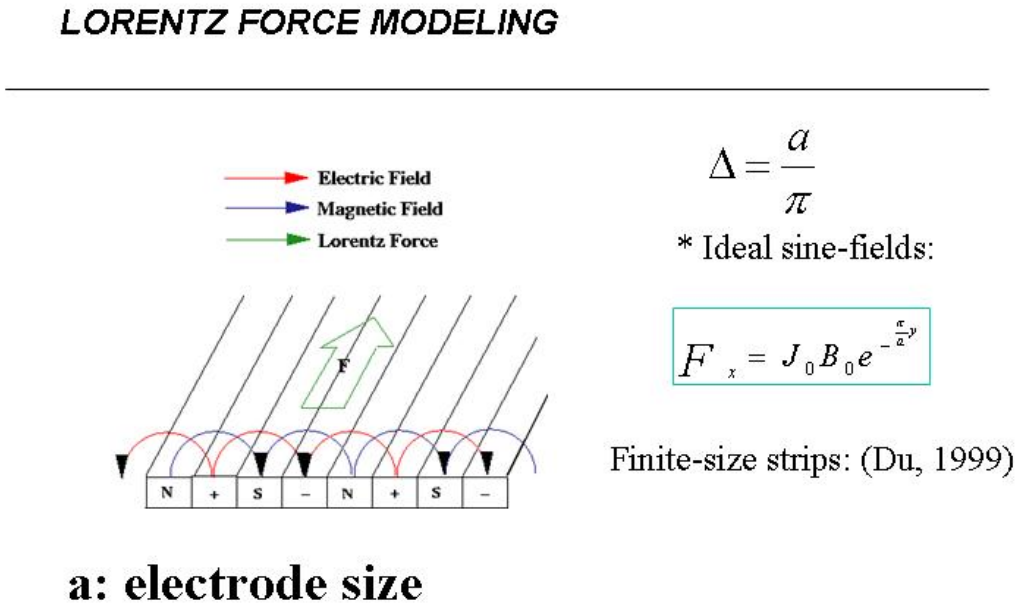

Figure 2.1.1 Diagram of a Lorentz Force Model [1]

Figure 2.1.1 shows an illustration of electric fields crossing magnetic fields creating a perpendicular force, which is the Lorentz force and is labeled 'F'. Changing the electrode size, (parameter a in the figure) will have an effect on the magnitude of the electric field generated. An electric field is generated in a fluid that is conductive by using an

electrode board which has long strips of electrodes. Since the fluid is conductive, the electric field is created from electrons traveling through the fluid from positive to negative charged electrodes. Any change in the electric field magnitude will result in a direct change in the magnitude of the Lorentz force. The following equation shows how the Lorentz force is dependent on the magnitudes of both the electric

$$F_x = J_0 B_0 e^{-\frac{\pi}{a} y}$$

and magnetic field, Jo being the magnitude of the electric field, and Bo being the magnitude of the magnetic field, as well as 'a', electrode size, and 'y', the distance in the vertical direction away from the surface of the electrode board. As one may expect the Lorentz force decays exponentially as the distance away from the surface of the electrode board increases. The implementation of hardware and electronic components capable of generating Lorentz forces for experimental work will be discussed in section 2.2.

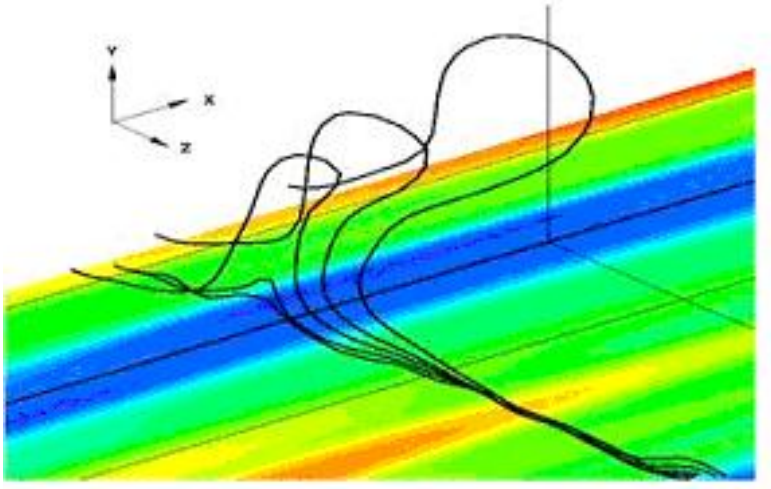

Figure 2.1.2 Hairpin Vortex Production near a flat plate [1]

Experimental analysis, numerical simulations, and theory have shown that in fluid flow over a flat plate, hairpin vortices are produced in and near the boundary layer. Figure 2.1.2 shows an illustration of such vortices formed near the surface of the flat plate where fluid is flowing in the +X direction. The production of near wall turbulent structures result in regions of higher surface velocity and is a characteristic behavior in flow past a flat plate. High surface velocity regions cause the formation of these hairpin

vortices. In regions where hairpin vortices are present, particularly in areas where there are high velocity streaks, drag over the surface of the plate is increased by a significant amount.

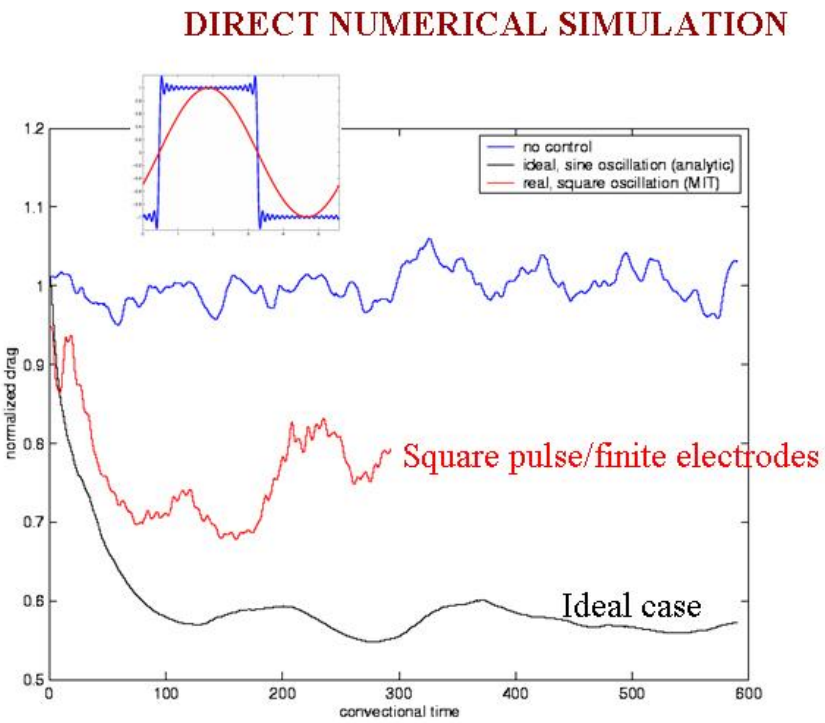

Figure 2.1.3 Direct numerical simulation showing drag reduction for different cases [1]

Brown University has developed numerical simulations to model the disruption of the creation of these turbulent structures. Simulations show that drag reduction is indeed present when these structures are disrupted by Lorentz force activation. Figure 2.1.3 shows data from a direct numerical simulation suggesting under both ideal and in real experimental conditions, that drag reduction is present. In this model, the Lorentz force sweeps back and forth always perpendicular to the flow and can be implemented by varying the direction of the current without having to vary the direction of the magnetic fields. An electronic setup capable of producing a square wave current signal can produce a Lorentz force which sweeps back and forth. A square wave setup would reduce the cost and complexity of the electronic driver system. The numerical simulation shows that in the ideal case, with infinitesimally thin electrodes, a sine field is produced,

and the drag reduction is greatest. A square wave oscillation, which was used in the experimental validation process, still results in drag reduction.

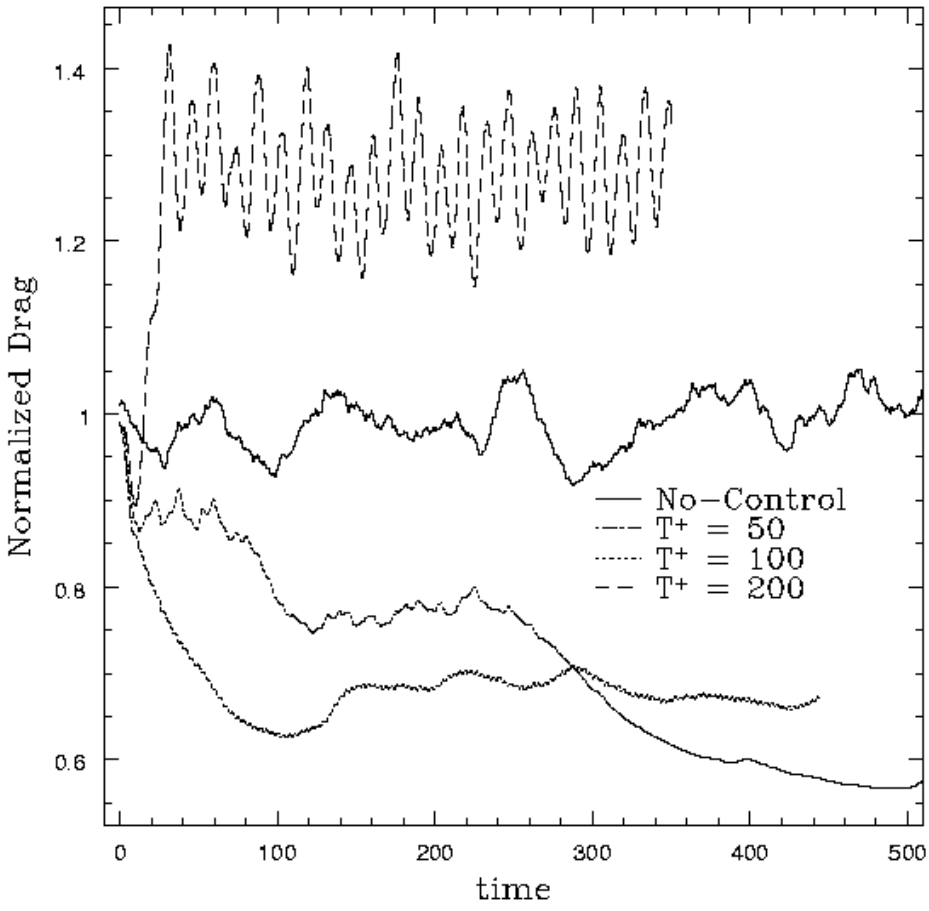

Figure 2.1.5 Numerical Simulation the baseline case leading to drag reduction [1]

A baseline case performed by the numerical simulations shows elimination of wall streaks, indicating that wall turbulent structures have been disrupted. Figure 2.1.5 shows a plot of predicted drag under no control and under Lorentz force disruption of the flow. Simulations indicate drag reduction of up to 30% is possible under these conditions. The baseline case was performed with an invariant parameter of 1, a forcing period of 50, and a penetration depth of 1/50. The simulations have predicted that those parameters will result in the maximum drag reduction for the square wave case. The validation of these drag reduction predictions was the next phase of this research project and involved experimental analysis conducted at the MIT water tunnel in 2002.

2.2 Experimental

Experimental work to validate the predicted drag reduction from numerical simulations was performed in the Marine Hydrodynamics Laboratory by MIT alumni Jaskolski in the fall and spring of 2001-2002 [2]. The hardware for the experimental setup consisted of a flat base plate machined out of white delrin plastic with a thickness of 1.5 inches, a length of 42.5 inches, and a width of 19.875 inches. Figure 2.2.1 shows a 3d solid model of the MHD (magneto-hydrodynamic) base plate as well as the electrode board which is an integrated part of the plate after its installation. The length of the base plate was designed to be 42.5 inches, long enough so that the flow over the long flat surface would produce near wall turbulent structures over the electrode board where Lorentz forces were generated and drag force measured. An elliptical nose was designed so as to create a smooth transition between flow moving over the lower wall of the water tunnel test section and over the flat delrin plate.

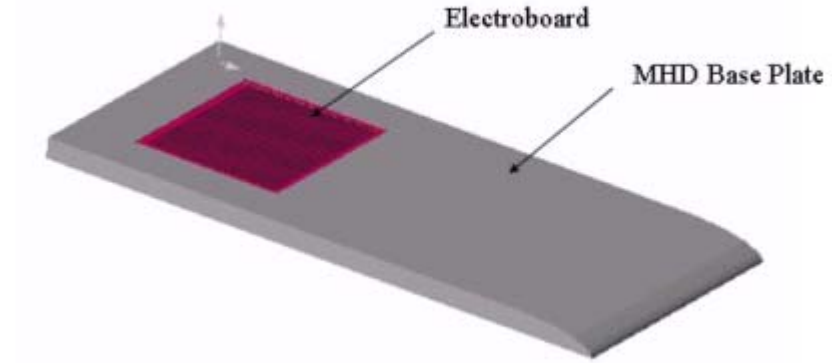

Figure 2.2.1 Flat plate hardware for Jaskolski's boundary layer experiment

The generation of a magnetic field was accomplished by having strips of magnets underneath and between the electrodes of the electrode board. The electrodes of the electrode board are $1/8^{th}$ inches wide and are spaced apart $1/8^{th}$ inches. The magnets are also $1/8^{th}$ inches thick and generate magnetic fields of up to 0.15 Tesla at the

surface of the electrode board which is exposed to the flow of water. If the fluid is conductive, current can travel from electrode to electrode in the fluid, in a plus to minus manner, and an electric field is generated.

Custom built driver electronics built by Jaskolski were connected to a power supply capable of generating up to 166 Amps of current and a frequency generator capable of outputting a square wave signal. The driver electronics allowed the current to switch directions by changing the polarity of the incoming current from the power supply. The resulting system was capable of producing square wave current signals with variable amplitude and frequency. The output of the electronic driver system was connected to the electrode board and a Lorentz force which switched back and forth in the crosswise flow direction could be produced with varying amplitude and frequency.

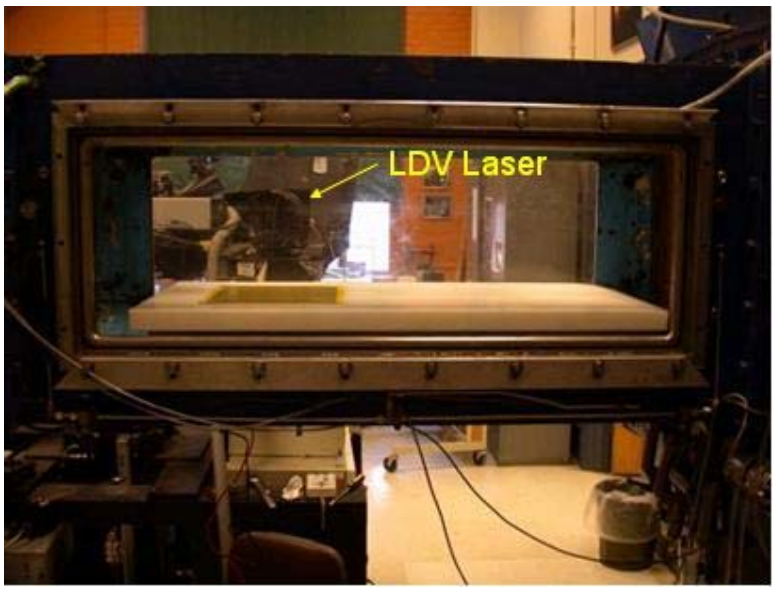

Figure 2.2.2 MHD plate setup in the MIT water tunnel

Experimental analysis was performed for various frequencies and amplitudes of current pumped into the electrode board, as well as for different fluid flow speeds generated by the water tunnel impeller. The data acquisition system used was an LDV (laser doppler velocimetry) system which consists of a laser mounted on a

traverse system. The LDV system in the marine hydrodynamics laboratory can detect particles of fluid moving in the flow and can accurately measure the flow speed in the horizontal and vertical directions. The laser shoots four beams into the test section window and into the flow, and the velocity measurement can be conducted where these beams intersect. The traverse system has a resolution of 0.01 mm and can accurately move to a desired position. Figure 2.2.2 shows a photograph of the MHD base plate installed in the water tunnel test section. Notice the positioning of the LDV laser and the electrode board installed in the MHD base plate. The hardware was setup in the test section, so that boundary layer profiles could easily be measured since the laser had the ability of taking measurements very close to the surface of the flat plate and of the electrode board.

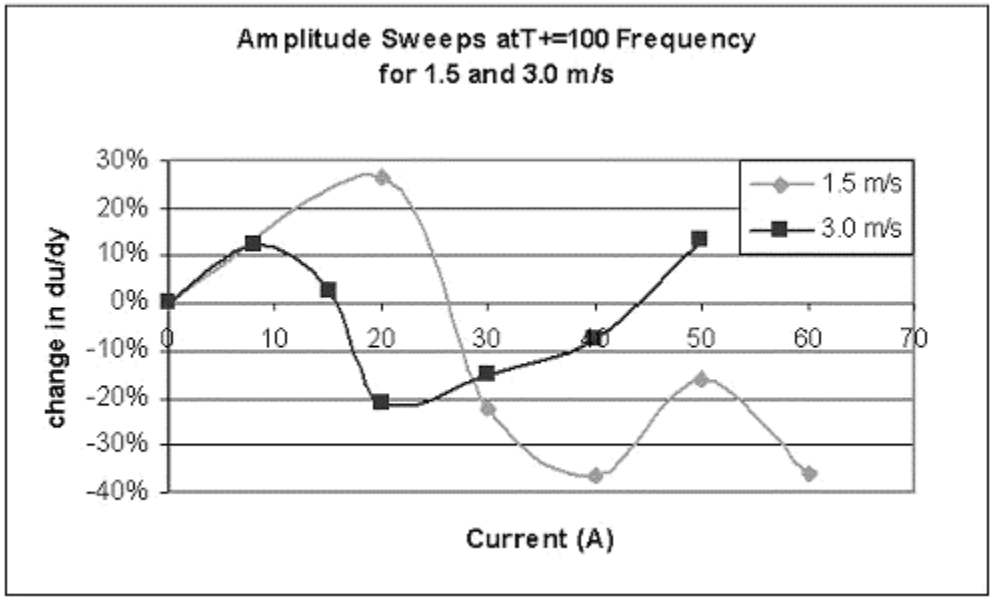

Figure 2.2.3 LDV data measurements performed by Corey Jaskolski – 2002 [2]

Boundary layer velocity profiles using Laser Doppler Velocimetry were measured for various frequencies and current amplitudes. At the optimum predicted forcing frequency of T+=100 by numerical simulations [1], the current was varied and velocity profiles measured yielded the local shear stress at the wall. The changes in the local shear stress are indicative of changes in drag. Figure 2.2.3 shows data measurements of the changes in du/dy as a function of current amplitude for both a tunnel flow speed of 1.5 and 3.0 m/s. The data clearly shows that a change in du/dy of about

26% is present at a current amplitude of 20 Amps for the 1.5 m/s second case, and at 40 Amps, the change in du/dy is -35%. This 35% change in du/dy agrees roughly with the predictions by numerical simulations of 30% drag reduction. Although the local changes in du/dy clearly show drag reduction locally, it is very difficult to make conclusions about drag reduction on a global scale for the entire surface area of the electrode board.

Some of the boundary layer profiles measured showed increase in drag in some areas over the electrode board, primarily over the electrodes themselves, and drag reduction in between the electrodes [2]. To make conclusions about drag reduction on a global scale with solely LDV acquired data would be inadequate. In pursuit of characterizing the global drag effects by Lorentz forcing in the fluid, implementation of a force measurement experiment to measure the global drag forces acting over the entire electrode board was carried out in the Marine Hydrodynamics Laboratory.

3.0 Test Setup and Hardware Design

3.1 Base plate/Cassette redesign

In preparation for the next round of experimental work, with the objective of quantifying global drag reduction, a major redesign of hardware and electronics was carried out in the spring of 2002 at the Marine Hydrodynamics Laboratory at MIT. The hardware redesign involved using the existing MHD baseplate, magnets, and the electrode board from previous work conducted by Jaskolski [2]. It was determined that the best method of measuring global drag force was to use load cells for a direct measurement of force. This could be accomplished by creating a square cutout in the MHD base plate, and having a square plastic delrin cassette which contained the rows of magnets and the integrated electrode board. The electrode board was mounted by four flat head screws on the corners, and a small 4-40 bolt in the center to keep the center of the board from bowing upwards and affecting the flow.

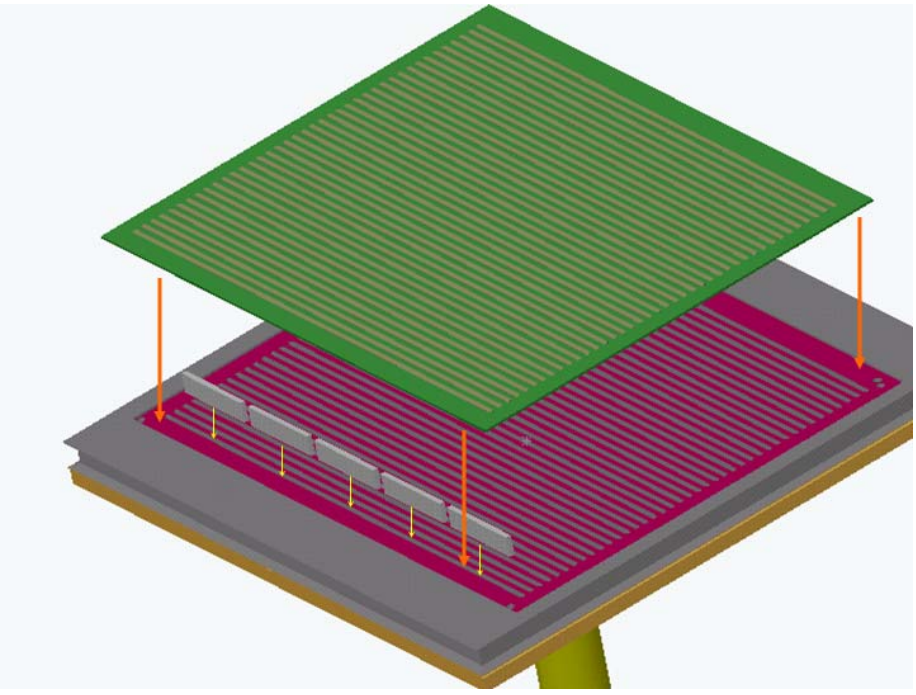

Figure 3.1.1 Solid model of magnet and electrode board assembly

The rows of magnets were positioned in such a manner that all the magnets of one row had the same orientation upwards, such as north, and adjacent rows would have magnets which were oriented south so as to create a magnetic field from row to row. Figure 3.1.1 shows a 3d model of how the magnets are placed into the slots. The magnet filled cassette sits flush with the MHD base plate and inside of the square cutout without touching any of the edges of the cutout but having a small clearance of about 0.005 inches around all four edges. Figure 3.1.2 shows a 3d solid model of the MHD base plate and the magnet filled delrin cassette.

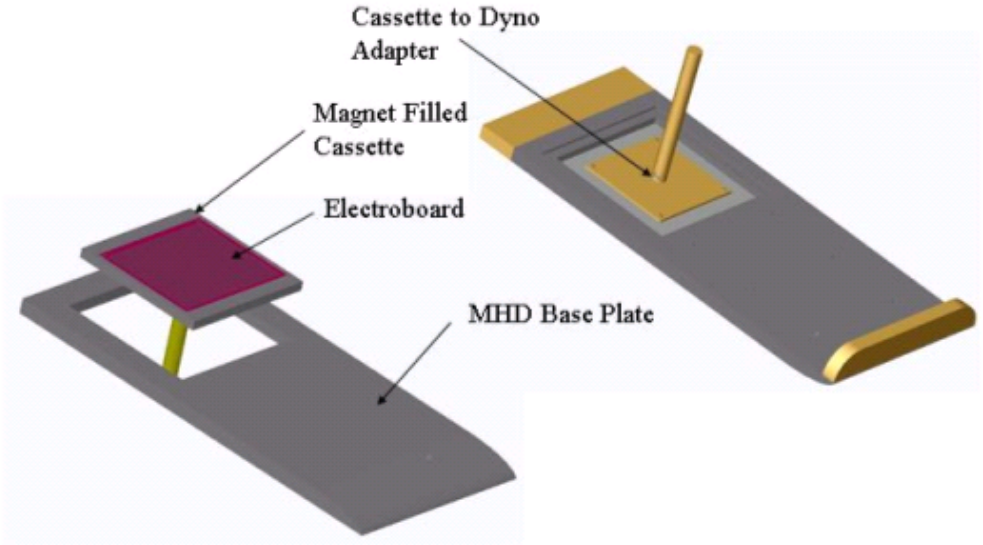

Figure 3.1.2 MHD base plate and cassette 3d solid assembly model

The cassette was designed to be 14 inches long and 14 inches wide with a thickness of 0.687 inches and with a ¼ inch thick steel plate mounted on the bottom which touches all of the rows of magnets and prevents any magnetic flux leakage from underneath the cassette. An adapter shaft attached served the purpose of fitting and clamping into the collet of a dynamometer which has integrated load cells for force measurements. The dynamometer was available in the lab and has been extensively used for measuring the drag and lift on hydrodynamic bodies such as hydrofoils. The assembly of the newly designed base plate, cassette, and dynamometer in the test section will be discussed further in section 3.2.

The design of new hardware for the upcoming experiment also involved the addition of a dam made of delrin plastic on the leading edge of the MHD plate and a rear extension block to cover the mounting hardware which extended past the rear of the MHD plate. Figure 3.1.3 shows the assembly of the MHD plate with the addition of the dam and the extension piece in the rear. The addition of the dam in the front, blocks the flow of water so that none of it can enter underneath the MHD plate and affect the mounting hardware and more importantly the shaft connected to the cassette which mounts into the dynamometer. If the flow of water underneath the MHD plate were not blocked, there would be flow induced vibrations on the shaft, and the load cells would measure these effects and give us inaccurate readings for drag force and side force. The extension block in the rear is not of critical importance but it was designed to reduce flow effects coming from objects other than the flat plate itself nearby the electrode board where sweeping Lorentz forces were generated.

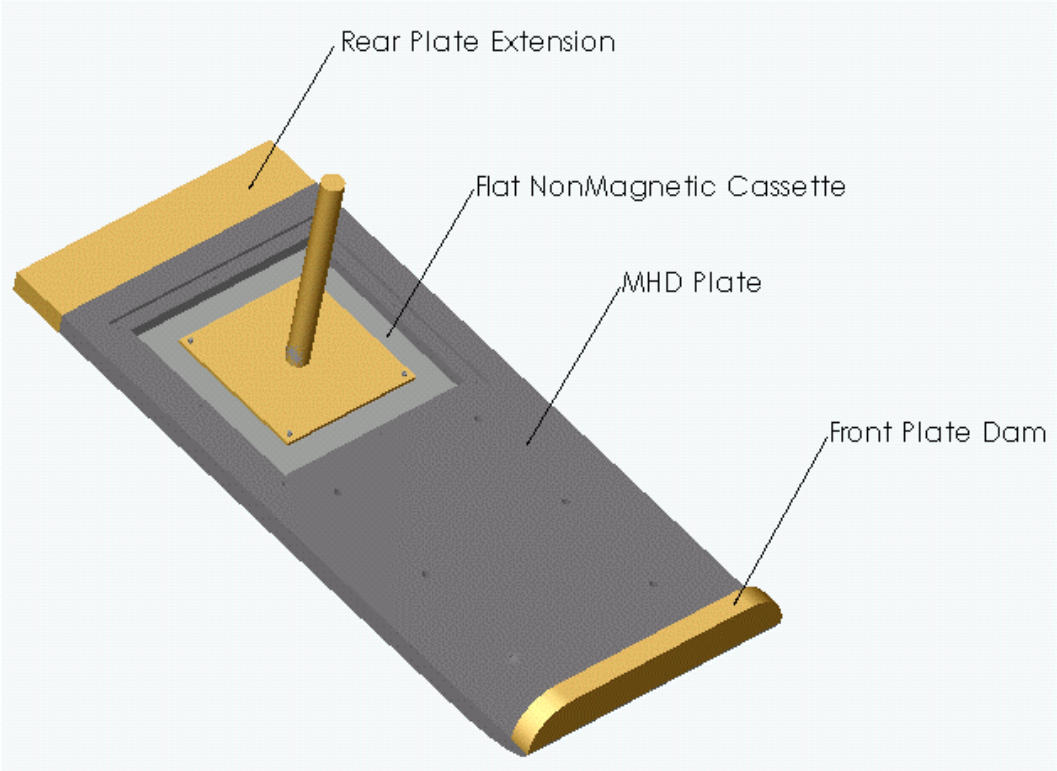

Figure 3.1.3 MHD Plate Assembly with Non Magnetic Cassette

Also, a second cassette with the same thickness, length, and width dimensions as the magnet filled cassette was designed and machined out of delrin plastic. This cassette had no magnets and no electrode board integrated and served as a baseline cassette for verification that the force gauge and cassette assembly systems were working properly. With this cassette, baseline drag measurements could be conducted and compared with LDV acquired data from Jaskolski's work [2] and with published data on drag over a flat plate surface. Figure 3.1.4 shows the non magnet filled cassette made of delrin, as well as the shaft adapter hardware required in mounting the cassette assembly into the dynamometer and into the MHD base plate cutout. If you notice in the figure you can see that an undercut chamfer has been added to the cassette edges on all four sides. This chamfer was also added to all four sides of the MHD plate square cutout and to the sides of the magnet filled cassette. These undercuts serve a critical role in acquiring accurate force measurements of drag and sideforce. The following paragraph explains why this is the case.

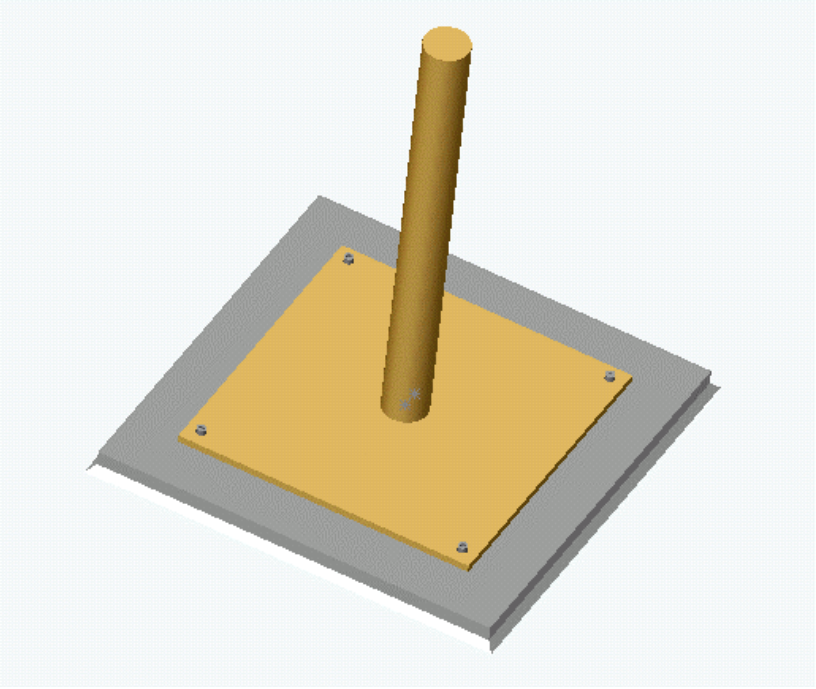

Figure 3.1.4 Non Magnetic Cassette Mounting Assembly

It is difficult to position the cassette exactly in the center of the cutout in the MHD plate, however it can be done to within a reasonable tolerance. This involves adjusting the position of the cassette with respect to the shaft adapter hardware. Since the location of the mounting hardware cannot be changed due to the shaft fitting into the dynamometer collet, the hardware has slots where it bolts to the underside of the cassette, allowing the adjustment of the cassette position, a process which can be very tedious and time consuming. Even so, it is likely there will be a small gap difference between the sides of the cassette and the MHD plate and the size difference depends on how accurately the cassette was centered. Figure 3.1.5 shows a cross section of the cassette mounted inside of the MHD plate cutout. The difference in gap at points A and B creates a difference in pressure along the cassette caused by water flowing through the gaps and acting on the side surfaces. This creates a force wanting to pull the cassette towards the direction of the bigger gap, towards the left in the figure. This force is significant enough to cause an effect on the force measurements measured by the load cells in the dynamometer.

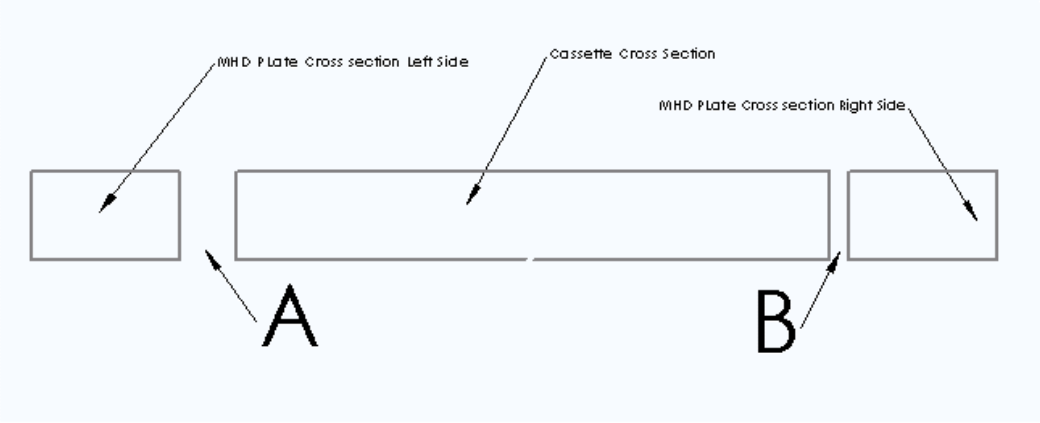

Figure 3.1.5 MHD Plate and Cassette Cross Section before undercuts

One solution to this problem would be to center the cassette exactly but this would require spending a lot of time getting it as accurate as possible. A more adequate solution to this problem was to add a chamfer to both the MHD plate and the cassette so as to create a sharp point on the edges of all four sides of the cassette and the base plate. Figure 3.1.6 illustrates a cross sectional view of the cassette installed inside of the base plate cutout with the undercut chamfers. The addition of these chamfers eliminates the

induced force caused by the gap differences at points A and B. If there is a gap difference at point A and B, the amount of area that is affected by the pressure in between the gaps is minimized to that of a knife edge allowing the force to be small and negligible.

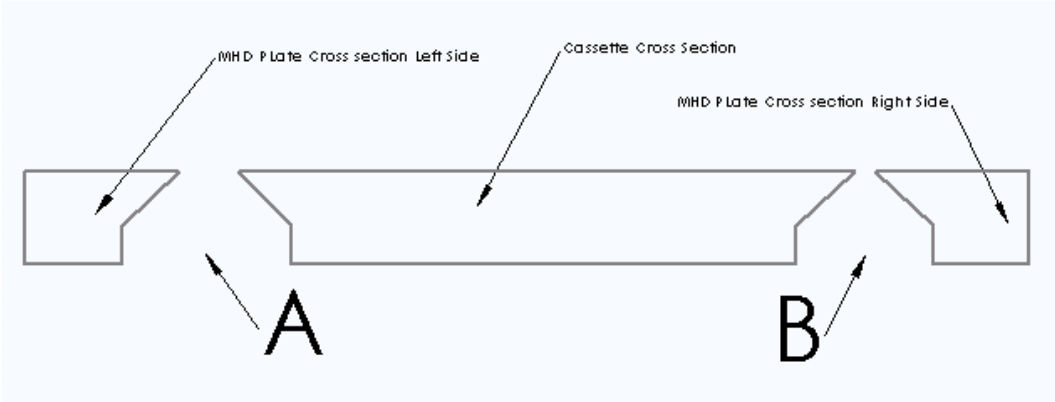

Figure 3.1.6 MHD & Cassette Cross Section after undercuts

3.2 Assembly of MHD Components & Water Tunnel Description

The hardware for the force measurement experiment consists of an assembly of components such as the magnet filled cassette and shaft adapter assembly, the MHD base plate, hardware for base plate to dynamometer window mounting, the dynamometer itself, and the load cells integrated into the isolation arm of the dynamometer. Figure 3.2.1 shows a 3D model, underside view of the dynamometer installed in the bottom of the water tunnel test section. Notice three load cells colored in darker grey which attach to the isolation arm of the dynamometer. The isolation arm is attached by thin rods at three points to the rest of the dynamometer.

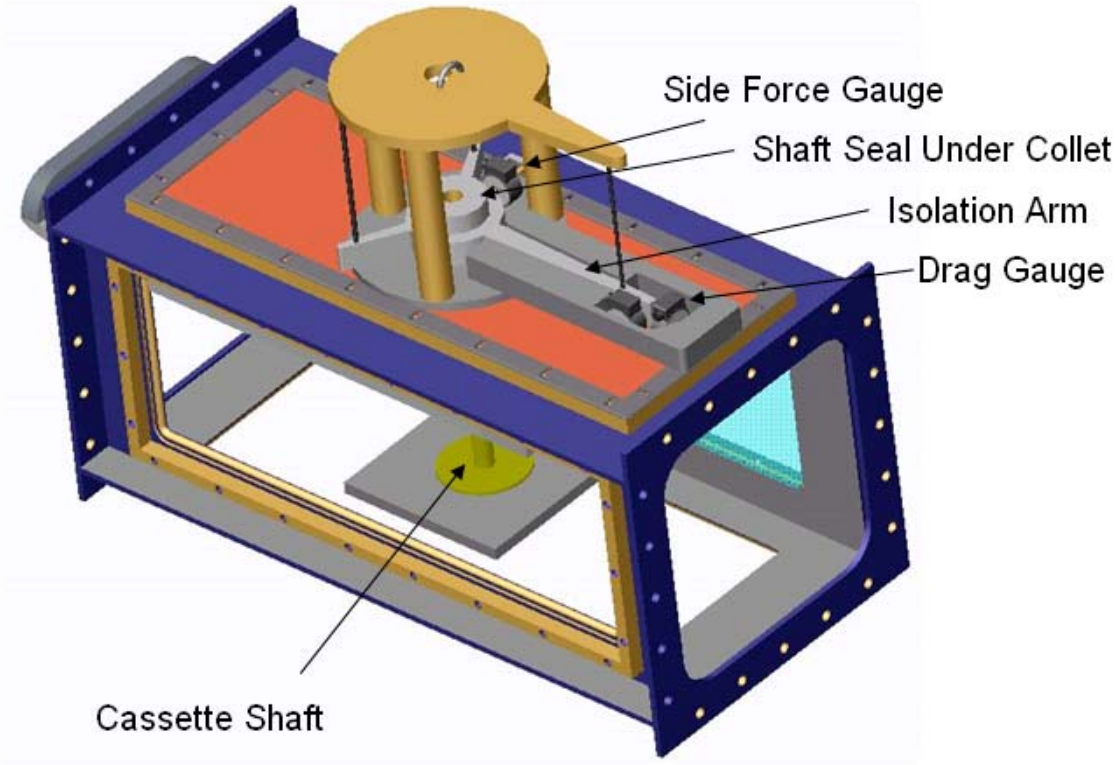

Figure 3.2.1 3D model of underside view of dynamometer, base plate, and cassette assembly

In this configuration, the load cells measure forces that are felt only by the isolation arm which has a collet with a 1.5 inch diameter hole where the shaft from the cassette is inserted and clamped with bolts. Figure 3.2.1 shows an exploded view of the cassette and

shaft aligned but not inserted into the collet of the dynamometer. The cassette shaft is inserted into the isolation arm, and the load cells are directly measuring forces felt by the cassette. The load cell used for the drag measurement was a 5 lb gauge and for side force a 20 lb gauge.

The dynamometer has the capability of rotating to a desired angle, but for the force measurement experiment, it was aligned perfectly parallel with the sides of the tunnel so that the load cell measuring drag would measure a force which was exactly in the direction of the flow, and load cell measuring side force would measure a force in the direction the Lorentz force was generated, perpendicular to the flow. A base plate spacer shown in figure 3.2.2 was used for mounting the base plate in the tunnel section with an offset of 2.8 inches from the dynamometer window. The base plate and the spacer are both secured with bolts, and for hydrodynamic efficiency, the bores in the base plate after the bolts have been inserted and tightened, are covered with silicone and then putty so as to create a smooth surface which blends with the rest of the delrin of the base plate.

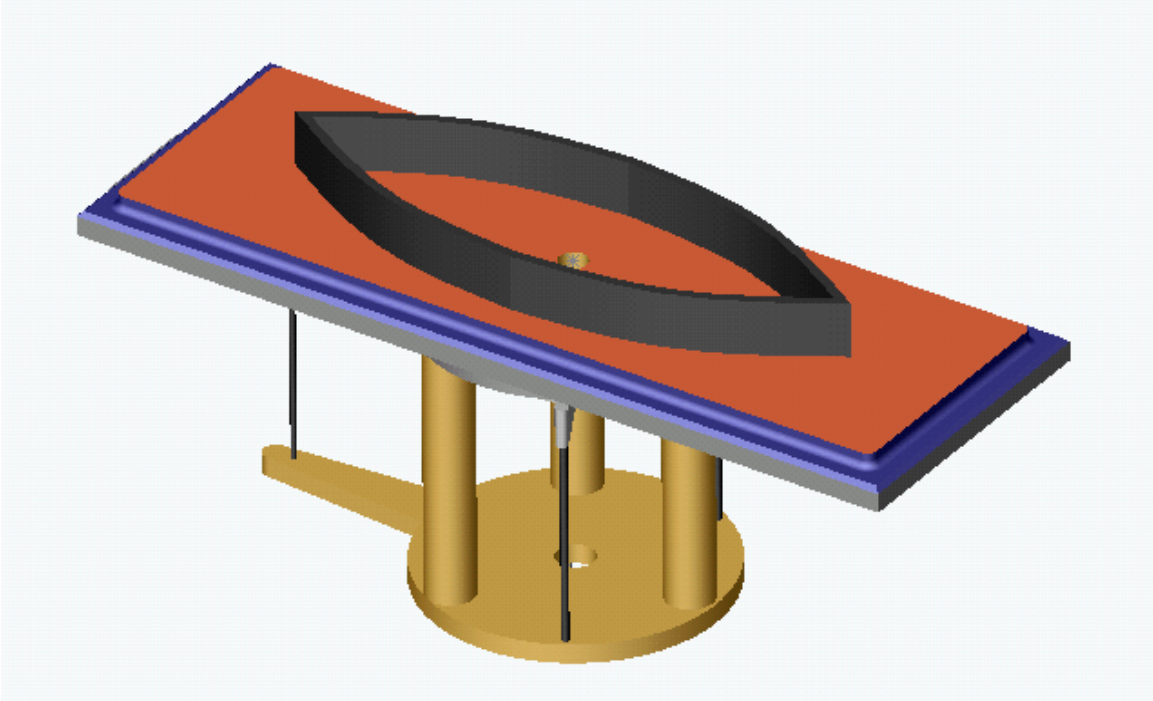

Figure 3.2.2 3D model of base plate spacer mounted to the dynamometer window

Figure 3.2.3 shows a photograph of the force measurement experiment hardware installed in the water tunnel test section with water filled and flowing from left to right. The red and green wires are run up through the hollow shaft adapter mounted to the cassette and are connected to each of the two terminals on the bottom side of the electrode board. After the wires have been connected, silicone is used to form a seal between the hollow shaft and where the wires run out. The photograph also shows the putty around the electrode board which appears as streaks of red which was used to create a smooth transition between the delrin of the cassette and the electrode board itself, since it did not sit perfectly flush when it was installed.

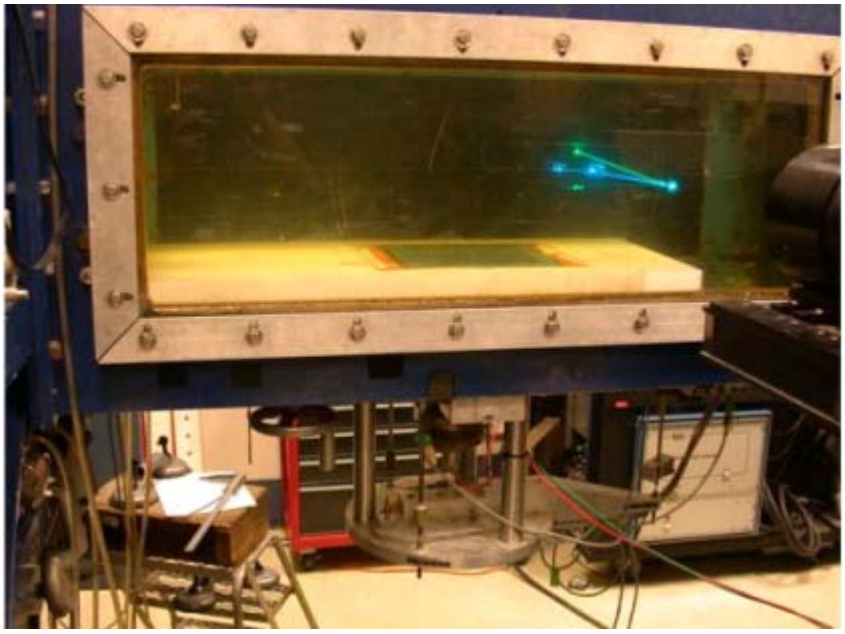

Figure 3.2.3 Photograph of MHD base plate installed in the test section

As seen in the figure, the LDV laser shoots four beams into the water and measures the speed of flow where these beams cross. The LDV system was used to record free stream velocities once the impeller of the tunnel was running and set to a certain RPM yielding a desired tunnel flow speed during the force measurement experiment. Figure 3.2.4 shows a schematic of the water tunnel in the Marine Hydrodynamics Laboratory. The water tunnel occupies two floors in building 3 at MIT, the bottom floor containing the impeller, and the storage tank, and the top floor containing the test section and sections of the tunnel which have flow straighteners such as stators and screen sections

which act to reduce turbulence in the free stream flow. The free stream turbulence of the tunnel is on the order of 3% - 5% and design work is in progress for the installation of a turbulence reduction mesh section capable of reducing the free stream turbulence to 1% or less.

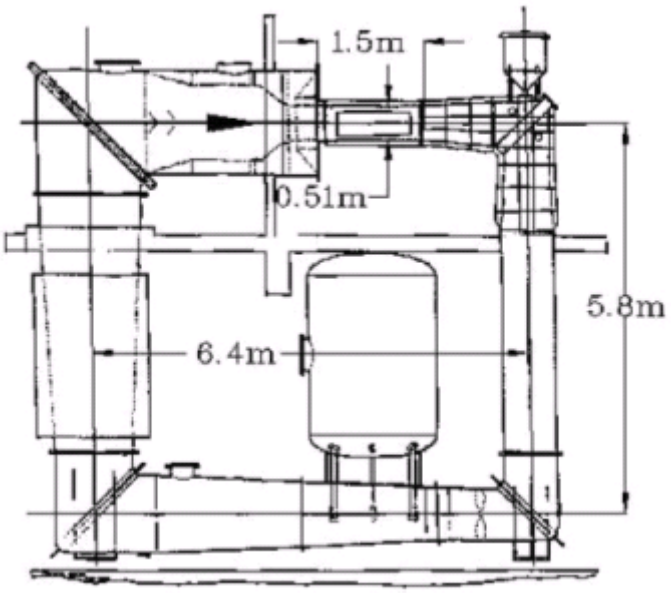

Figure 3.2.4 Schematic of MHL Water Tunnel

3.3 Electronics

Lorentz force activation requires the generation and crossing of magnetic and electric fields. The magnetic fields were created by installing rows of magnets an $1/8^{th}$ of an inch apart and integrating them into the cassette just below the electrode board. To create an electric field in the flow, current needs to be pumped through the electrodes of the electrode board. The transmission path for current flow is through wires connecting the outputs of four MOSFET's (connected to a power supply and driver electronics) to the electrode terminals located on the bottom of the electrode board.

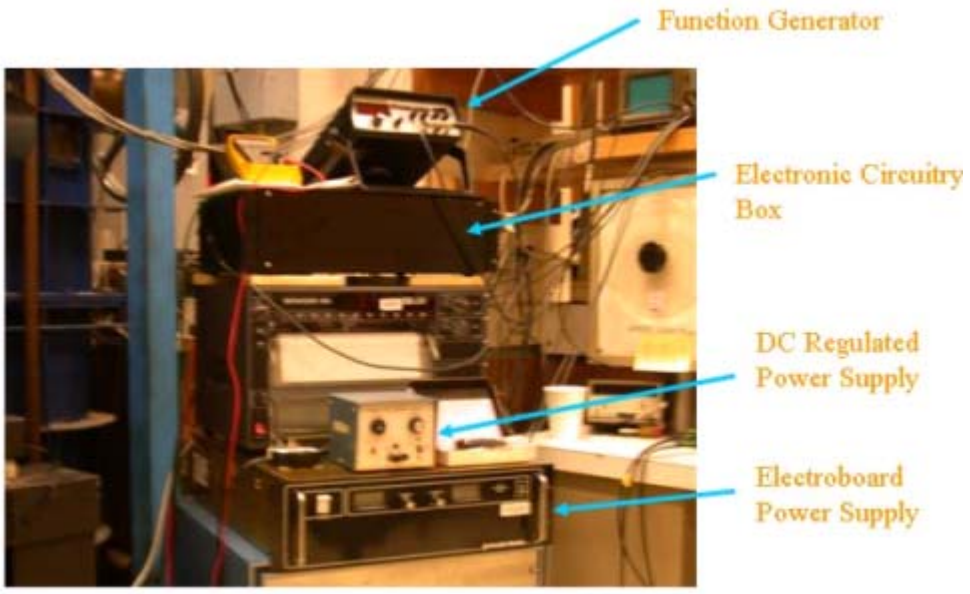

Figure 3.3.1 The main electronic components for Lorentz force activation

In order to verify maximum drag reduction predicted by numerical simulations, the current direction must be switched back and forth, with a magnitude that switches from plus to minus and minus to plus, thus creating a Lorentz force which alternates in crosswise flow direction from right to left and left to right. The amount of drag reduction observed is a function of the frequency and amplitude of the Lorentz force and to validate such effects, a requirement in the design of the electronics system was the capability of being able to produce an adjustable current signal with a desired frequency and amplitude. Figure 3.3.1 shows a photograph of the main electronic components required

in generating Lorentz force activation. The function generator serves the role of generating a square wave signal and has adjustable frequency and an output which is connected to the input of the driver electronics circuitry box.

For our new round of force measurement experiments Hydro Technologies of Severance Colorado, upgraded the electronic gate driver circuitry used in Jaskolski's Lorentz force activated measurements. The new driver electronics contain a Schmidt trigger, a high frequency driver chip, and other electronic components such as capacitors, resistors, and power supplies. To power the driver electronics, a DC regulated power supply capable of producing 15 volts was needed. The newly designed electronic circuitry components allowed current polarity to be switched at a frequency of up to several hundred hertz. The old circuitry worked reliably up to only about 120 Hz. Because power supplies are not capable of producing wave forms with a frequency greater than a few hertz, an h-bridge type switch was needed to produce the desired wave form from a DC current output from the power supply used. The outputs of this circuitry were connected to the gates of four MOSFET's, which were then connected to the outputs of the main power supply capable of generating 166 amps of current and to the wires connecting to the terminals of the electrode board. The outputs of the driver circuitry were connected in such a manner that they would open and close the gates of the MOSFET's repeatedly, thus changing the polarities of the two wires which connected to the electrode board and allowing the generation of a square wave current signal which alternated from plus to minus and minus to plus. Schematics of the electronics can be found in the Appendix section.

4.0 Results

4.1 Magnetic and Electric Field Mapping

Magnetic and electric field mapping were performed in an effort to verify that both the electric fields and magnetic fields were present over the electrode board in order to produce Lorentz force activation. The magnetic flux was measured using a gauss probe meter and was mounted to the LDV laser traverse so that positions for desired probe location could be programmed and data acquired for various points across and above the surface of the electrode board. Figure 4.1.1 shows a photograph of the major components used in the magnetic field mapping as well as the coordinate system used.

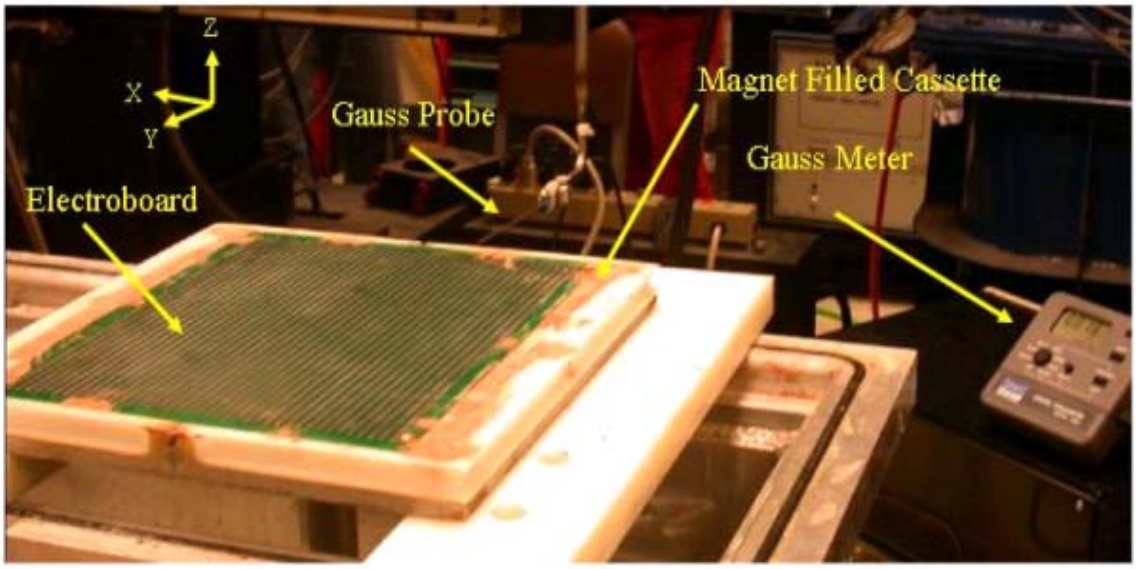

Figure 4.1.1 Photograph of components used in magnetic flux measurements

The magnet filled cassette was set on top of a cart and delrin bars, and was aligned with the probe so that movement of the probe would be perpendicular or parallel to the rows of magnets and electrodes. Each of the magnets that make up the rows in between the electrodes are 0.5 Tesla magnets, and the polarities in the rows alternate. For example

one row will contain magnets that are all oriented south and the two adjacent rows will contain magnets oriented north.

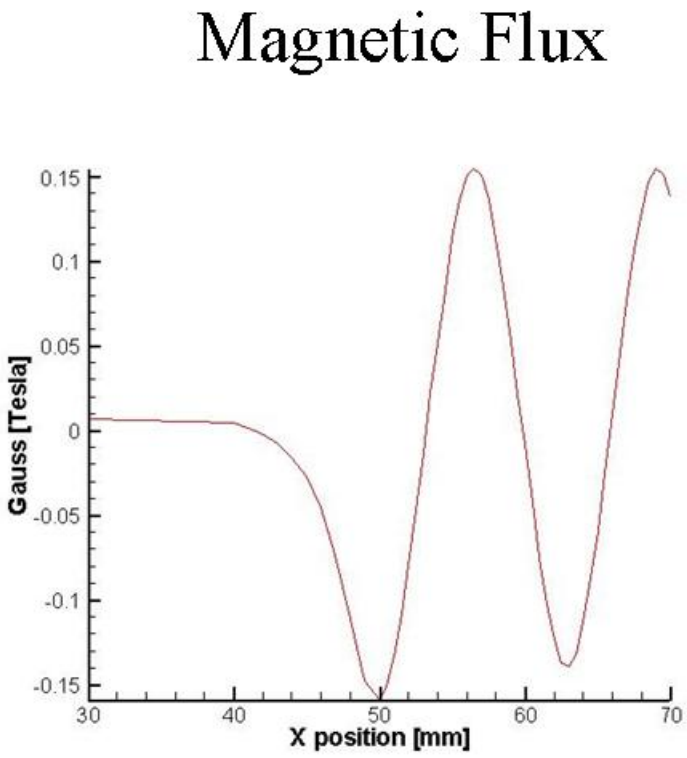

Figure 4.1.2 Plot of magnetic flux vs x position over electrode board

Figure 4.1.2 shows a plot of the magnetic flux as a function of position x. Notice from the plot that the maximum and minimum readings are 0.15 and -0.15 Tesla. The probe position was setup so that x = 0 was the edge of the electrode board which stuck out past the rows of magnets, thus no flux is present until an x position of about 42 mm. At values of x = 56 mm and x = 68mm, the peaks are positive with magnitudes of 0.15 Tesla. These are locations of the centers of rows of magnets oriented north, and at x = 50 and x = 63 mm the peaks are negative with magnitudes of -0.15 Tesla and are centers of rows of magnets oriented south. The widths of the magnets are 3.1 mm and the spacing in between rows is also 3.1 mm. Also notice from the plot that the maximum magnitude measured at the surface of the electrode board was +/- 0.15 Tesla. Although the cassette was filled with rows of 0.5 Tesla magnets, the probe was

measuring very close to the surface of the electrode board but at a distance of 0.06 inches above the actual surface of the magnet rows. This distance above the magnet rows is equivalent to the thickness of the electrode board

A similar verification process was carried out to verify that current was being pumped into the electrodes of the electrode board. This test was a rather simple one since it involved measuring voltage at the terminals where the wires connected and supplied current coming from the power supply and driver electronics. A voltmeter was sufficient enough to carry out this procedure. This test was performed on a spare electrode board since it needed to be submerged in conductive water and it would have been difficult to perform this procedure with the electrode board installed in the cassette and in the water tunnel.

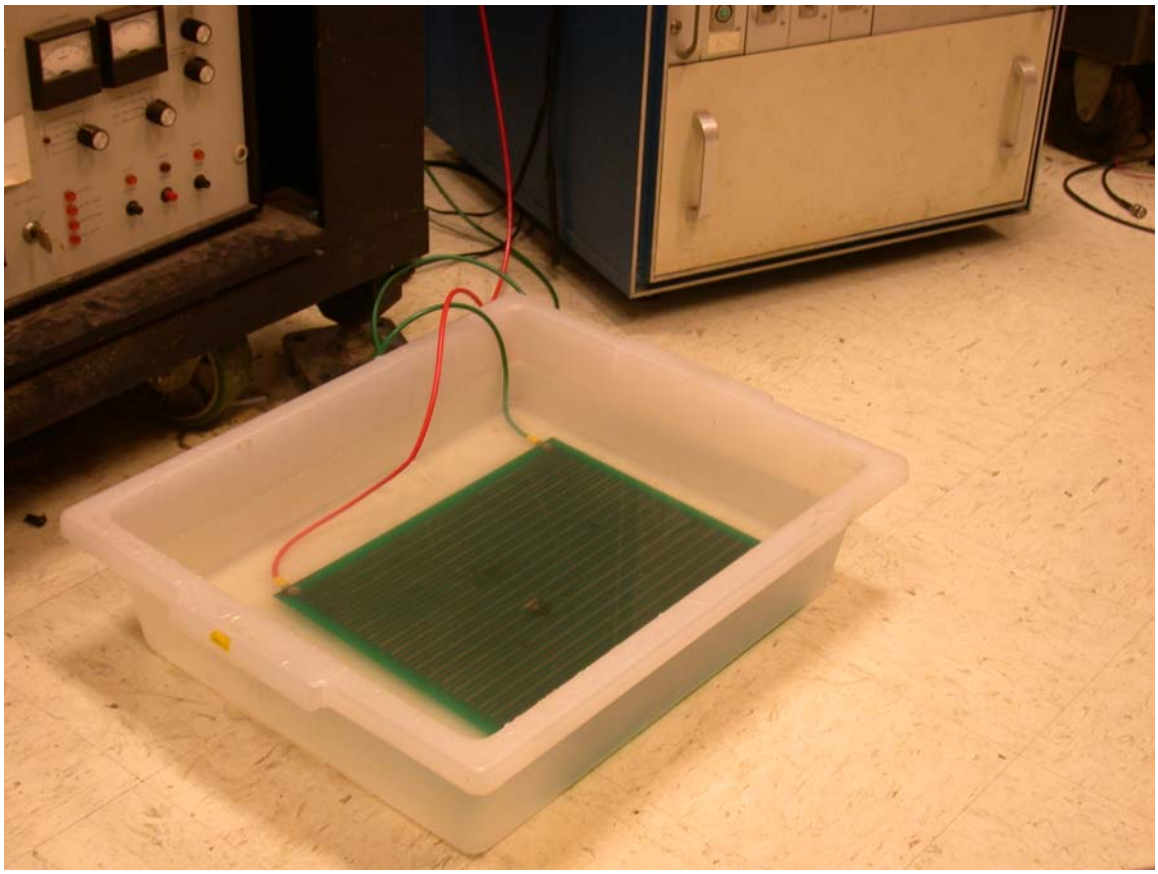

Figure 4.1.3 Photograph of voltage mapping experimental setup

Figure 4.1.3 shows a photograph of the test bed setup which had water filled half way and with the electrode board submersed. Salt was added to the water to make it

conductive so electric fields could be created in the fluid at the surface of the electrode board. In the water tunnel, roughly 800 lbs of sodium nitrite was added for 6000 gallons of water in order to create conductive properties equal to half of sea water conductivity which is in the range of 4.29 siemens/m [3]. The current output of the power supply was set to 30 Amps and the function generator output was set to 20Hz and various voltages at positions along the electrodes of the electrode board were measured with the voltmeter.

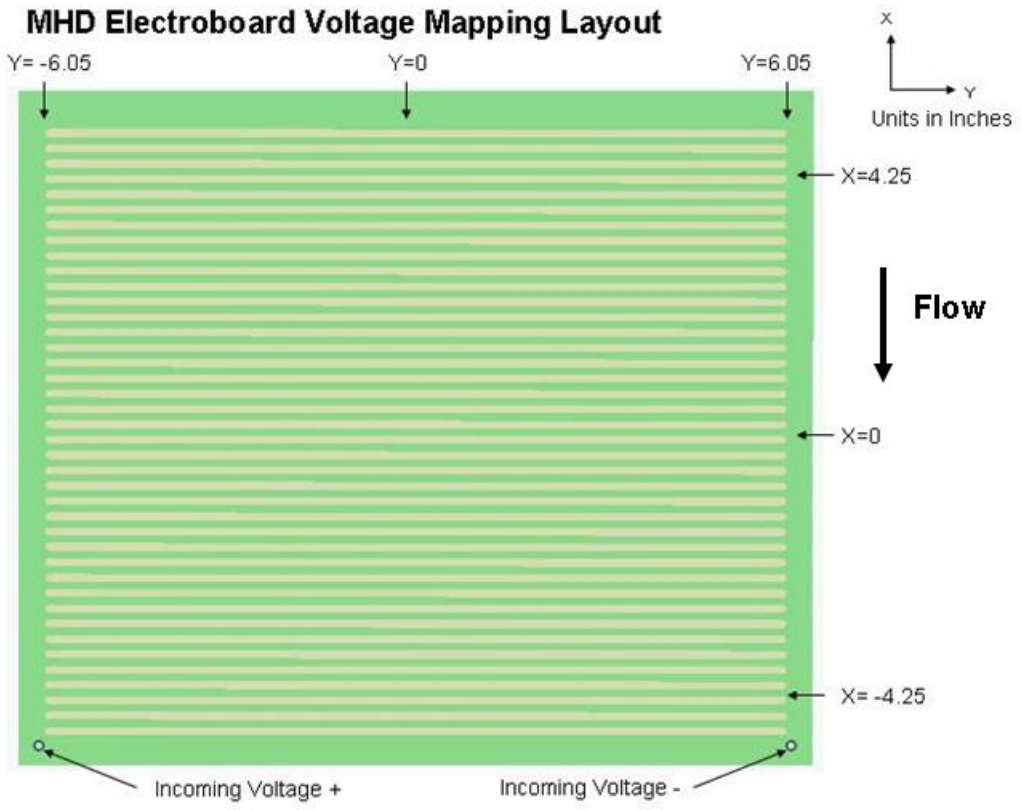

Figure 4.1.4 Diagram of voltage mapping layout

Figure 4.1.4 shows a diagram of the mapping layout where voltages were measured. Three sweeps were made at locations of X = -4.25, 0, and 4.25 inches. At these X locations 10 evenly spaced points from Y = -6.05 to Y = 6.05 inches were measured. These measurements were made on two electrode boards, one of them was a previously used board and had electrodes with widths of 1/8 inches and 1/8 inch spacing and the other board was a brand new electrode board which had electrodes with widths of 1/16

inches and an electrode spacing of 1/8th inches. Figure 4.1.5 shows plots of the three different X locations of voltage as a function of y position along the electrode board. At X = -4.25 there is almost no variation in voltage along the Y axis, but for X = 0 and X = 4.25 the variation around Y = - 3 inches is significant and is due to the electrodes in that region being corroded as well as the presence of epoxy which was accidentally spilt from some other experimental work occurring in the lab.

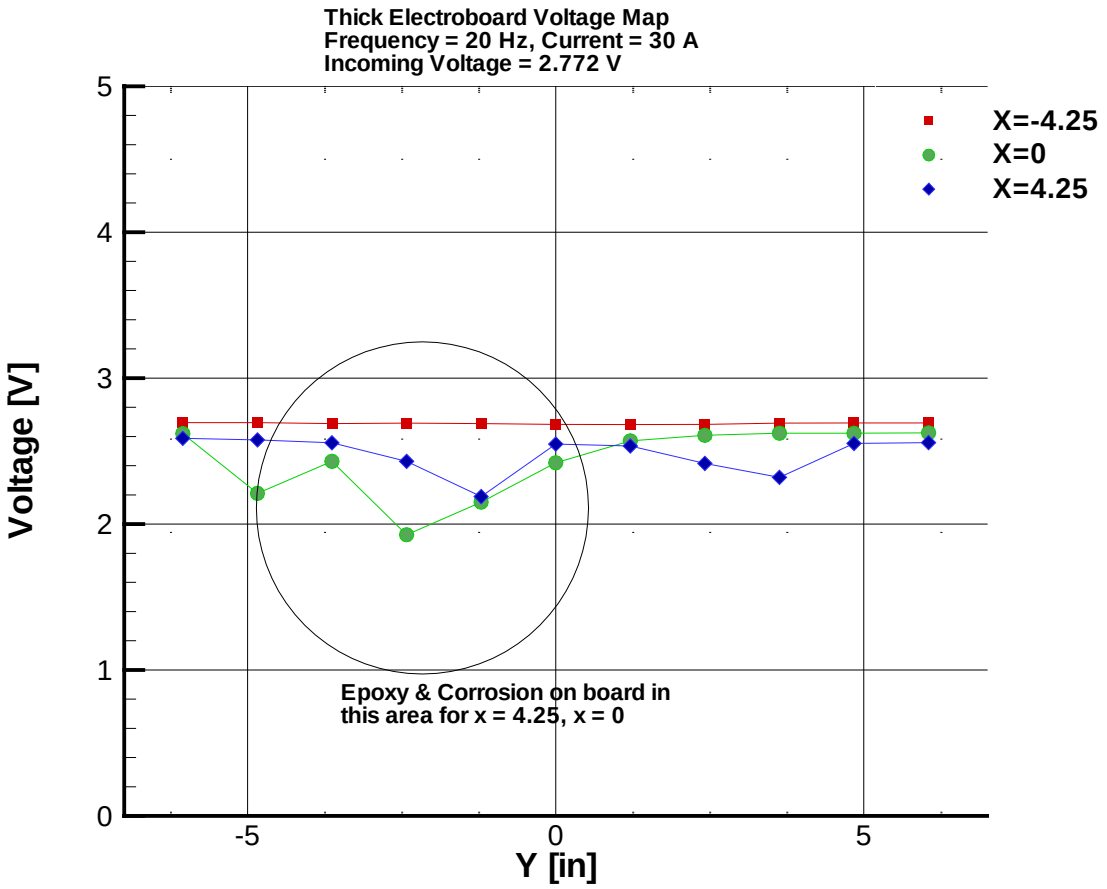

Figure 4.1.5 Thick electrode board voltage mapping plot

This same test was also conducted on a new electrode board with thinner electrode widths in order to verify that the variation seen in the thick electrode board was in fact due to corrosion and effects of the epoxy. Figure 4.1.6 shows plots of the voltages as a function of y position for the sweeps at the three different X positions. This data shows no variations such as those that were found in the thick electrode board containing those

regions of corrosion and epoxy. There is some variation in voltage between the different X positons, and the trend seems to be that voltage drops with increasing X, which is further away from the terminals of where the current is supplied by the power supply and driver circuitry. This drop in voltage is not drastic enough that Lorentz force activation becomes greatly affected in regions further away from the incoming current terminals. However, there is a voltage drop of about 5% between the electrode at X = -4.25 and at X = 4.25. This will affect the magnitude of the Lorentz force generated in this region somewhat, but will likely not have any significant impact on the global drag and side forces measured by load cells in the dynamometer.

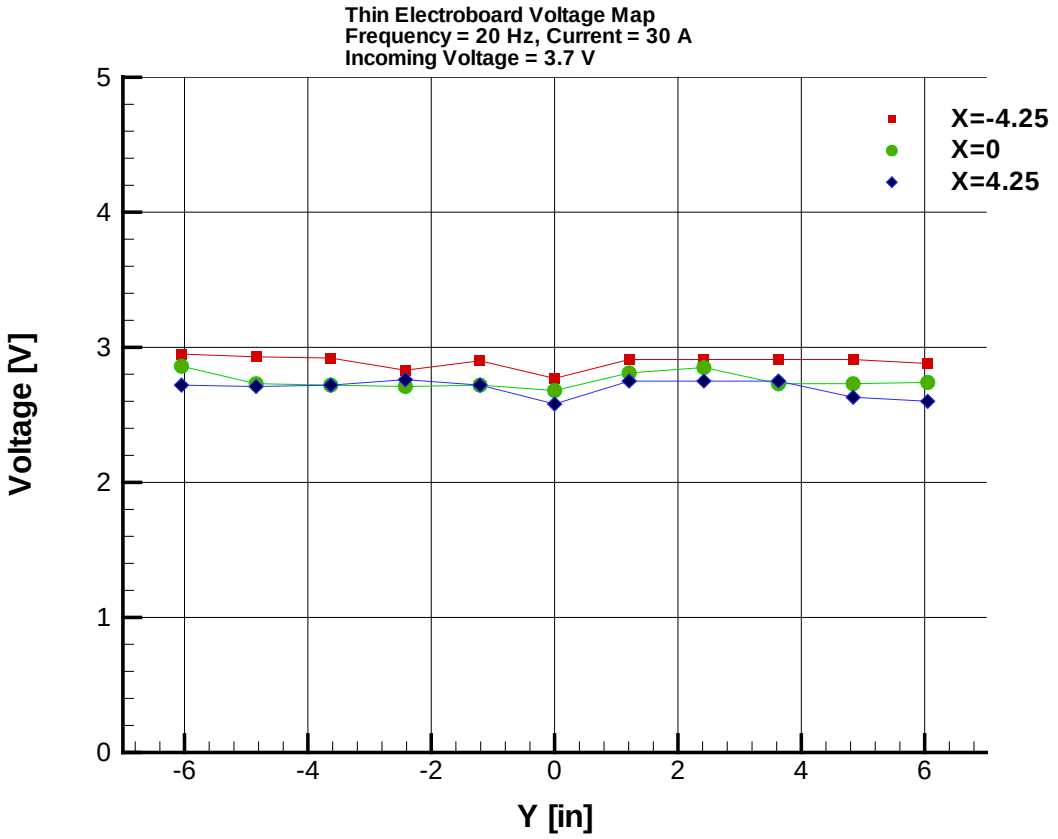

Figure 4.1.6 Thin electrode board voltage mapping plot

4.2 Boundary layer measurements

4.2.1 Boundary layer data

In order to characterize local effects induced by Lorentz force activation, the LDV data acquisition system was used to measure velocity profiles in the boundary layer of flow over the electrode board. Local changes in Du/Dy, the shear stress at the wall, are directly associated with changes in the drag force. One of the first LDV measurements made in the March 2003 experiment was shear stress sensitivity in the cross flow direction. This data would indicate whether there is any change in the drag across the board perpendicular to the flow. We expect there to be little or no variation in drag in this direction.

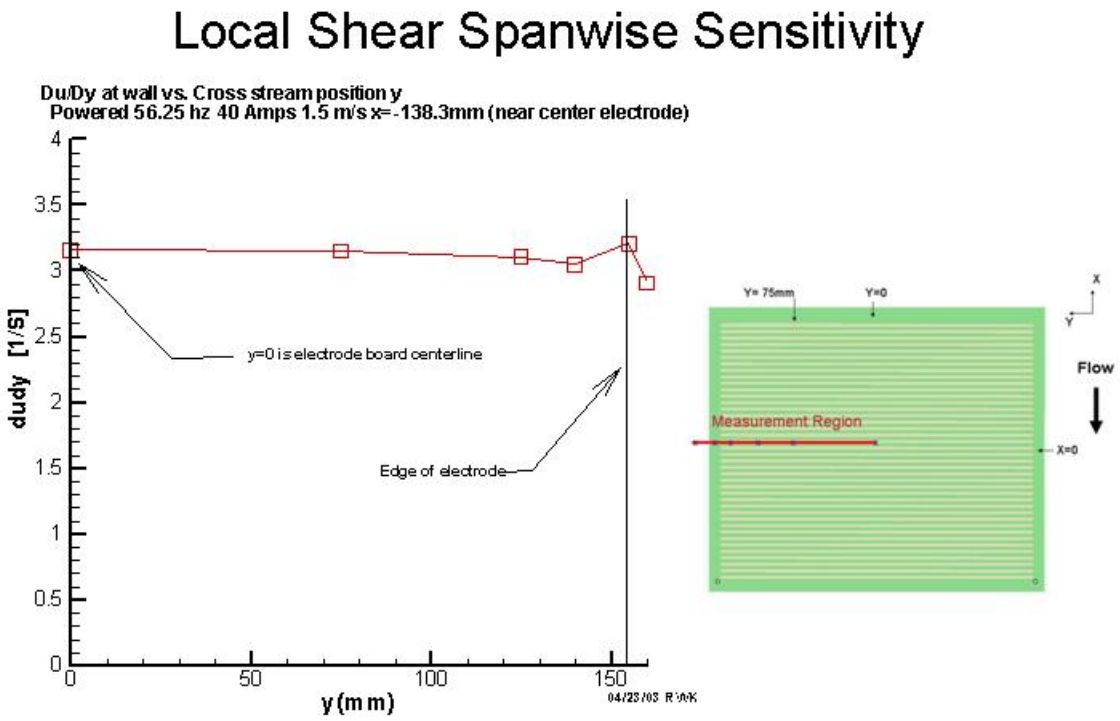

Figure 4.2.1 Variation in wall shear across electrode board

Figure 4.2.1 shows the variation in wall shear across the electrode board at one streamwise position between electrodes 19 and 20. Note there is very little change

from the centerline of the board all the way to the edge of the electrodes, thus validating the off center measurements (y = 75mm) of most of the LDV measurements performed later in March 2003.

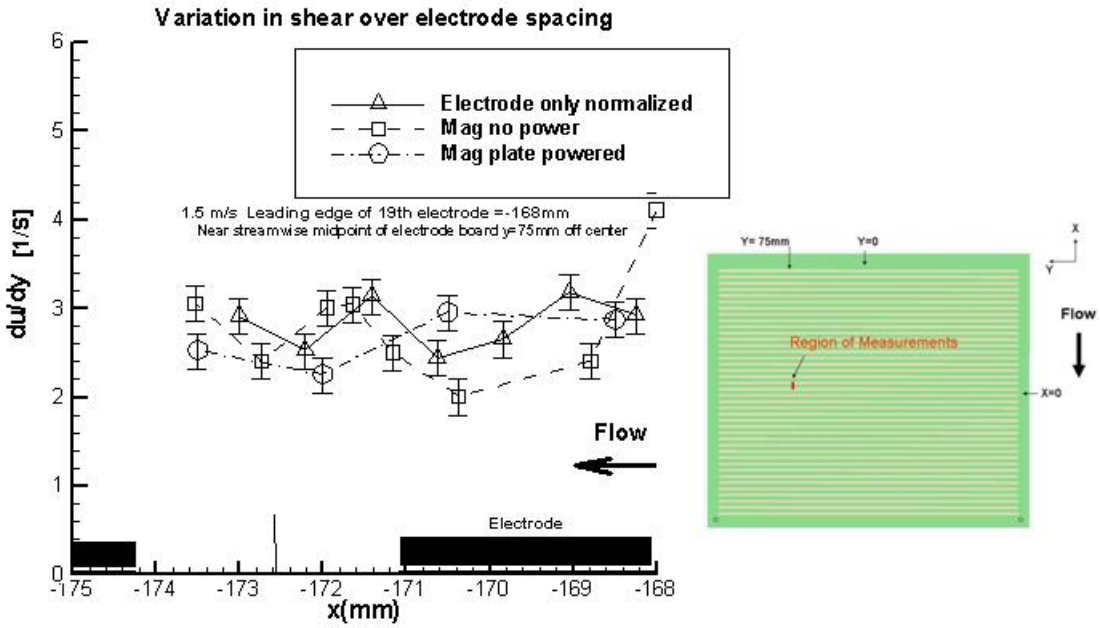

Figure 4.2.2 Plot of variation in shear over electode spacing

Measurements in variation of shear over an electrode spacing in the flow direction were also conducted. Figure 4.2.2 shows the variation in wall shear over the actual extent of an electrode spacing. Three cases are shown, one with the cassette with the electrode board but no magnets, another with the entire electromagnetic cassette unpowered, and the last with the electromagnetic cassette powered at 56.25 Hz, and 40 amps. The cases shown are at 1.5 m/s free stream velocity. For the electromagnetic cassette powered, the trend seems to show a reduction in du/dy between the electrodes indicating that drag reduction is occurring in between the electrodes. Although there is some variation in du/dy for the electromagnetic board with no power and for the cassette with no magnets, it is not evident that drag reduction is occurring in between the electrodes.

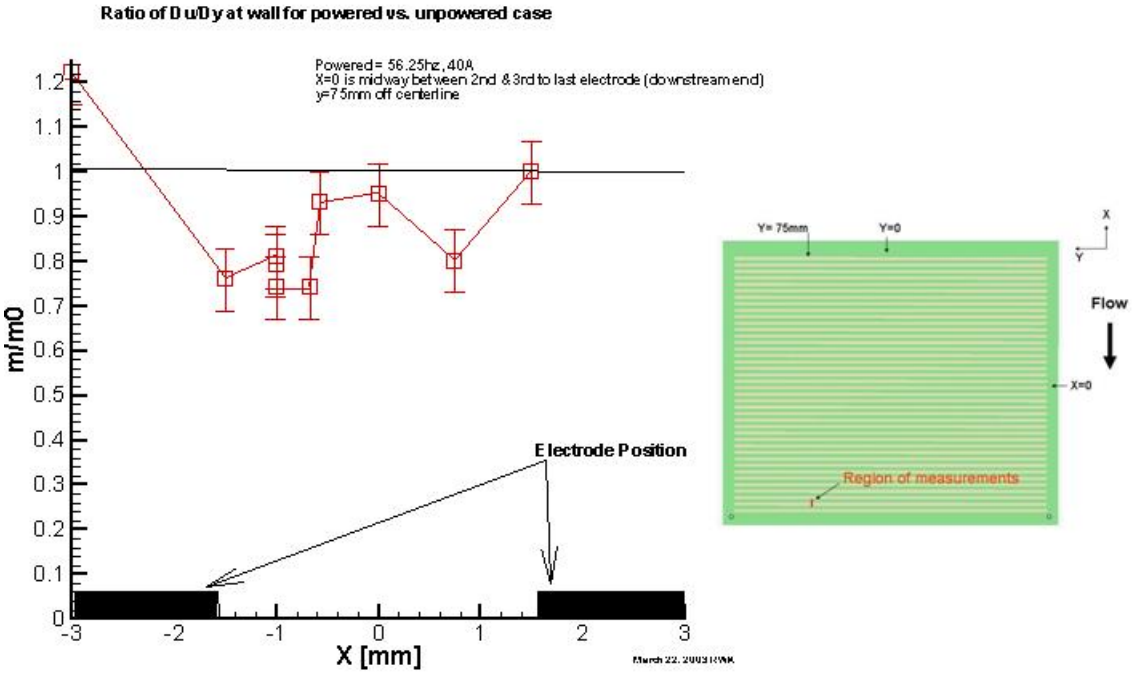

Figure 4.2.3 Plot of wall shear over an electrode spacing

Figure 4.2.3 shows the deviation in wall shear across an electrode spacing for the powered case at 56.25 Hz and 40 Amps. This data was measured between the 2nd and 3rd to last electrodes 75mm off the centerline. This case also shows lower wall shear between the electrodes and higher wall shear over the electrodes indicating drag reduction between electrodes and drag increase over electrodes. This is in contradiction with the prediction from the numerical simulations. Moreover, this data shows the large variation in wall shear over the electrode spacing, thus showing that inferring drag from a single point wall shear measurement will not be adequate to infer the global drag. This validates previous conclusions involving the need to measure drag force directly and globally using a load cell setup.

Variation in cross stream velocity was also measured for the electromagnetic board powered and unpowered. The measurement was conducted half way between the center electrodes. Figure 4.2.4 shows that the maximum electromagnetic action penetrates the

boundary layer to about 0.5 mm. This roughly agrees with penetration depths predicted by the numerical simulations. The change in magnitude of RMS is about 0.04 m/s maximum, but it should be noted that due to the low data rate of these measurements, this magnitude is not very reliable.

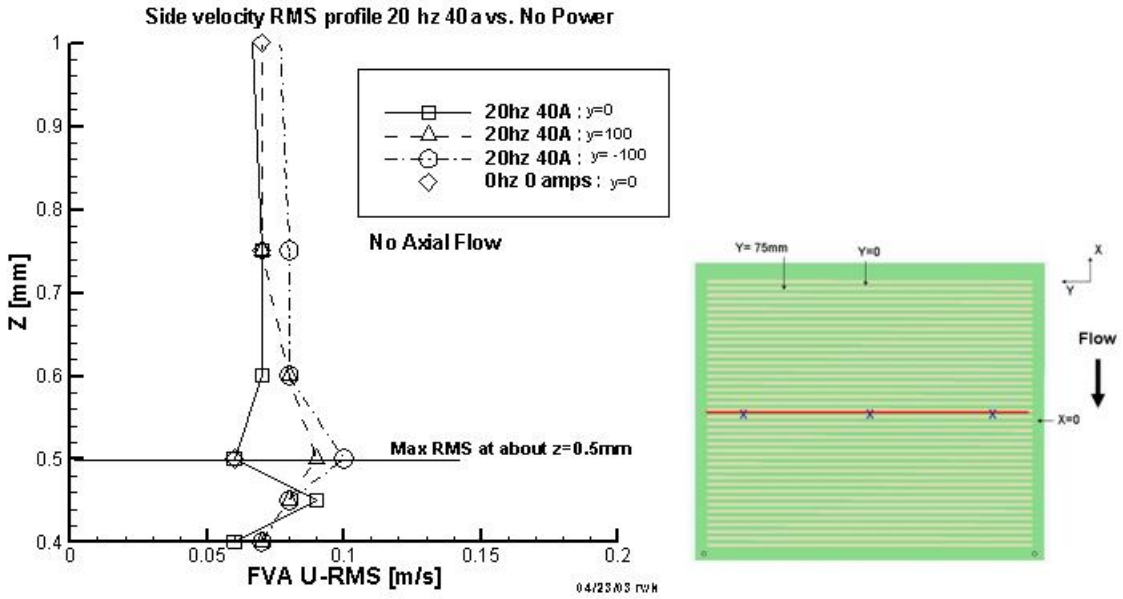

Figure 4.2.4 Plot of variation in cross-stream velocity

4.2.2 Comparisons to prior work

Measurements of wall shear as a function of current amplitude were performed between the 2nd and 3rd to last electrodes and 75mm off the center of the electrode board. The figure below compares the data of Jaskolski 2002 [2] to measurements conducted in March 2003. The data was collected at the same location over the electrode board for both cases at 1.5 m/s and at frequencies of T+ = 100. The data shows similar trends for both data though the magnitude of the maximum wall shear variation is lower for the 2003 data. Instead of a magnitude of about 36% in change in du/dy for a current amplitude of 40 amps measured by Jaskolski [2], the recent measured magnitude for change in du/dy was about 28%. This change could be due to the high sensitivity to axial position on the wall shear.

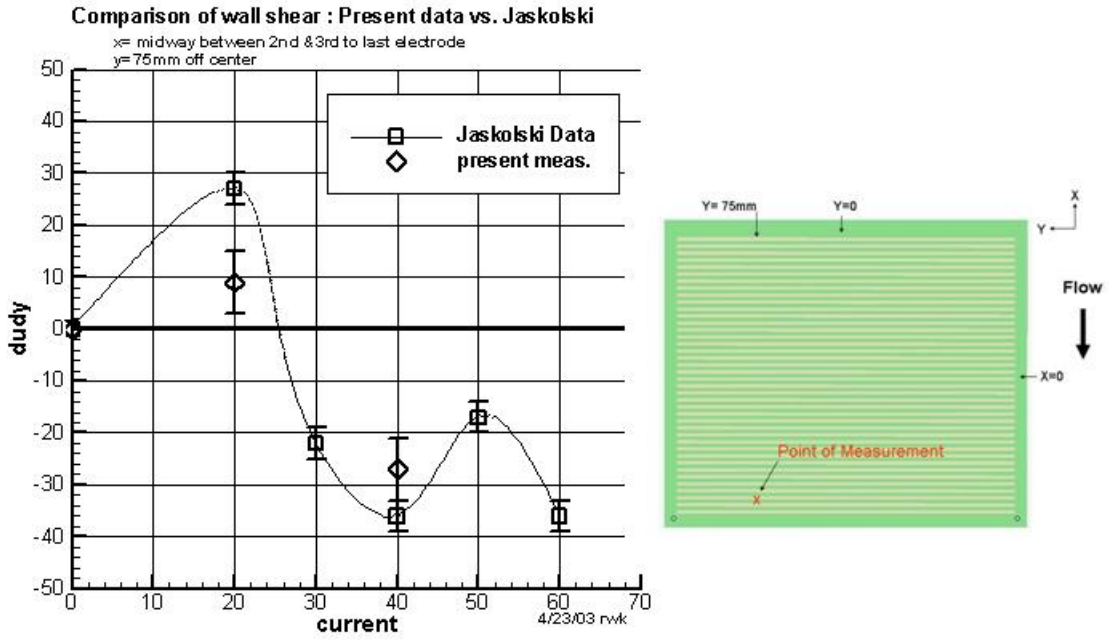

Figure 4.2.5 Wall shear comparison: Present vs. Jaskolski at 1.5 m/s

4.3 Force Measurements

4.3.1 Background

As part of verification that our force measurement system was capable of measuring drag and lift forces accurately, baseline drag force measurements were conducted in the summer of 2002. Baseline curves for drag vs speed were measured for both the baseline plate which was the flat delrin cassette with no magnets or electrode board and for the electromagnetic cassette but unpowered. Figure 4.3.1 shows the drag of the delrin flat plate and of the electromagnetic plate. The drag as a function of speed of the delrin baseline plate rises as the square of the tunnel speed, and is consistent with slightly rough plates at high Reynold's numbers. This verifies that our force measurement setup was working properly.

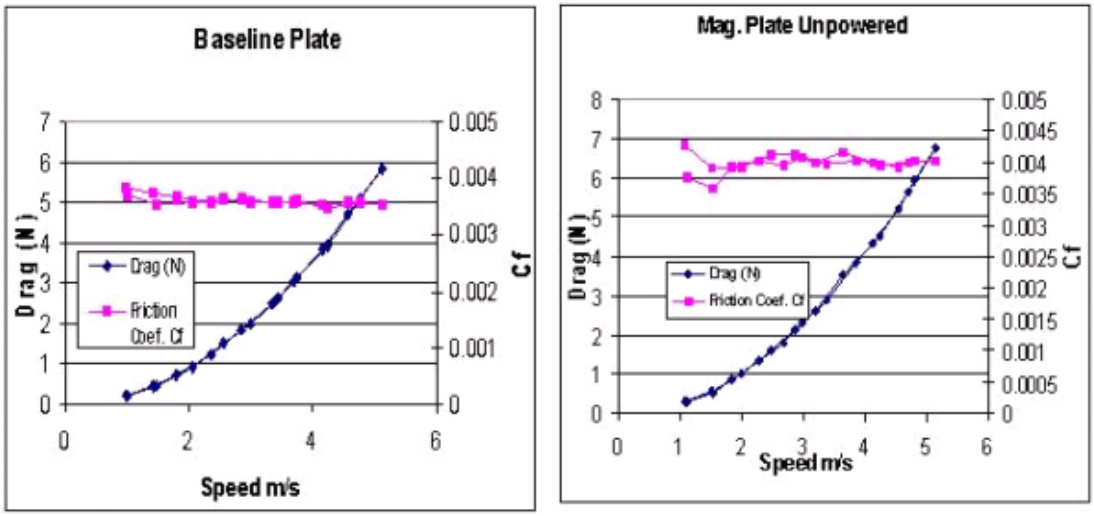

Figure 4.3.1 Plots of drag vs speed for the baseline and magnetic unpowered plate cases

The two plots show that for friction coefficients Cf of the two plates, the electromagnetic plate has an average Cf of about 0.004 and the baseline delrin plate has a Cf of about 0.0035. The baseline plate is slightly higher than the predicted drag from theory which is 0.003 and is likely due to extra roughness from the delrin surface. The

increase in the drag of the electromagnetic plate is probably due to the extra roughness of the electrodes of the electrode board protruding from the surface.

4.3.2 Drag Force Measurements

The process of measuring drag forces in an attempt to verify global drag reduction as a result of Lorentz force activation was carried out experimentally in March of 2003. Other attempts had been made in January of 2003 but because of driver electronics and data acquisition problems, no reliable drag force measurements were conducted. In the March 2003 force measurement experiment, data acquisition and driver electronics issues were taken care of and reliable drag measurements were made.

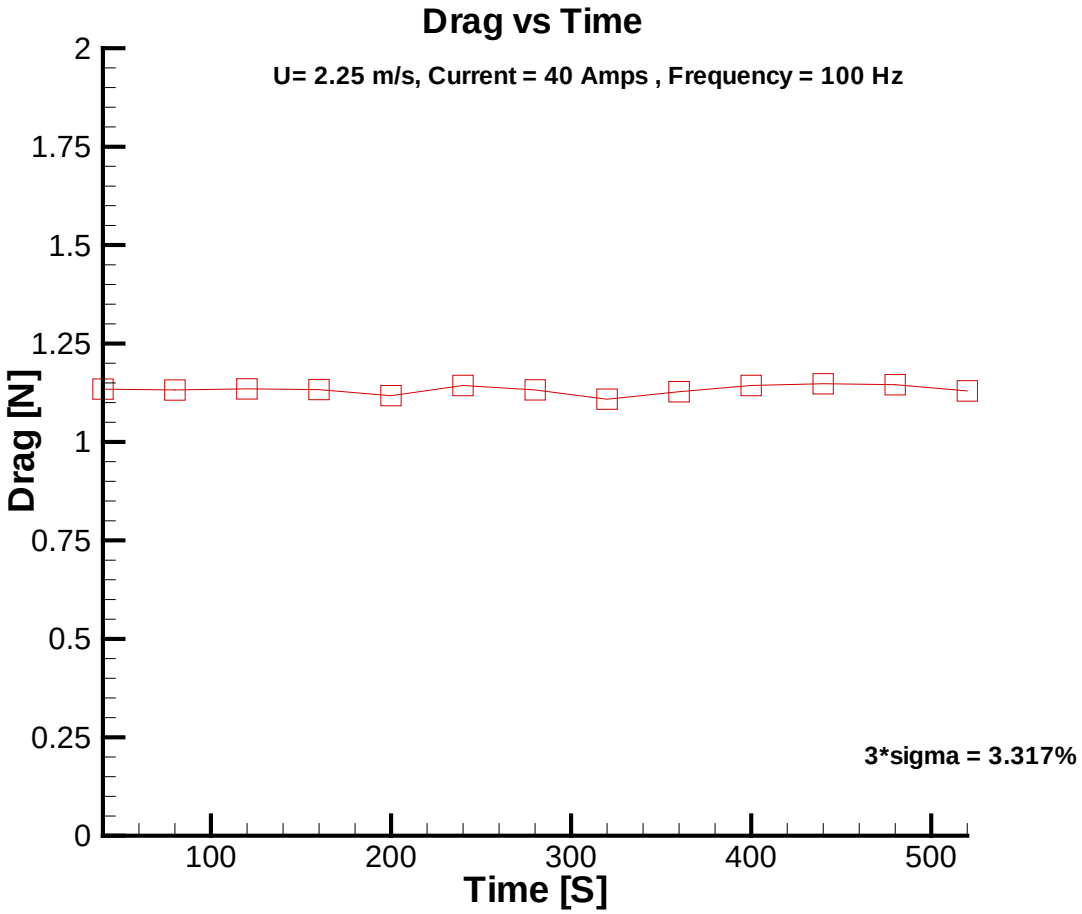

Figure 4.3.2 Plot of drag vs time an operating point of U=2.25 m/s, Current = 40 A, Frequency = 100Hz

From this experimental work, figure 4.3.2 shows the repeatability of the drag measurement at one point. The operating point for this data is at a tunnel speed U

equal to 2.25 m/s, a current of 40 Amps, and a driving frequency of 100Hz. This data has a 3 sigma variation of 3.317% which was used as the error bound for subsequent drag measurements. In this calculated error bound, the contributions are likely to be from the resolution of the data acquisition system and from small fluctuations in tunnel speed which is controlled manually. When controlling tunnel speed, the LDV laser system is used to measure the flow speed in the free stream. The person running the experiment will periodically check the flow speed acquired by the LDV system and adjust the tunnel speed accordingly. After the tunnel impeller has been running for about a half hour, the resolution of tunnel speed control is 0.01 m/s, which is remarkably good.

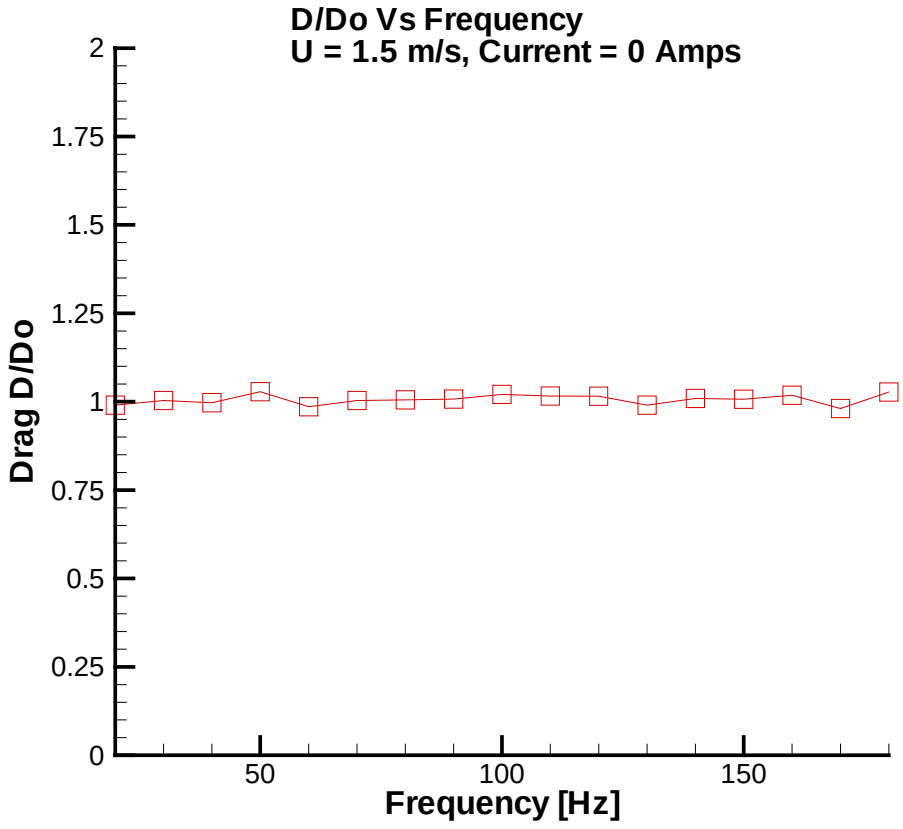

Figure 4.3.3 Plot of drag D/Do vs frequency

Drag measurements were also conducted with the tunnel speed at 1.5 m/s and with the electromagnetic board unpowered (0 Amps) but at different frequencies. We expect there to be almost no variation in this case since the output amperage on the power supply

with it turned on was set to zero for each of these data points. Figure 4.3.3 shows the actual data of drag D/Do as a function of frequency when the board was unpowered. D/Do is the dimensionless value of drag and is calculated by dividing drag measurements at various powered points by the average value of drag for the unpowered sweep. The data shows little variation in drag as a function of frequency given the error due to drift in zeros.

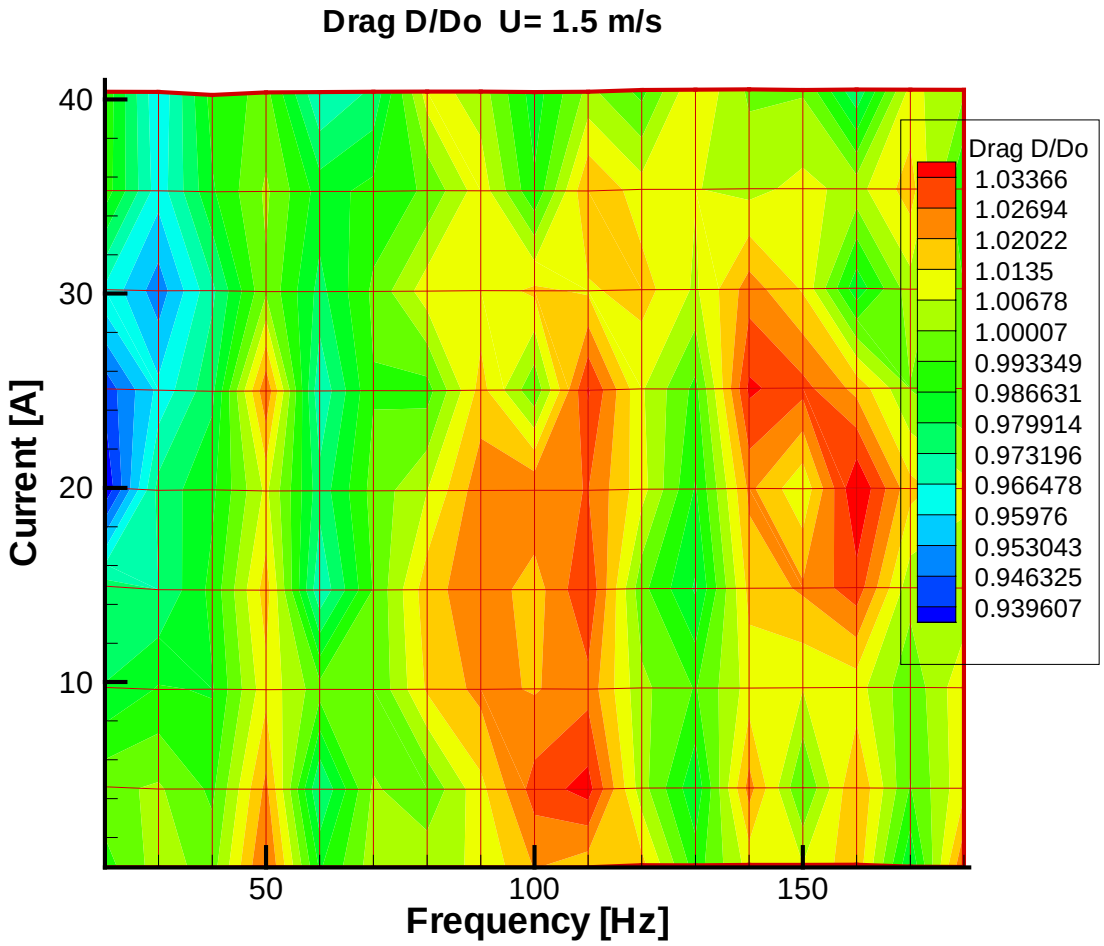

Figure 4.3.4 Countour of drag D/Do vs frequency and current

Drag force measurements were also conducted for various frequencies and amplitudes of current. Sweeps at different frequencies where the current varied from 0 to 40 amps in increments of 5 amps were performed. The frequencies of these sweeps were performed from 0 to 180 Hz and were incremented by 10Hz. Since load cell zero positions shift, the

zeros were recorded before and after each of these sweeps by turning off the tunnel flow speed, turning off the power supply, and then acquiring data from the load cell. The zeros would then be recorded so that linear interpolations could be applied in the data processing phase for each sweep. Figure 4.3.4 shows the drag change D/Do (powered over unpowered) for the entire electromagnetic plate at 1.5 m/s as a function of drive frequency and current. Each of the data points acquired was taken over a period of 40 seconds and 40,000 samples were acquired and averaged. Noting that the repeatability of the drag measurements is +/- 3.317%, there is little evidence of drag change throughout the contour. Small amounts of drag reduction may be present at the lower frequencies but the data in this area should be repeated to validate this. These areas of possible drag reduction are shown in figure 4.3.5 for current amplitudes of 20, 30, and 40 Amps and appear to be in the lower frequency range. The data shows no more than a few percent drag reduction at best.

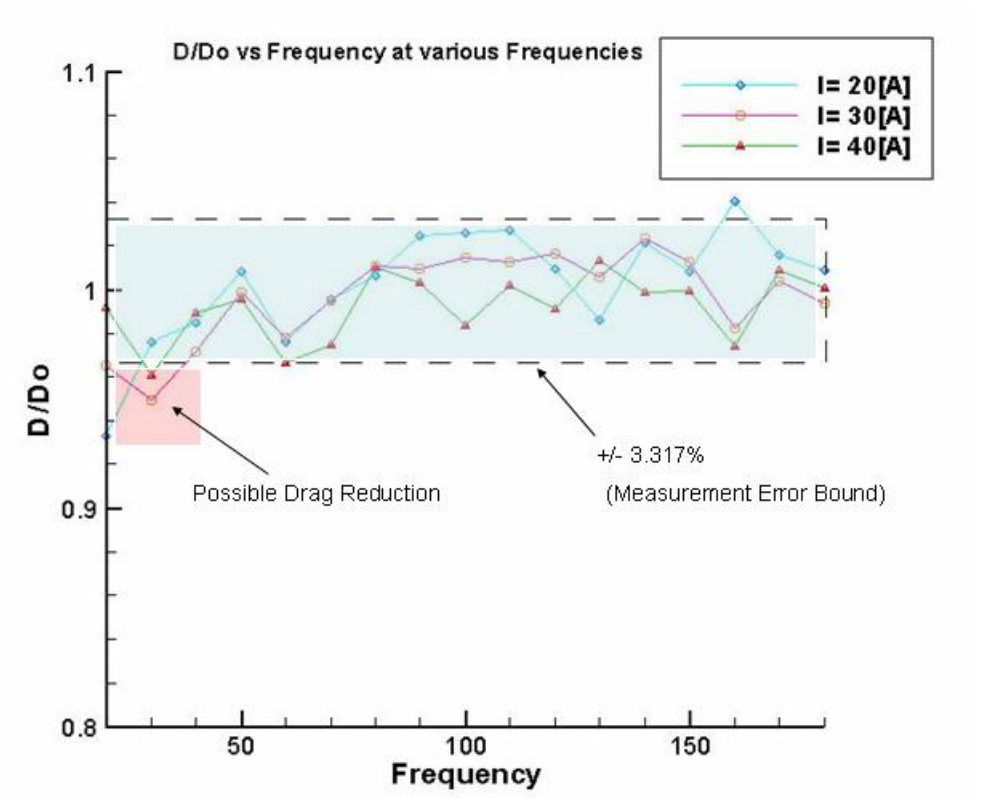

Figure 4.3.5 D/Do vs frequency for various amplitudes of current

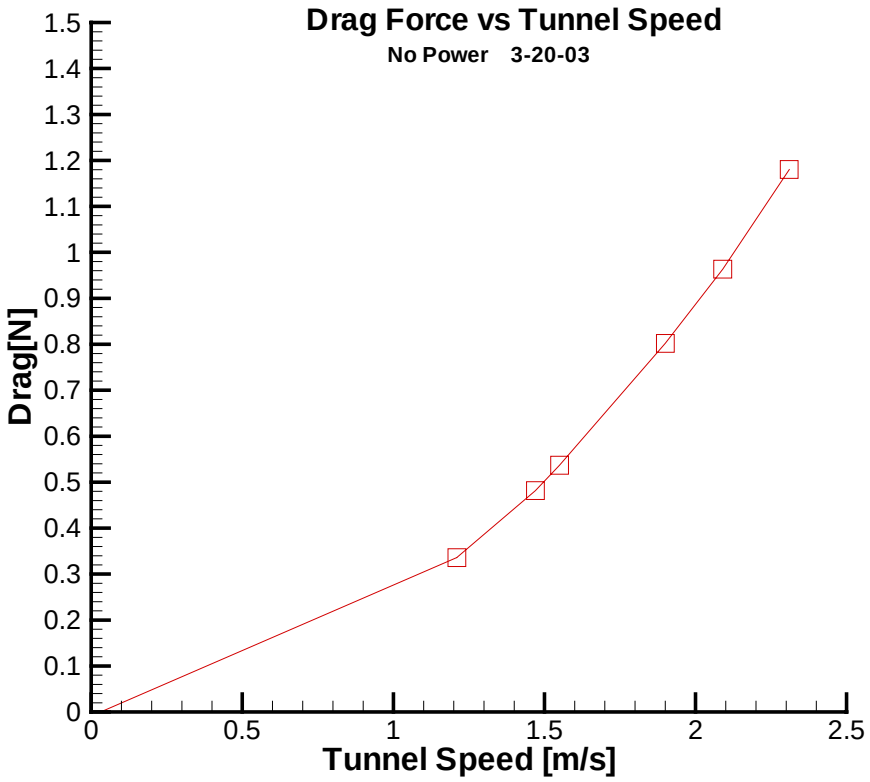

Figure 4.3.6 Plot of drag force vs Tunnel Speed

Since a greater amount of drag reduction was expected, verifications that the force measurement setup was working properly were conducted. One of the first verification tests was acquiring data to construct a drag force vs tunnel speed plot such as the ones performed in the summer of 2002. Figure 4.3.6 shows a plot of this data, and the trend follows the expected drag increase as a function of tunnel velocity squared. In comparison to the drag vs speed plots from summer of 2002, both plots agree but there are slight differences outside the error bound of +/- 3.317%. From the same data acquired, drag coefficients were calculated and plotted as a function of tunnel speed.

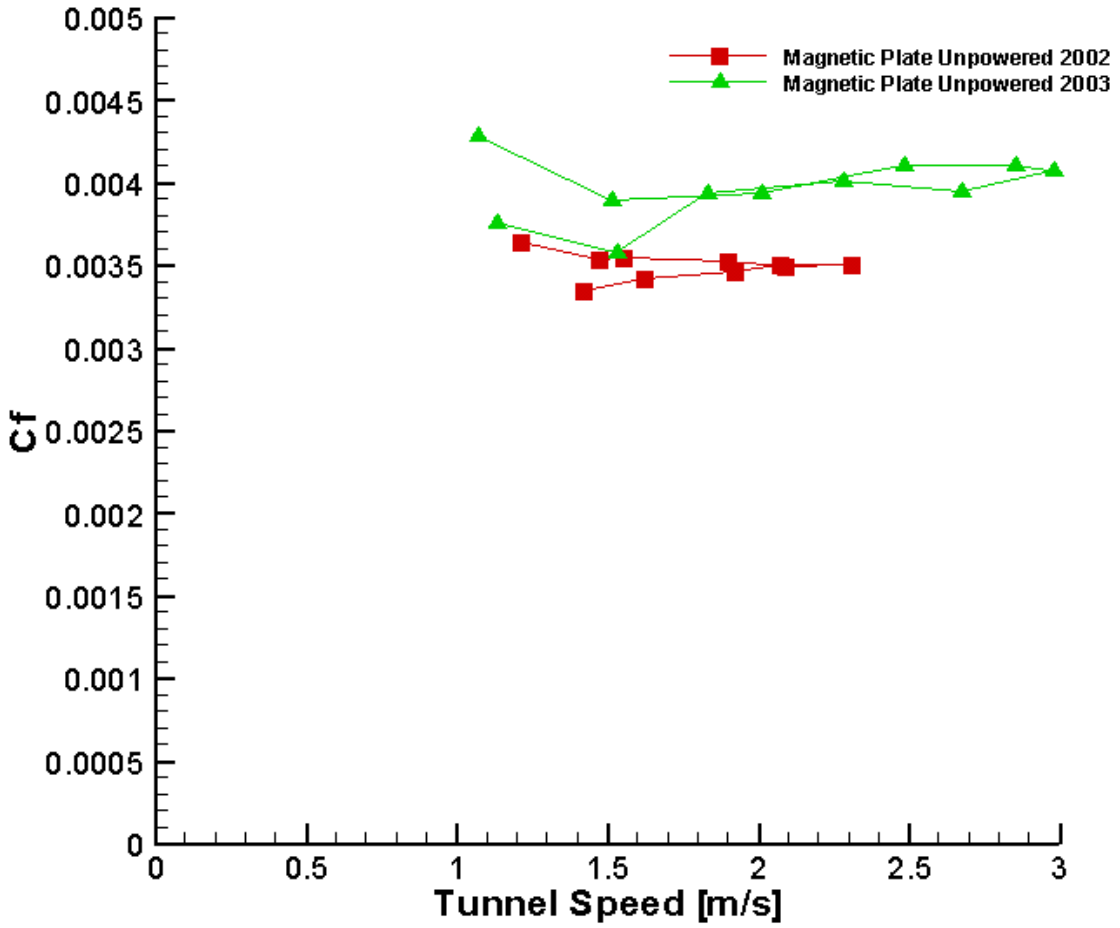

Figure 4.3.7 Plot of Drag Coefficient vs Tunnel Speed for electromagnetic plate

Figure 4.3.7 shows the drag coefficient for the electromagnetic plate as a function of speed. Note the variation in Cf at 1.5 m/s is about 5% of the total drag. The variation in drag at lower speeds is due to the decreasing resolution of the drag measurement, since drag force goes as the square of the velocity. When the data was acquired, the tunnel speed was varied up to 4m/s and then back down again to a lower speed, hence there is more than one data point for Cf at some tunnel speeds. Notice there are slight differences in the drag coefficient for 2002 and 2003 and is likely due to the small bolt in the center of the electrode board used in the 2003 measurements to keep the board from bowing. This data verified that the small percentage of global drag reduction was not due to any problems in the measurement setup. We then proceeded to performing a force time trace analysis to determine if the electromagnetic forcing had any effect in the fluid.

4.3.3 Force time trace data

Force time trace data was taken for a variety of operating points at different frequencies, amplitudes of current, and tunnel speeds. At some of the operating points, the effects due to electromagnetic activation were certainly visible. Figure 4.3.7 shows the time trace and subsequent spectrum of the drag and side forces as well as the current. In this case, the free-stream tunnel velocity is 0m/s and the board is driven at 100 Hz, and the drag shows little effect due to electromagnetic forcing. There is some 60 Hz noise getting into the drag signal. The side force spectrum shows significant content at 100Hz indicating that electromagnetic force is being input into the fluid. The content at lower frequencies in both drag and side force are due to resonances in the dynamometer and is not indicative of any electromagnetic related effects.

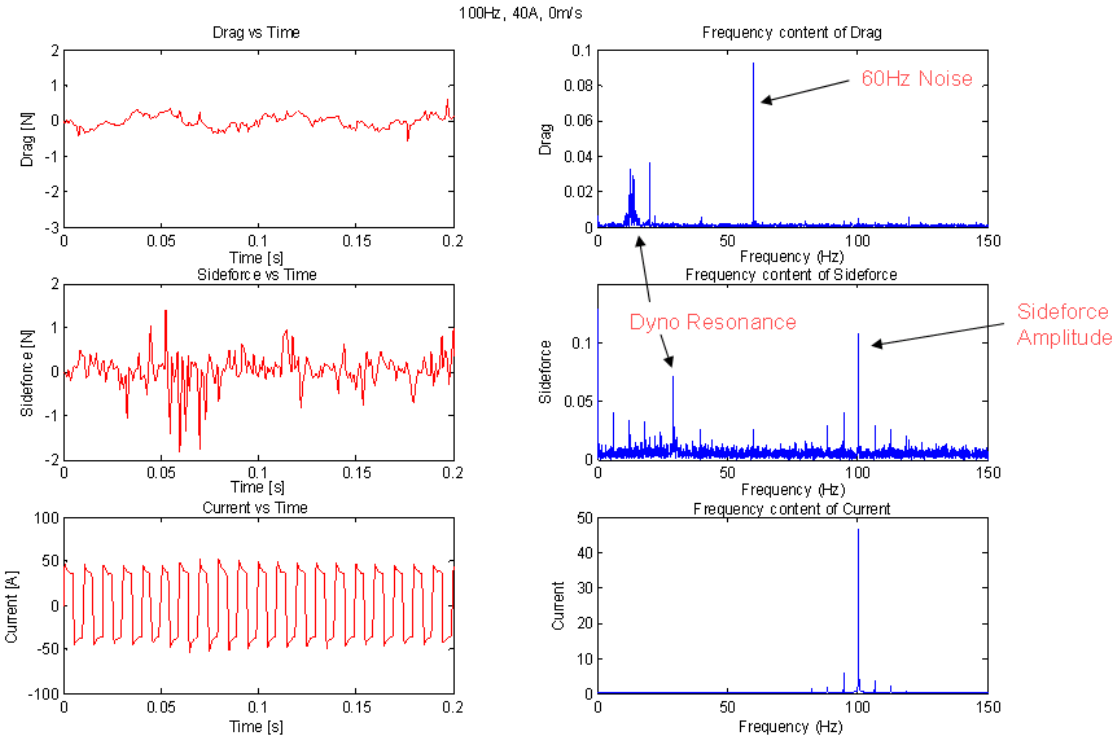

Figure 4.3.7 Time trace data and spectra for drag, lift and current

For drag, the plots show that the dynamometer resonance is at about 15 Hz, and for side force, 28 Hz. In other plots of frequency spectra for side force, for currents of 40

amps and frequencies of 100 Hz, but different tunnel speeds greater than zero, the frequency content almost disappears at 100 Hz. This may be due to a mechanical interference at flow speeds greater than 1 m/s, where forcing from the fluid on the floating cassette is masking the electromagnetic forcing effects. It is not ideal for the frequencies of the responses from electromagnetic forcing to be greater than the dynamometer resonances for drag and lift. For the case of 3 m/s, the magnitude of the side force at 100Hz drops to about 0.075 N from the 0.15 N at the 0 m/s case. These plots can be found in the appendix section. Plots which show the response at no power were performed on the electromagnetic cassette with the power supply turned off. The time traces of current for the no power condition at different flow speeds show some signal getting in, but this is likely due to signal noise or occasionally induced currents which have magnitudes of less than an amp.

The 28 Hz resonance is present even in the time traces with no power, thus validating that this resonance is not related to electromagnetic forcing. The data shows that the frequency of side force is always a multiple of 28Hz, for instance at 100 Hz, 20 Amps, and 1.5 m/s, there are side force responses at 28Hz and at 56Hz. The frequency spectrum plots for side force have shown that Lorentz forcing is indeed having an effect in the fluid at 0 m/s, however for the greater than 0 m/s flow speeds, more research is needed to determine the cause and effects of the mechanical interference, and whether or not it is associated with such a low global drag reduction measured in the force measurement experiment.

5.0 Conclusions

Experimental work in the fall and spring of 2002-2003 has shown that Lorentz force activation does indeed affect the fluid on a local scale. From LDV measurements which were first acquired by Jaskolski in the spring of 2002, and later validated in the spring of 2003, we can infer that the local drag reduction primarily in between electrodes on the electrode board was indeed on the order of 30%, a drag reduction amount predicted by numerical simulations. However, the results from the direct force measurements for drag with a dynamometer and load cell setup have shown that drag change for a variety of frequencies and amplitudes of currents have only been on the order of a few percent taking into consideration that the measurement repeatability was on the order of 3.3%. This is far less reduction than expected for global drag and the results force us to consider some of the issues that may have been a factor. Some of these are listed as follows:

- **Conductivity:** The conductivity of the water in the experimental work was half of sea water. Since force is proportional to current, a direct impact on force is not expected, but conductivity may effect ionization, hydrogen formation, iode heating, and other electrochemical effects. These are expected to be minor effects.
- **Magnetic Flux:** The magnetic flux at the surface of the electrode board is much less, on the order of 0.15 Tesla. Decreasing the electrode board thickness would increase the amount of flux present at the surface of the electrode board exposed to the flow of water.
- **Center bolt in electrode board:** This bolt produces locally unwanted drag and turbulence but is needed to keep the board flat and from bowing at the center. A better, less intrusive method to hold the board center down would be some type of adhesive applied to the bottom surface.
- **Dynamometer resonance:** An unsteady force measurement system whose resonances are much higher than the drive signal is desirable. Currently, the resonance response is large compared to the measured forces. The dynamometer resonances may also cause mechanical interferences with the electromagnetic forcing.

- **Base plate turbulence stimulation:** Current plate setup has no trips to stimulate turbulence, thus the transition point could be moving significantly. Installing trips on this setup would allow more control over turbulence location.
- **Base plate flexing at higher speeds:** The delrin base plate is not secured at the leading edge. Some flexing may have occurred. A stiffer plate made of aluminum with fastening hardware for the leading edge would eliminate any flexing.
- **Salt vs sodium nitrite:** Electrochemical and ionization differences between salt and sodium nitrite are expected to cause minor if not negligible effects.
- **Square wave improvement:** The square wave setup produces less drag reduction as predicted by numerical simulations.

Another issue that needs to be investigated is whether local drag reduction in between the electrodes, and drag increase over the electrodes leads to a net drag change of zero for the entire electrode board. Consultation with Professor Karniadakis to discuss these issues will be made before any future work is performed on electromagnetic boundary layer control.

The numerical simulations show that greater drag reduction is present with a traveling wave Lorentz force, as opposed to a Lorentz force that travels back and forth in the crosswise flow direction. This would also require more complicated electronic driver circuitry to create a current wave that travels along the entire electrode board. Hydro Technologies is currently developing new driver electronics for an experiment with General Atomics Corp which will be conducted in the water tunnel of the Marine Hydrodynamics Laboratory in June of 2003. The design of the hardware for this experiment is currently in progress and involves designing a base plate made of aluminum, as well as a magnetic filled cassette also made of aluminum that is twice as long but with the same width as the delrin cassette used in the force measurements in March of 2003. Flexing of the base plate will be eliminated since the aluminum plate will be much stiffer and new mounting hardware for setup in the water tunnel is currently being designed. The electrode board will also have twice the length and will be much thinner and will allow for a traveling wave that can travel twice the distance. The

magnetic flux at the surface of the electrode board is expected to be higher since the thickness of the new electrode board will be reduced significantly.

Our goals at the Marine Hydrodynamic Laboratory, after having conducted the traveling wave Lorentz force experiment in June are reliable measurements of drag reduction as well as a better understanding of why experimental work showed local drag reduction over the electrode board as predicted by numerical simulations, but global drag reduction much less than expected. We also hope to identify the possible mechanical interferences in the dynamometer setup and repeat force time traces once the issues have been resolved. In the experimental quest for observing a much greater global drag reduction from Lorentz force activation, we hope to find results that will contribute to drag reduction efforts that have been carried out for several years in the hydrodynamics field.

References

[1]. Y. Du, V. Symeonidis and G.E. Karniadakis, “Drag reduction in wall-bounded turbulence via a transverse traveling wave”, J. Fluid Mech., Vol. 457, pp.1-34.

[2]. Jaskolski, Corey, “Experimental Implementation of Lorentz Force Actuators for Hydrodynamic Drag”, (Master’s Thesis, Massachusetts Institute of Technology, May 2002).

[3] UNESCO International Equation of State (IES 80) as described in Fofonoff, JGR, Vol 90 No. C2, pp 3332-3342, March 20, 1985.

6.0 Appendix

6.1 Force Time Trace Series

Case 1: 0 m/s

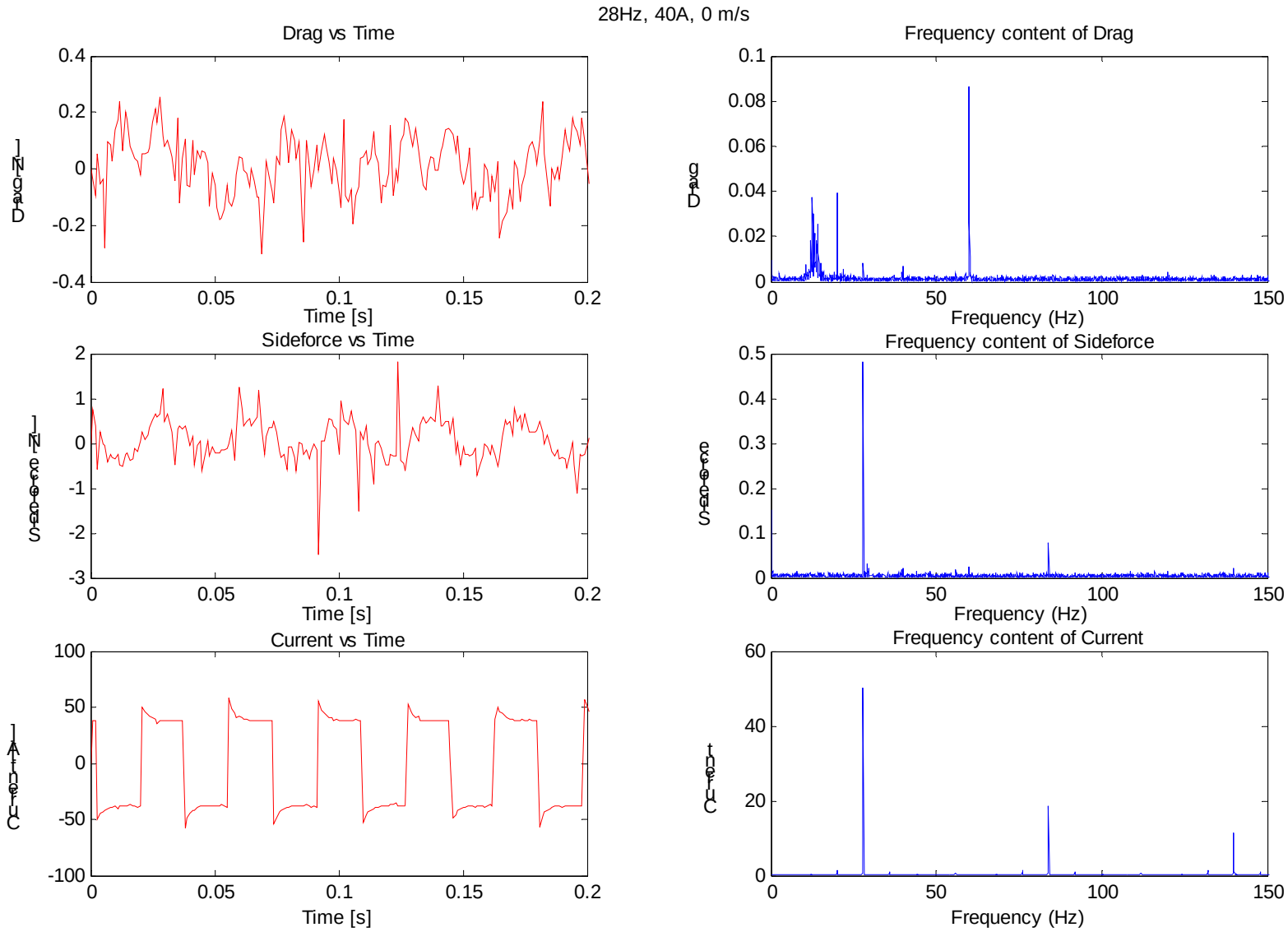
28Hz, 40A, 0 m/s
Drag vs Time
Drag [N]
Time [s]
Frequency content of Drag
Drag
Frequency (Hz)
Sideforce vs Time
Sideforce [N]
Time [s]
Frequency content of Sideforce
Sideforce
Frequency (Hz)
Current vs Time
Current [A]
Time [s]
Frequency content of Current
Current
Frequency (Hz)

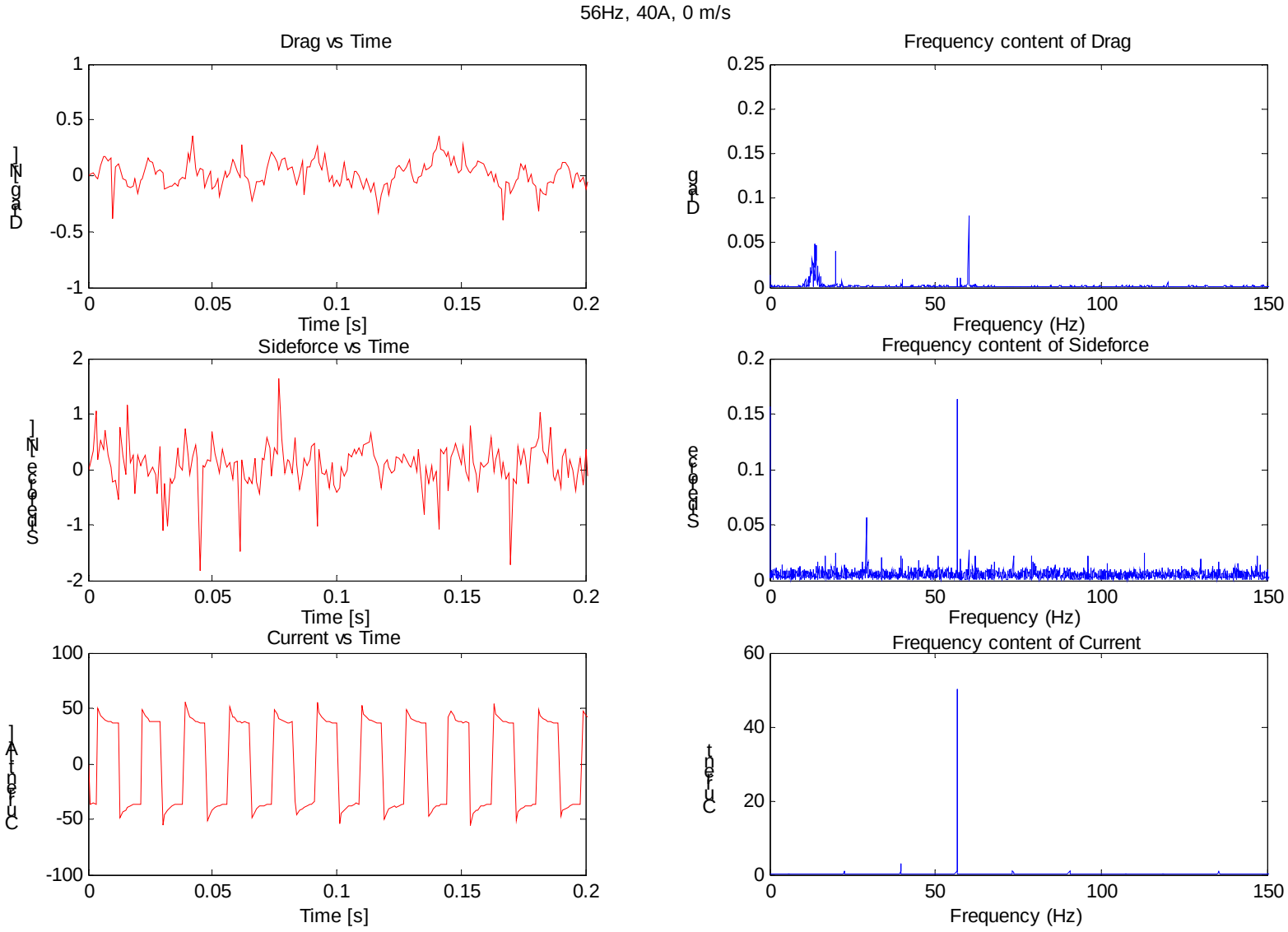
56Hz, 40A, 0 m/s
Drag vs Time
Drag [N]
Time [s]
Frequency content of Drag
Drag
Frequency (Hz)
Sideforce vs Time
Sideforce [N]
Time [s]
Frequency content of Sideforce
Sideforce
Frequency (Hz)
Current vs Time
Current [A]
Time [s]
Frequency content of Current
Current
Frequency (Hz)

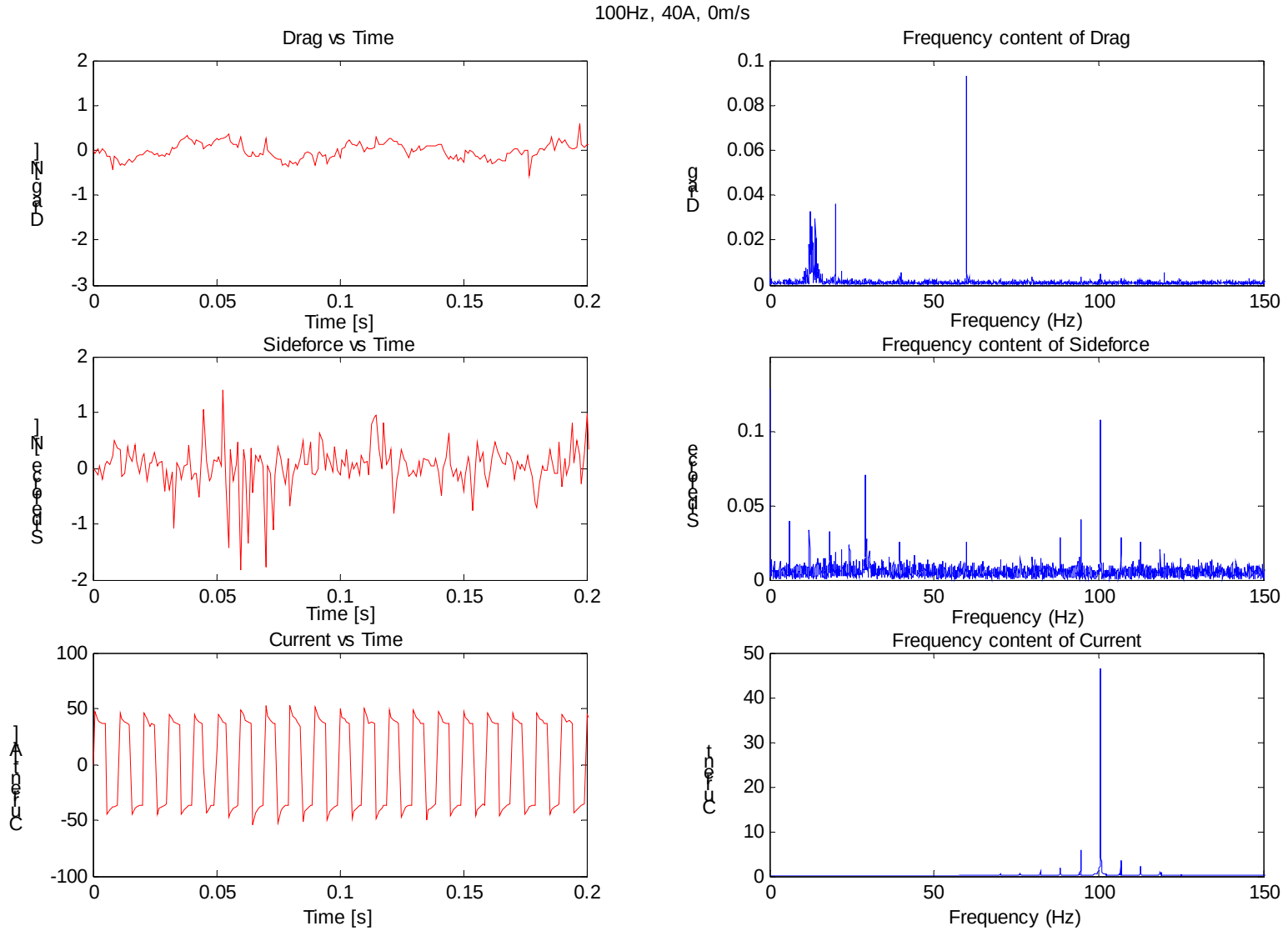
100Hz, 40A, 0m/s
Drag vs Time
Drag [N]
Time [s]
Frequency content of Drag
Drag
Frequency (Hz)
Sideforce vs Time
Sideforce [N]
Time [s]
Frequency content of Sideforce
Sideforce
Frequency (Hz)
Current vs Time
Current [A]
Time [s]
Frequency content of Current
Current
Frequency (Hz)

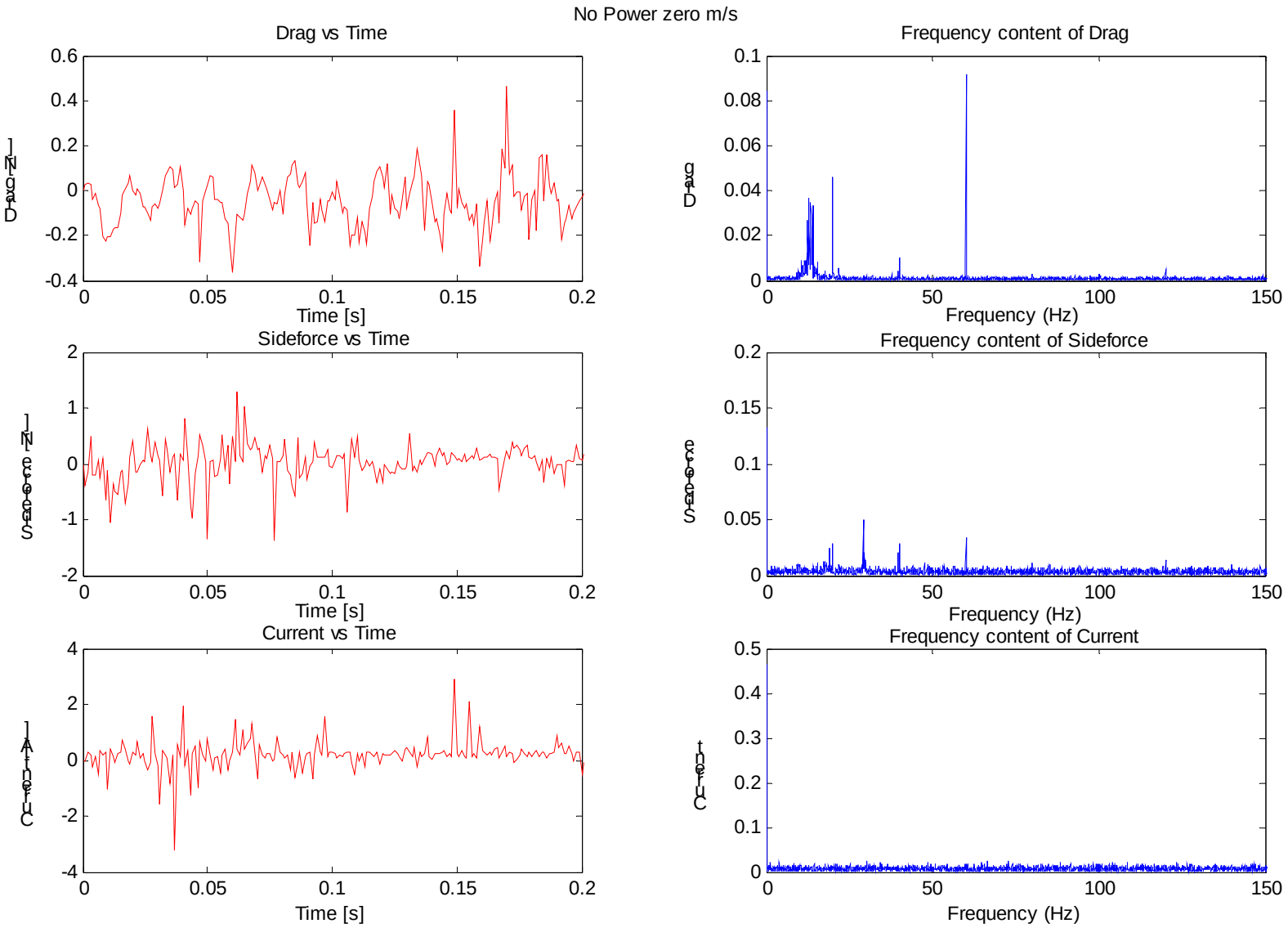
No Power zero m/s
Drag vs Time
Drag [N]
Time [s]
Frequency content of Drag
Drag
Frequency (Hz)
Sideforce vs Time
Sideforce [N]
Time [s]
Frequency content of Sideforce
Sideforce
Frequency (Hz)
Current vs Time
Current [A]
Time [s]
Frequency content of Current
Current
Frequency (Hz)

Case 2: 1.5 m/s

20hz, 1A, 1.5m/s

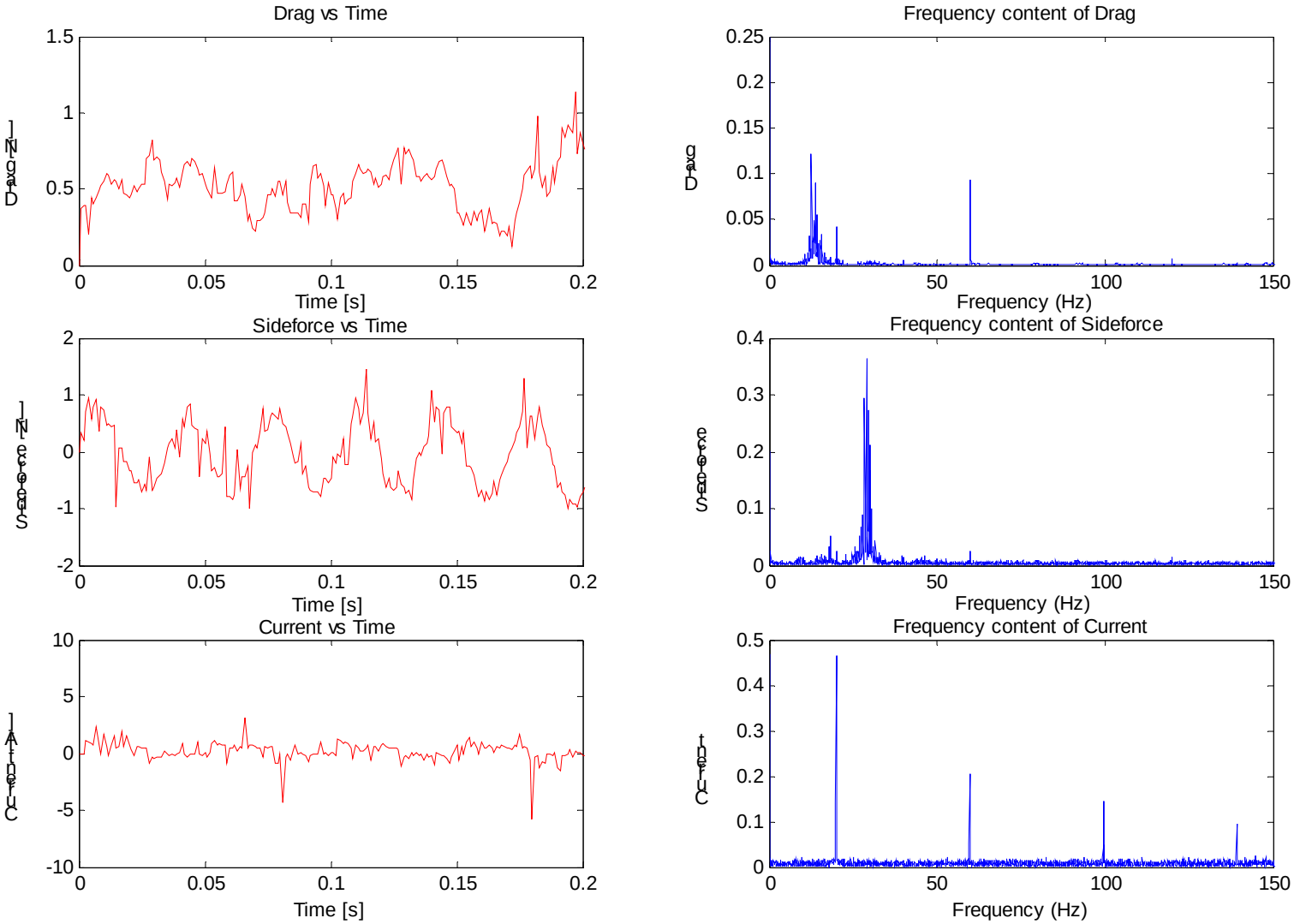
Drag vs Time
Drag [N]
Time [s]
Frequency content of Drag
Drag
Frequency (Hz)
Sideforce vs Time
Sideforce [N]
Time [s]
Frequency content of Sideforce
Sideforce
Frequency (Hz)
Current vs Time
Current [A]
Time [s]
Frequency content of Current
Current
Frequency (Hz)

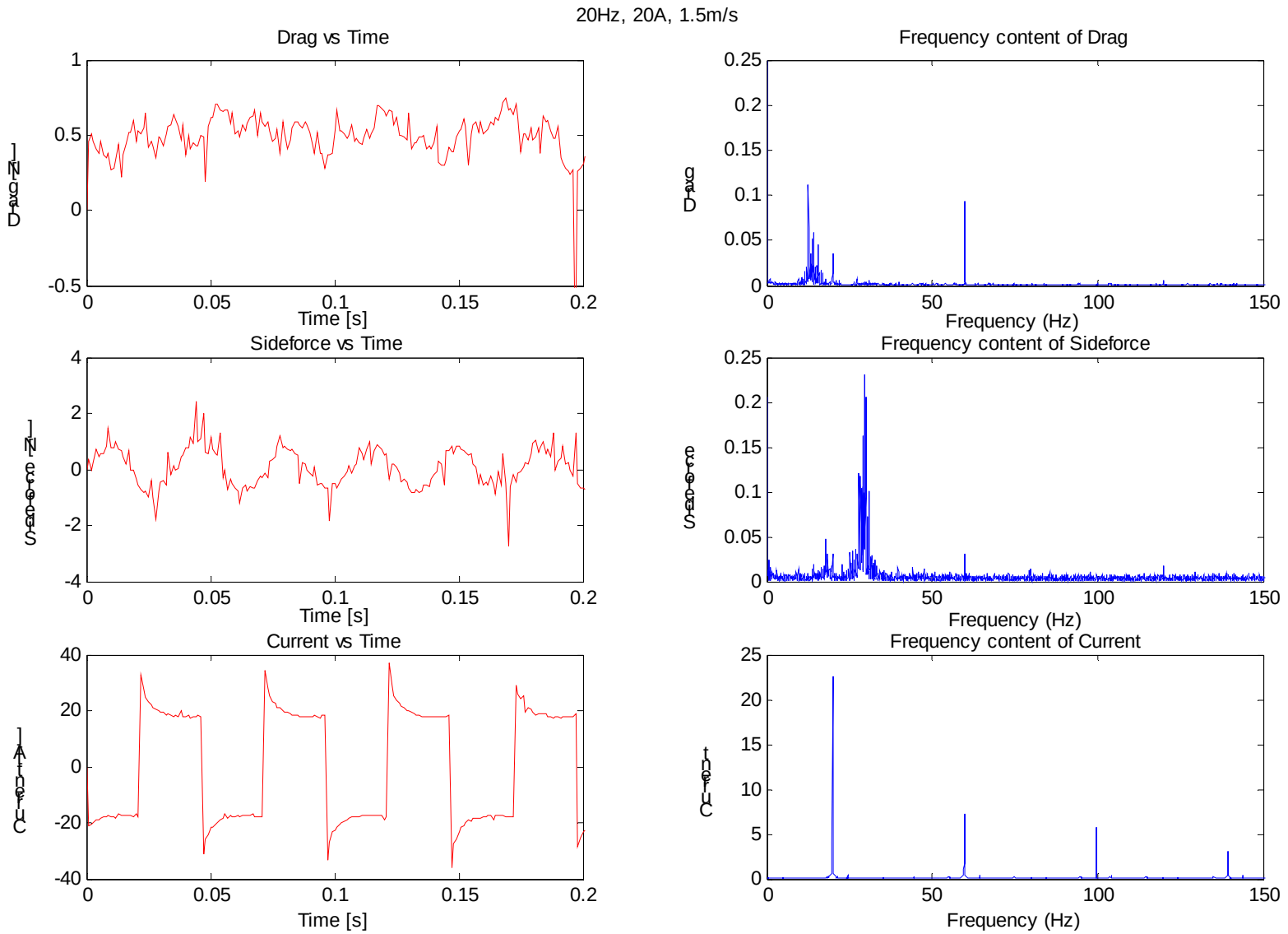
20Hz, 20A, 1.5m/s
Drag vs Time
Drag [N]
Time [s]
Frequency content of Drag
Drag
Frequency (Hz)
Sideforce vs Time
Sideforce [N]
Time [s]
Frequency content of Sideforce
Sideforce
Frequency (Hz)
Current vs Time
Current [A]
Time [s]
Frequency content of Current
Current
Frequency (Hz)

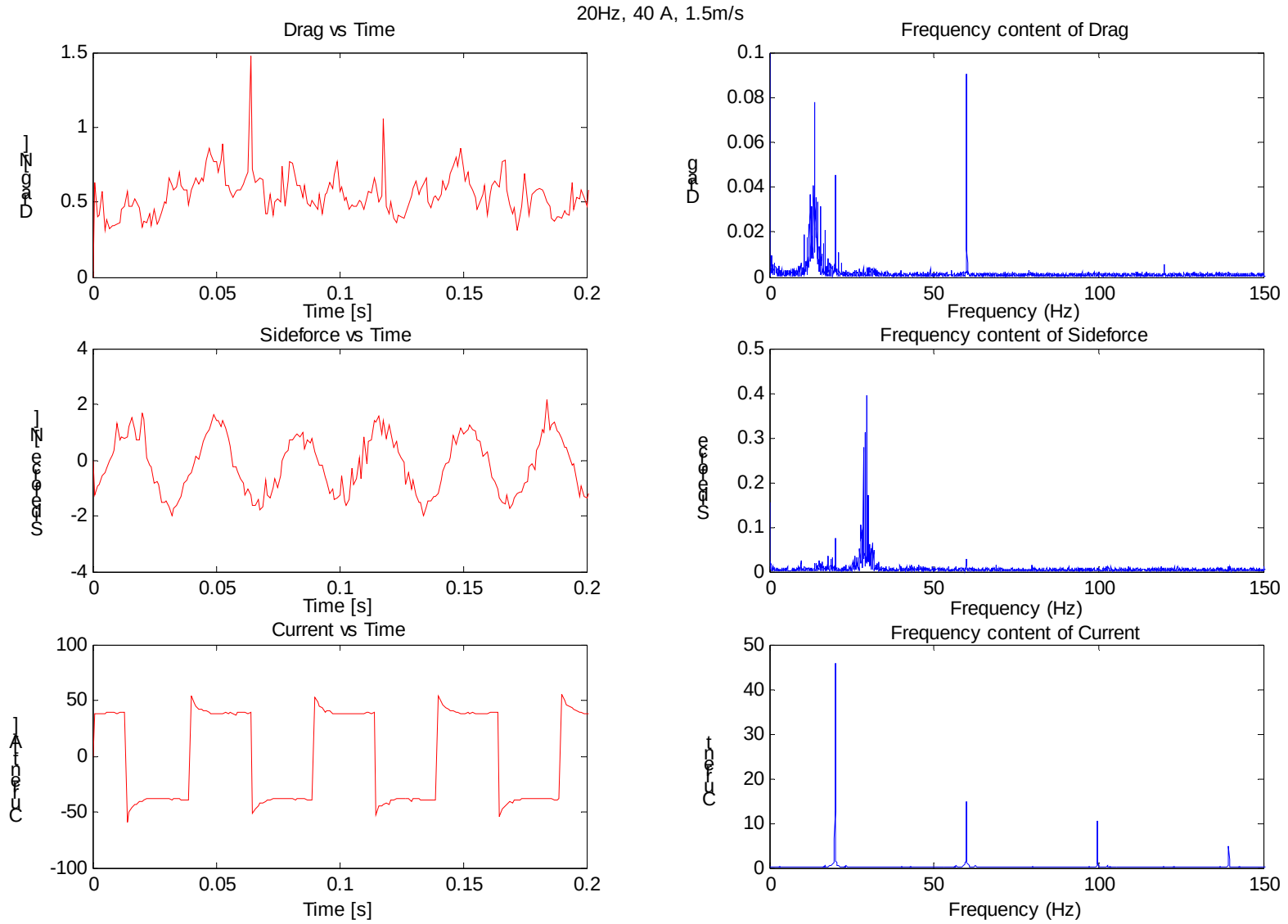
20Hz, 40 A, 1.5m/s
Drag vs Time
Drag [N]
Time [s]
Frequency content of Drag
Drag
Frequency (Hz)
Sideforce vs Time
Sideforce [N]
Time [s]
Frequency content of Sideforce
Sideforce
Frequency (Hz)
Current vs Time
Current [A]
Time [s]
Frequency content of Current
Current
Frequency (Hz)

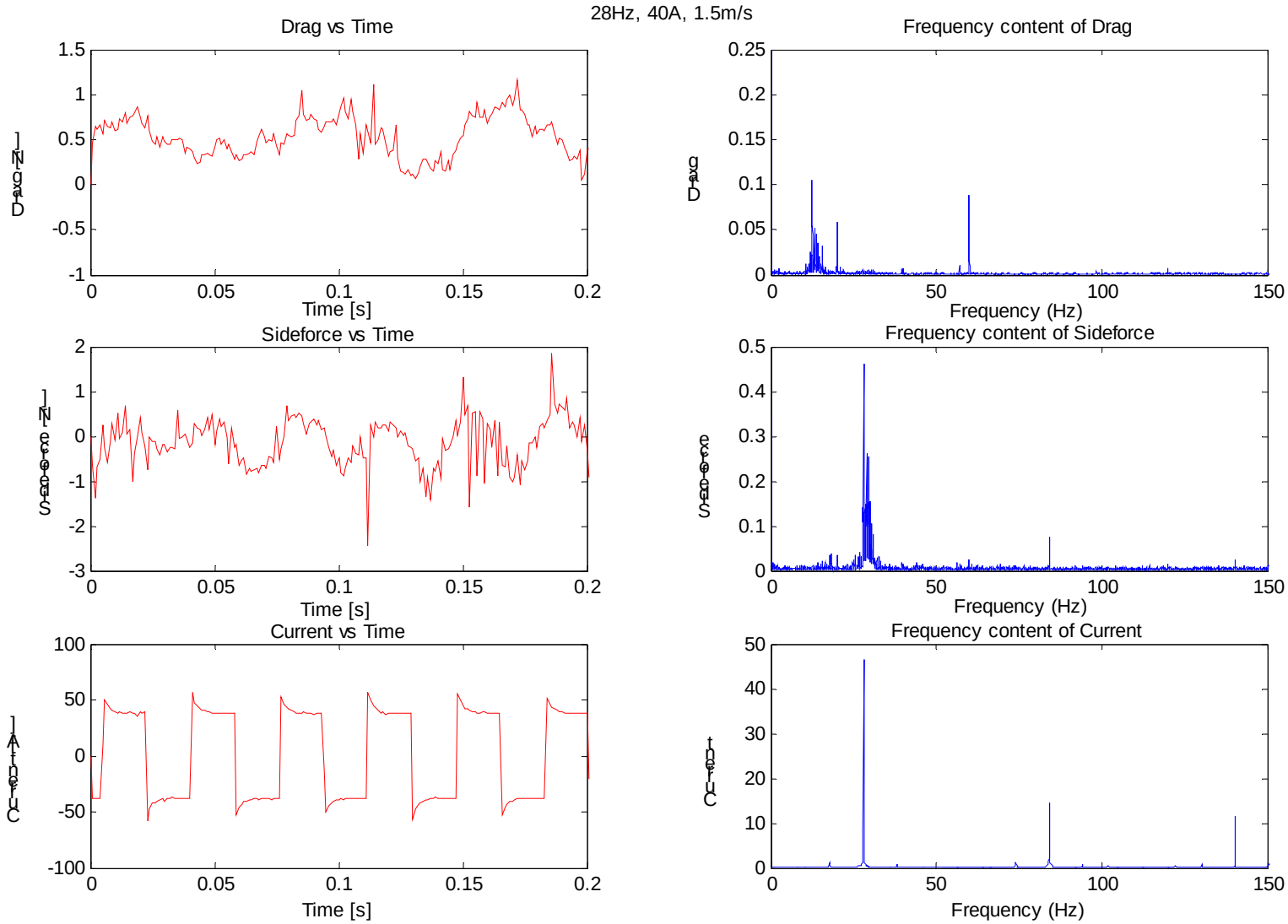
28Hz, 40A, 1.5m/s
Drag vs Time
Drag [N]
Time [s]
Frequency content of Drag
Drag
Frequency (Hz)
Sideforce vs Time
Sideforce [N]
Time [s]
Frequency content of Sideforce
Sideforce
Frequency (Hz)
Current vs Time
Current [A]
Time [s]
Frequency content of Current
Current
Frequency (Hz)

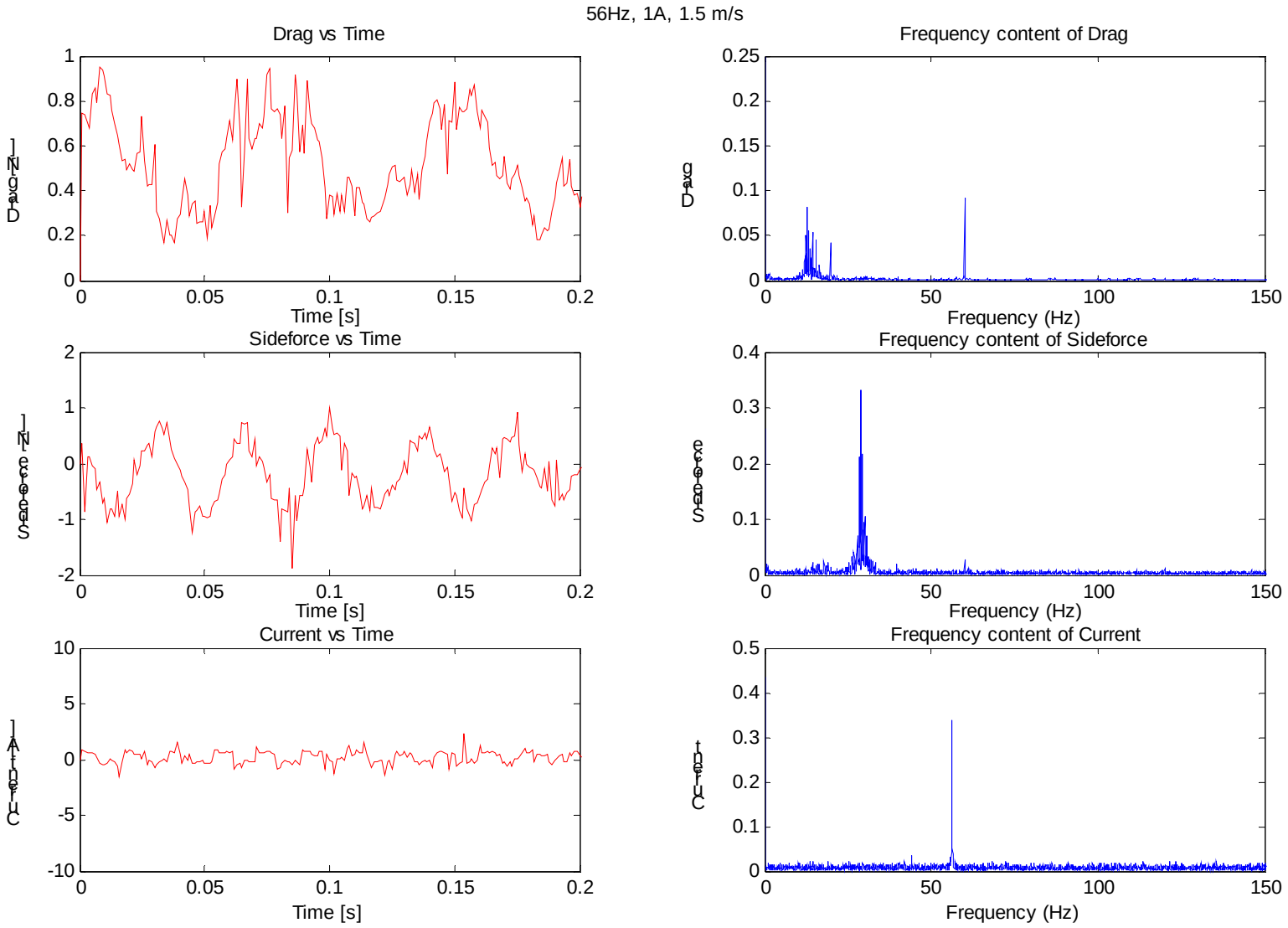
56Hz, 1A, 1.5 m/s
Drag vs Time
Time [s]
Frequency content of Drag
Frequency (Hz)
Sideforce vs Time
Time [s]
Frequency content of Sideforce
Frequency (Hz)
Current vs Time
Time [s]
Frequency content of Current
Frequency (Hz)

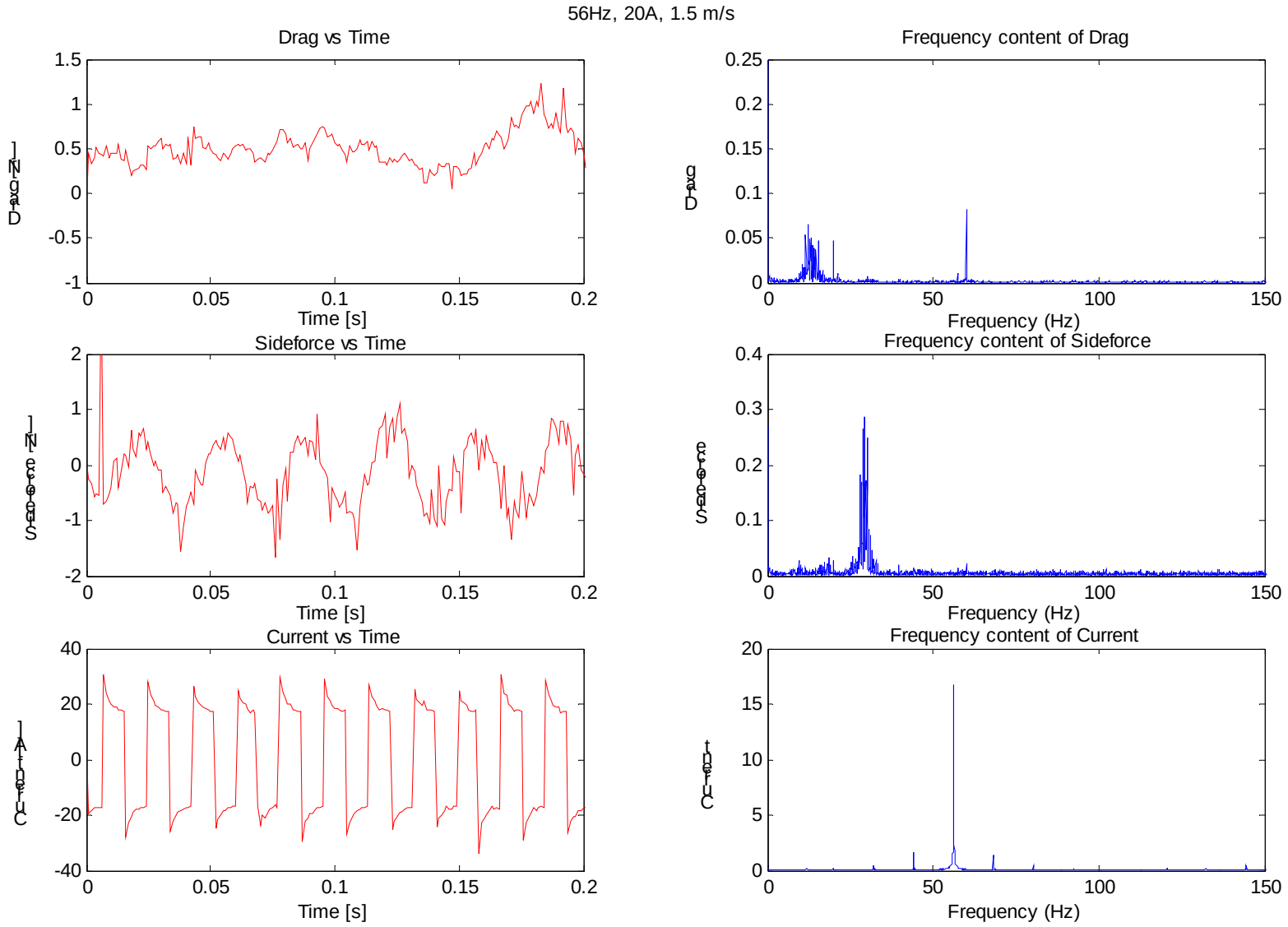
56Hz, 20A, 1.5 m/s
Drag vs Time
Drag [N]
Time [s]
Frequency content of Drag
Drag
Frequency (Hz)
Sideforce vs Time
Sideforce [N]
Time [s]
Frequency content of Sideforce
Sideforce
Frequency (Hz)
Current vs Time
Current [A]
Time [s]
Frequency content of Current
Current
Frequency (Hz)

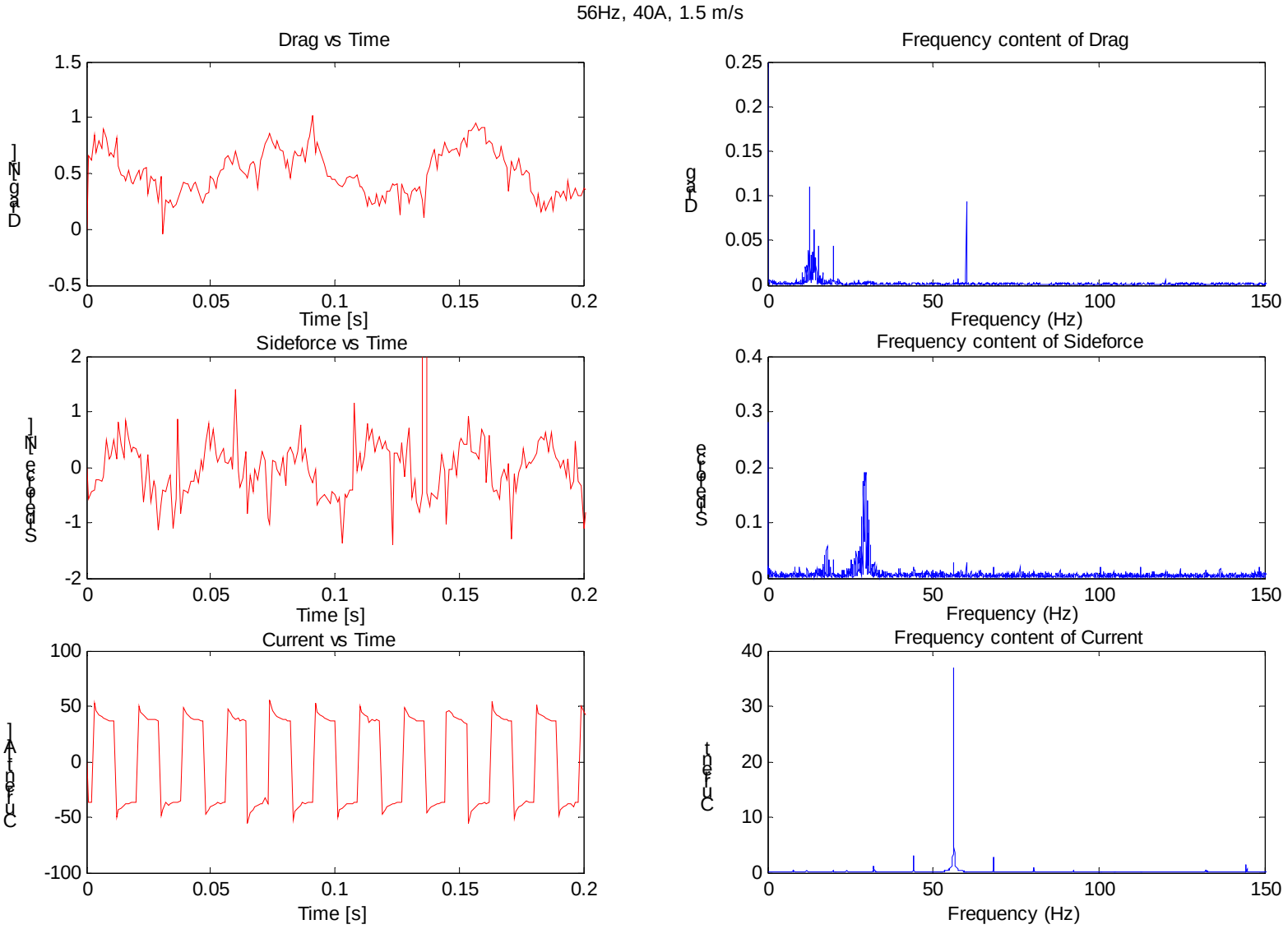
56Hz, 40A, 1.5 m/s
Drag vs Time
Drag [N]
Time [s]
Frequency content of Drag
Drag
Frequency (Hz)
Sideforce vs Time
Sideforce [N]
Time [s]
Frequency content of Sideforce
Sideforce
Frequency (Hz)
Current vs Time
Current [A]
Time [s]
Frequency content of Current
Current
Frequency (Hz)

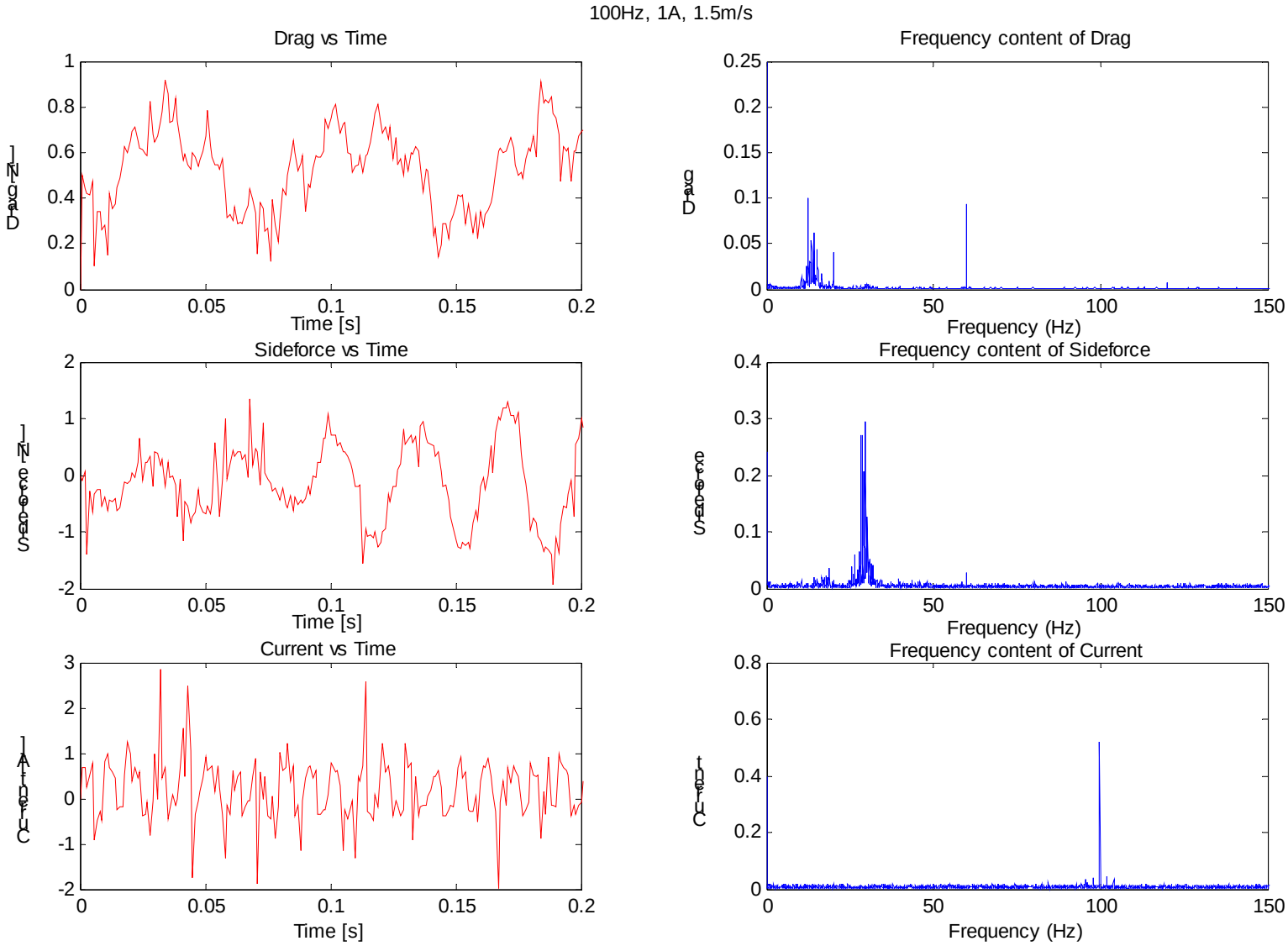
100Hz, 1A, 1.5m/s
Drag vs Time
Drag [N]
Time [s]
Frequency content of Drag
Drag
Frequency (Hz)
Sideforce vs Time
Sideforce [N]
Time [s]
Frequency content of Sideforce
Sideforce
Frequency (Hz)
Current vs Time
Current [A]
Time [s]
Frequency content of Current
Current
Frequency (Hz)

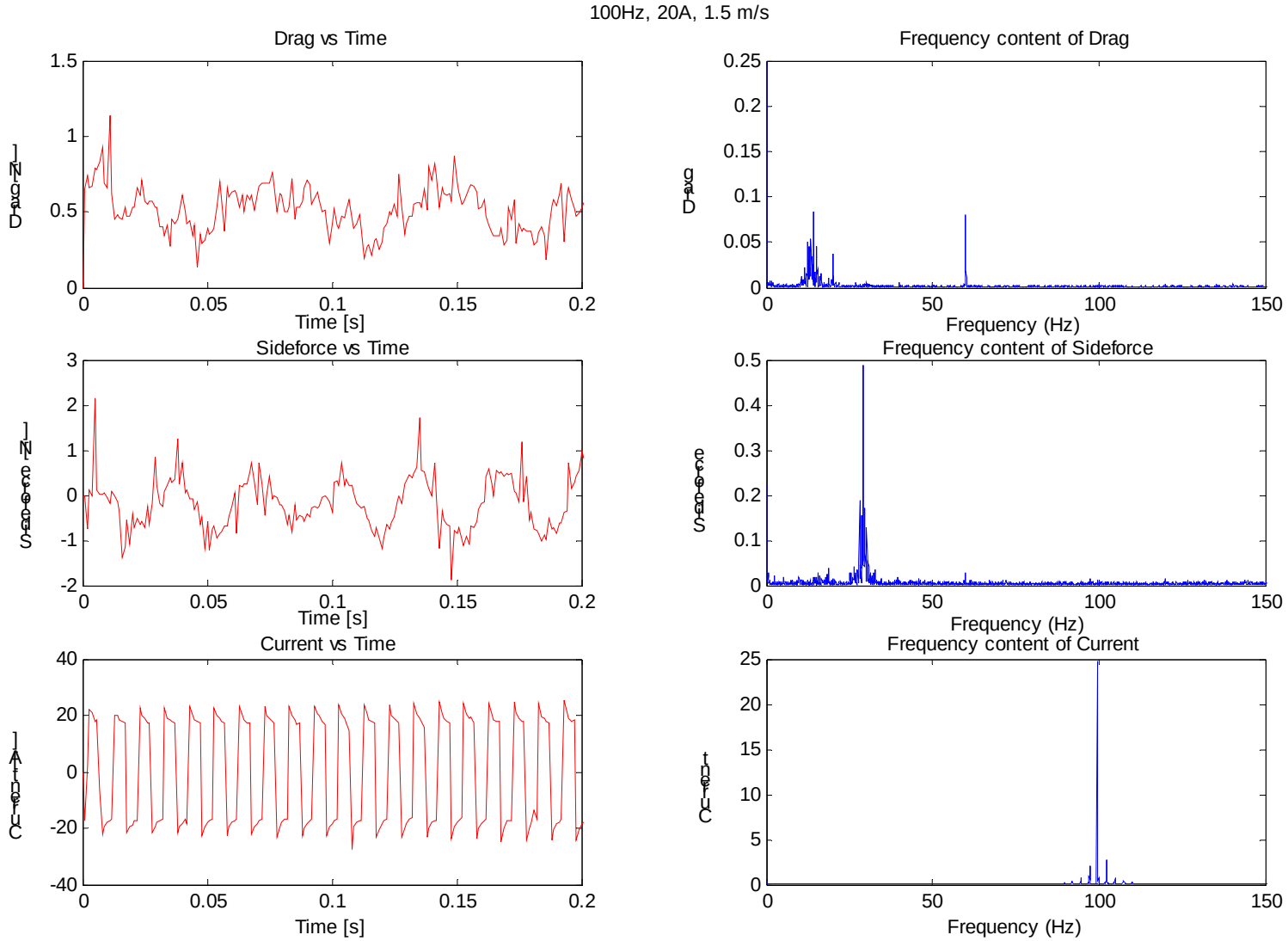
100Hz, 20A, 1.5 m/s
Drag vs Time
Drag [N]
Time [s]
Frequency content of Drag
Drag [N]
Frequency (Hz)
Sideforce vs Time
Sideforce [N]
Time [s]
Frequency content of Sideforce
Sideforce [N]
Frequency (Hz)
Current vs Time
Current [A]
Time [s]
Frequency content of Current
Current [A]
Frequency (Hz)

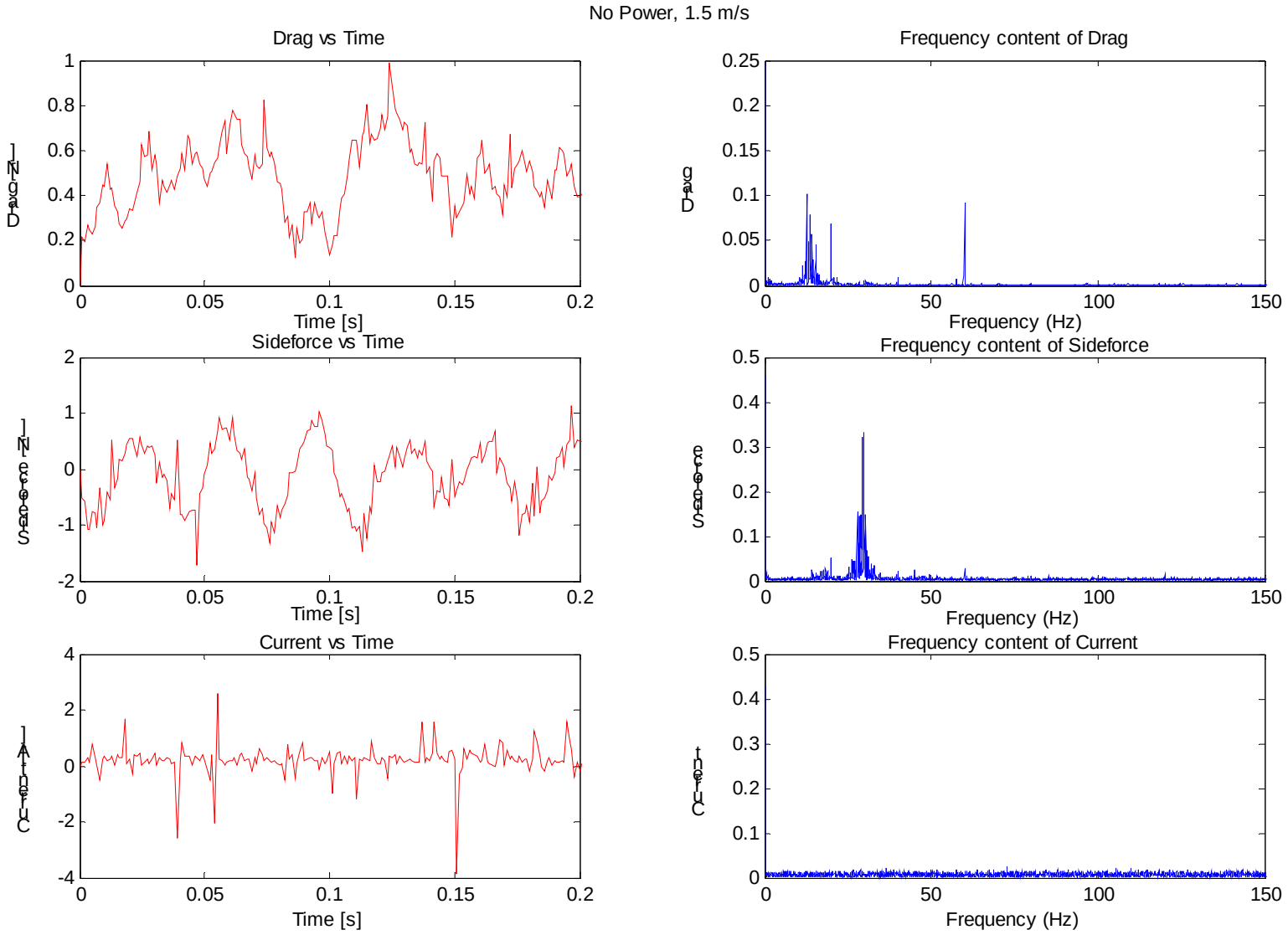
No Power, 1.5 m/s
Drag vs Time
Time [s]
Frequency content of Drag
Frequency (Hz)
Sideforce vs Time
Time [s]
Frequency content of Sideforce
Frequency (Hz)
Current vs Time
Time [s]
Frequency content of Current
Frequency (Hz)

Case 3: 3.0 m/s

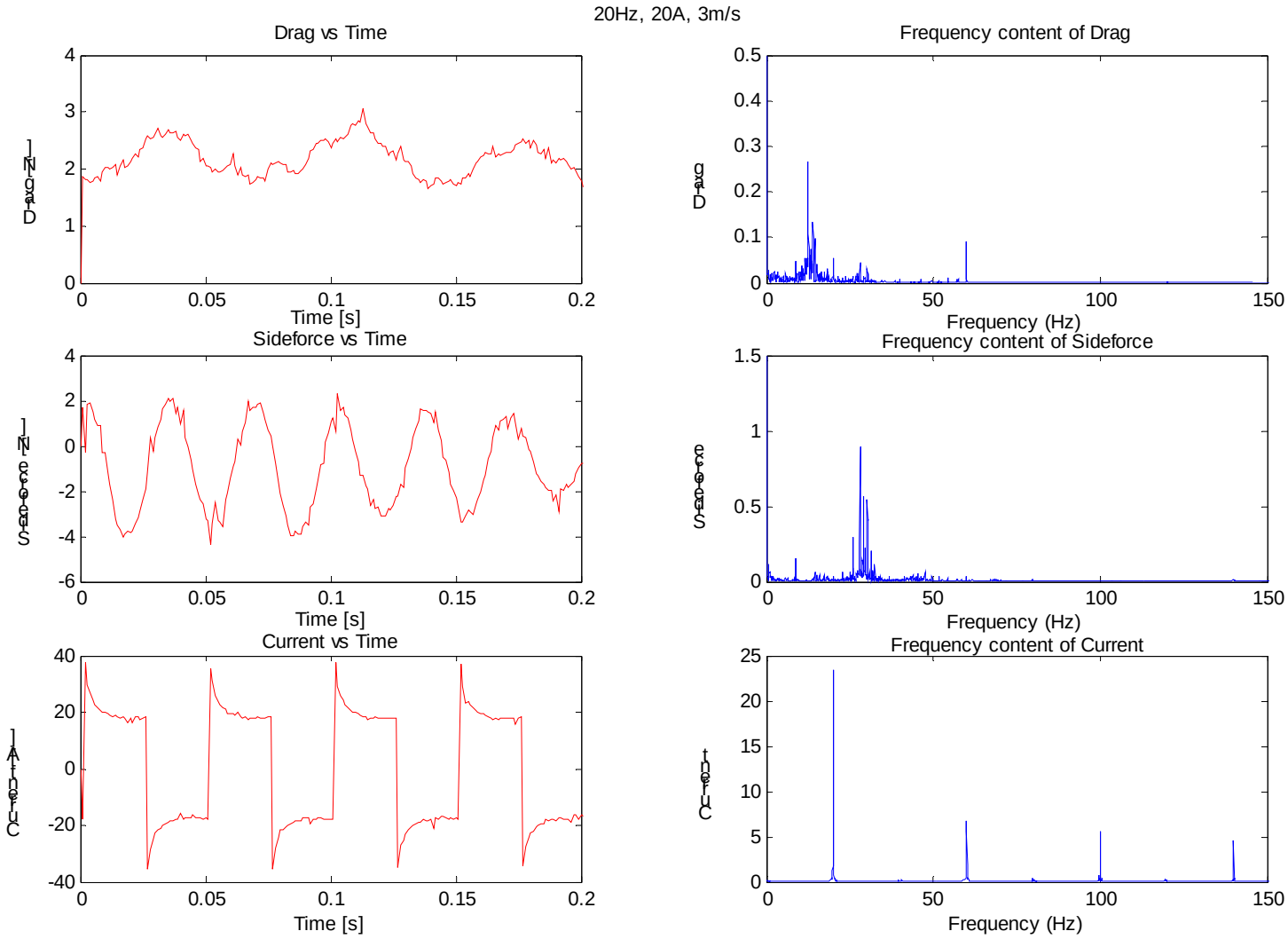
20Hz, 20A, 3m/s
Drag vs Time
Drag [N]
Time [s]
Frequency content of Drag
Drag
Frequency (Hz)
Sideforce vs Time
Sideforce [N]
Time [s]
Frequency content of Sideforce
Sideforce
Frequency (Hz)
Current vs Time
Current [A]
Time [s]
Frequency content of Current
Current
Frequency (Hz)

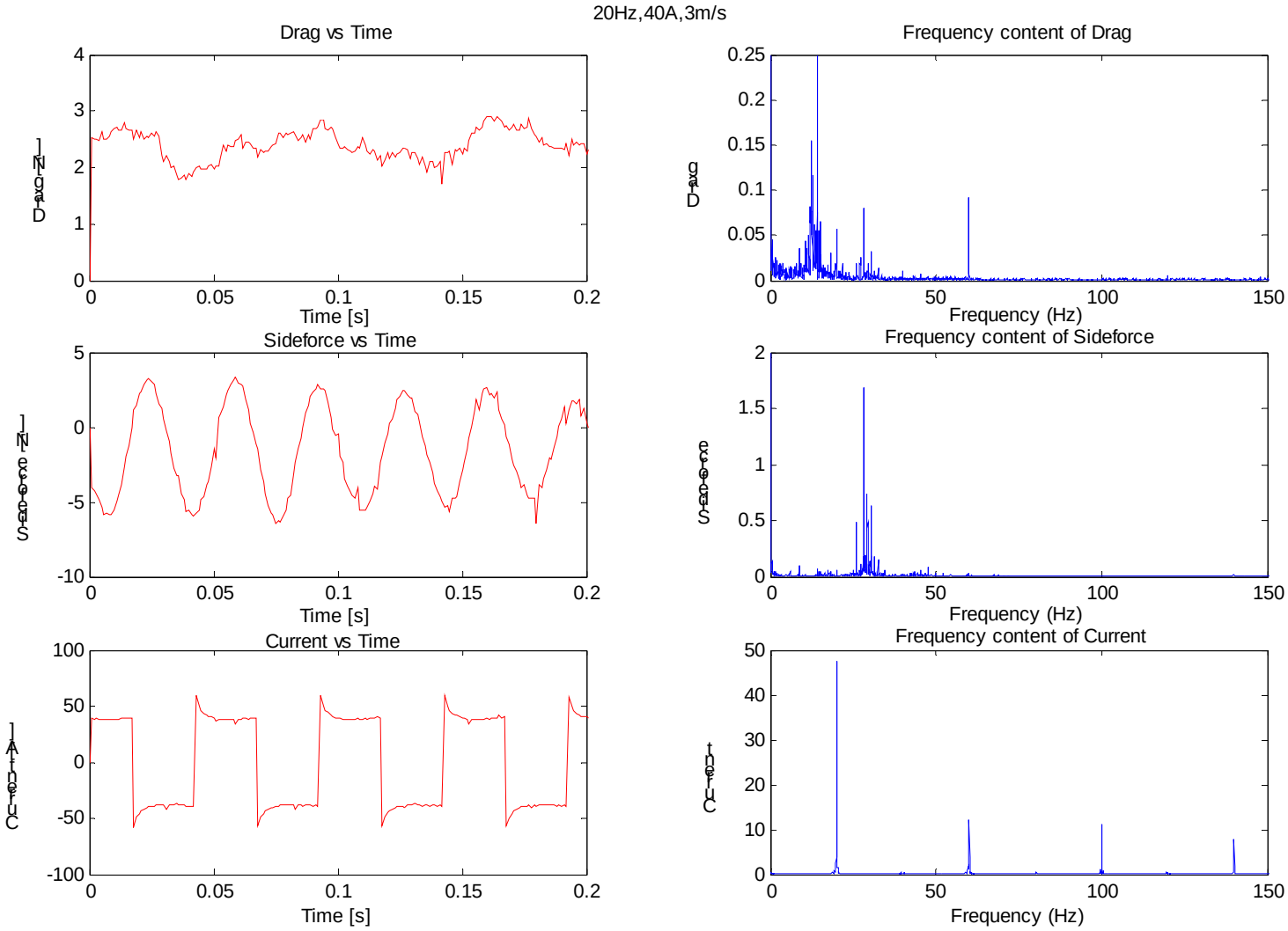
20Hz,40A,3m/s
Drag vs Time
Drag [N]
Time [s]
Frequency content of Drag
Drag
Frequency (Hz)
Sideforce vs Time
Sideforce [N]
Time [s]
Frequency content of Sideforce
Sideforce
Frequency (Hz)
Current vs Time
Current [A]
Time [s]
Frequency content of Current
Current
Frequency (Hz)

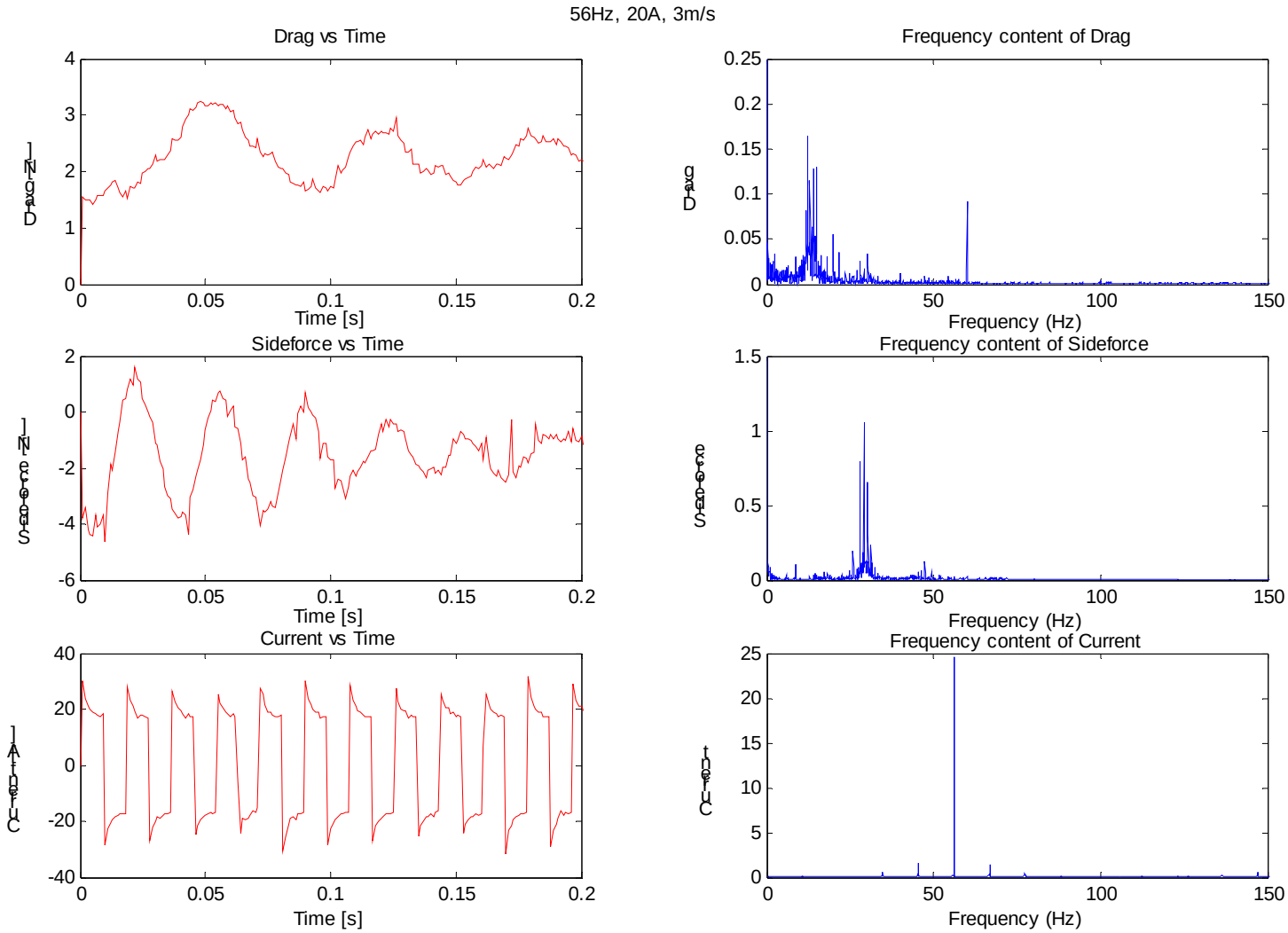
56Hz, 20A, 3m/s
Drag vs Time
Drag [N]
Time [s]
Frequency content of Drag
Drag
Frequency (Hz)
Sideforce vs Time
Sideforce [N]
Time [s]
Frequency content of Sideforce
Sideforce
Frequency (Hz)
Current vs Time
Current [A]
Time [s]
Frequency content of Current
Current
Frequency (Hz)

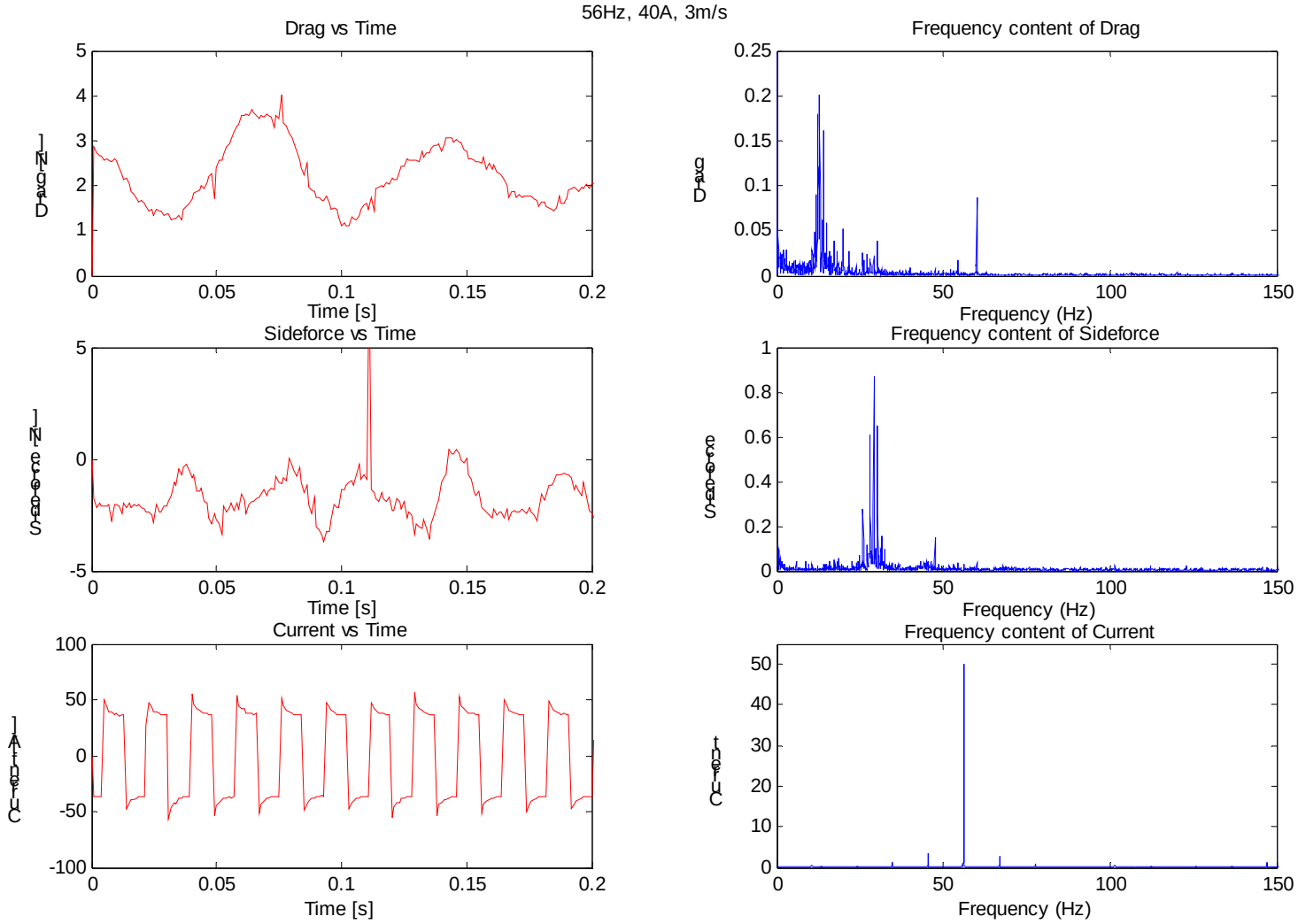
56Hz, 40A, 3m/s
Drag vs Time
Drag [N]
Time [s]
Frequency content of Drag
Drag
Frequency (Hz)
Sideforce vs Time
Sideforce [N]
Time [s]
Frequency content of Sideforce
Sideforce
Frequency (Hz)
Current vs Time
Current [A]
Time [s]
Frequency content of Current
Current
Frequency (Hz)

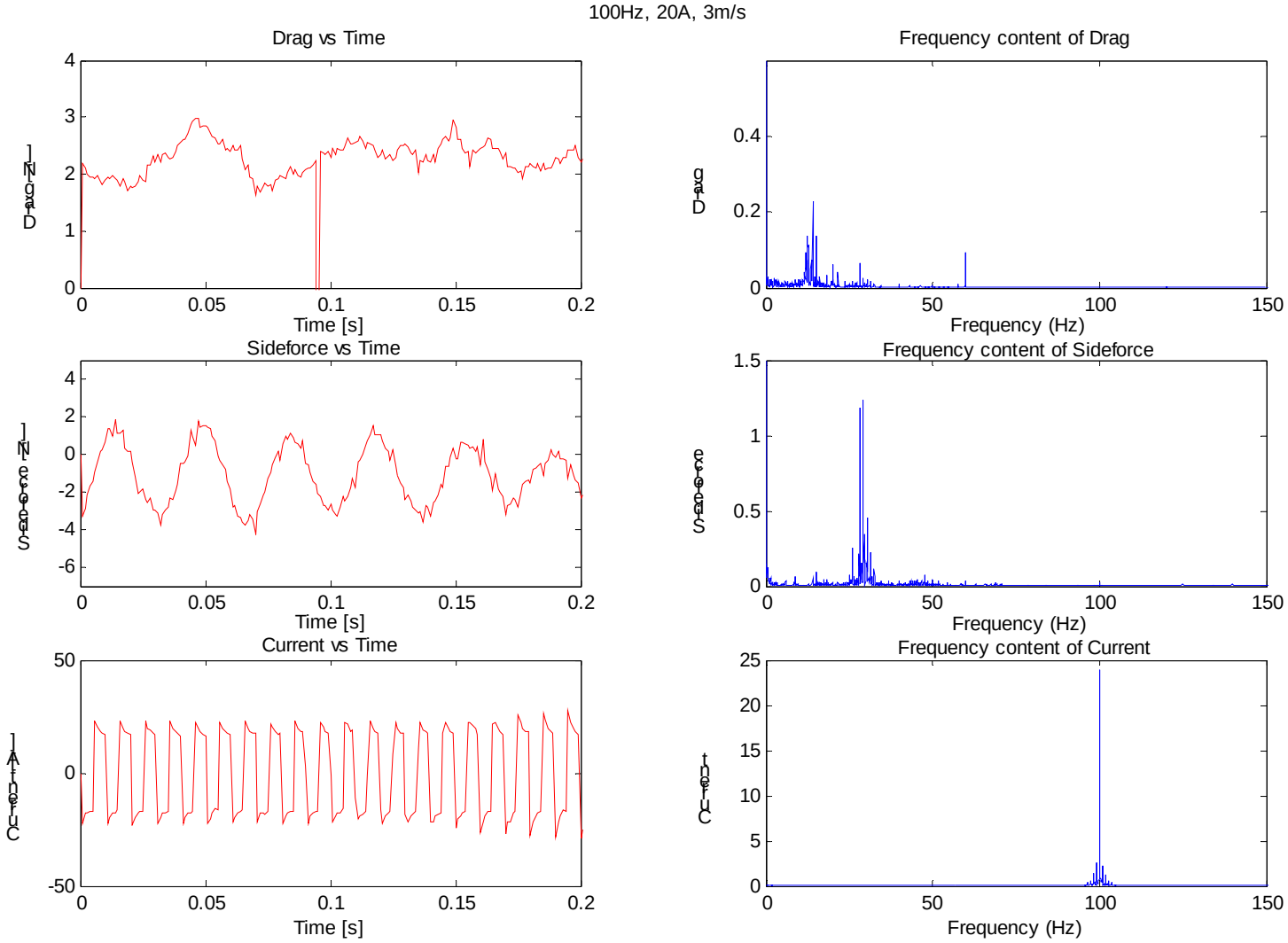
100Hz, 20A, 3m/s
Drag vs Time
Drag [N]
Time [s]
Frequency content of Drag
Frequency (Hz)
Sideforce vs Time
Sideforce [N]
Time [s]
Frequency content of Sideforce
Frequency (Hz)
Current vs Time
Current [A]
Time [s]
Frequency content of Current
Frequency (Hz)

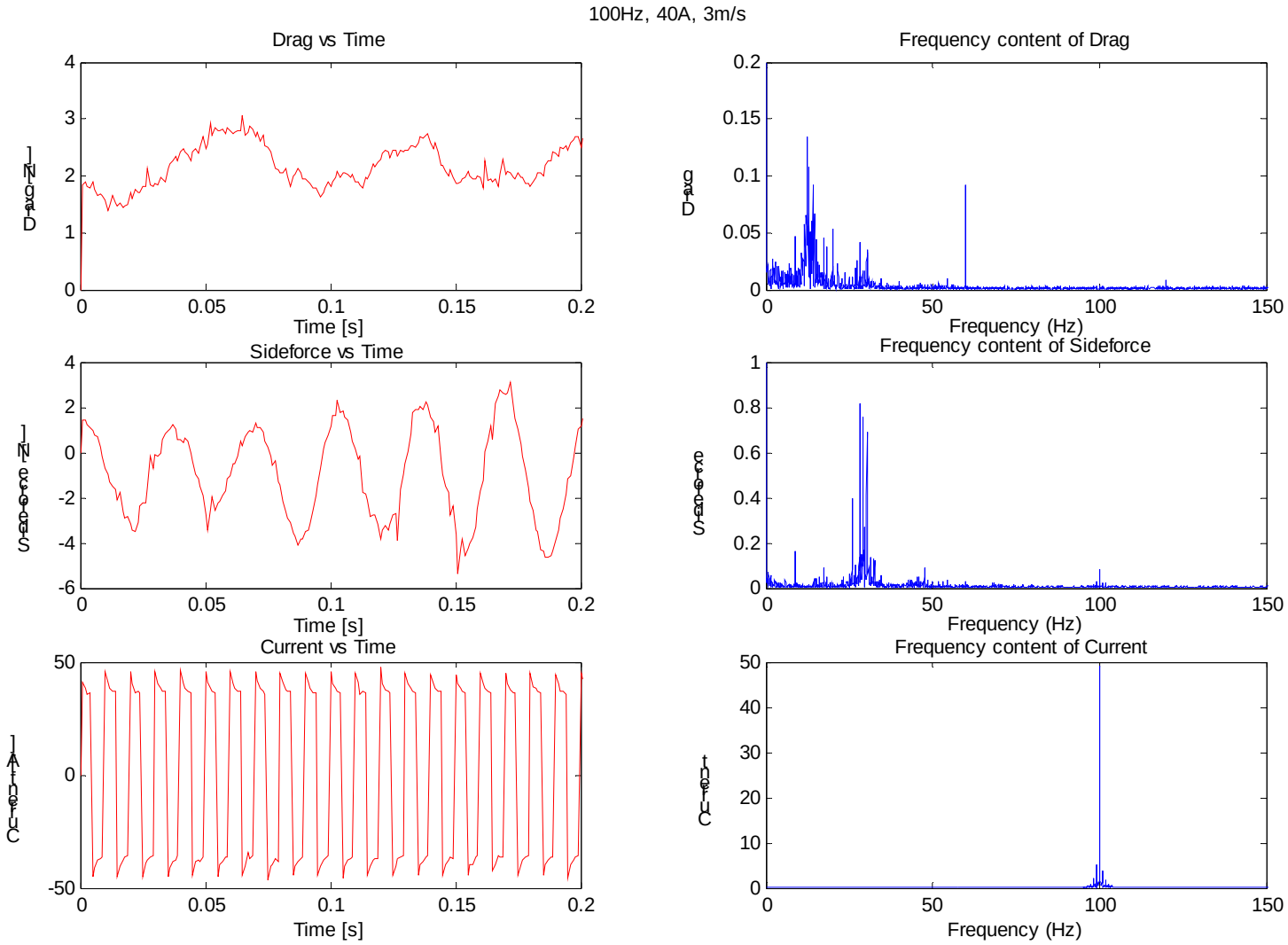
100Hz, 40A, 3m/s
Drag vs Time
Drag [N]
Time [s]
Frequency content of Drag
Drag
Frequency (Hz)
Sideforce vs Time
Sideforce [N]
Time [s]
Frequency content of Sideforce
Sideforce
Frequency (Hz)
Current vs Time
Current [A]
Time [s]
Frequency content of Current
Current
Frequency (Hz)

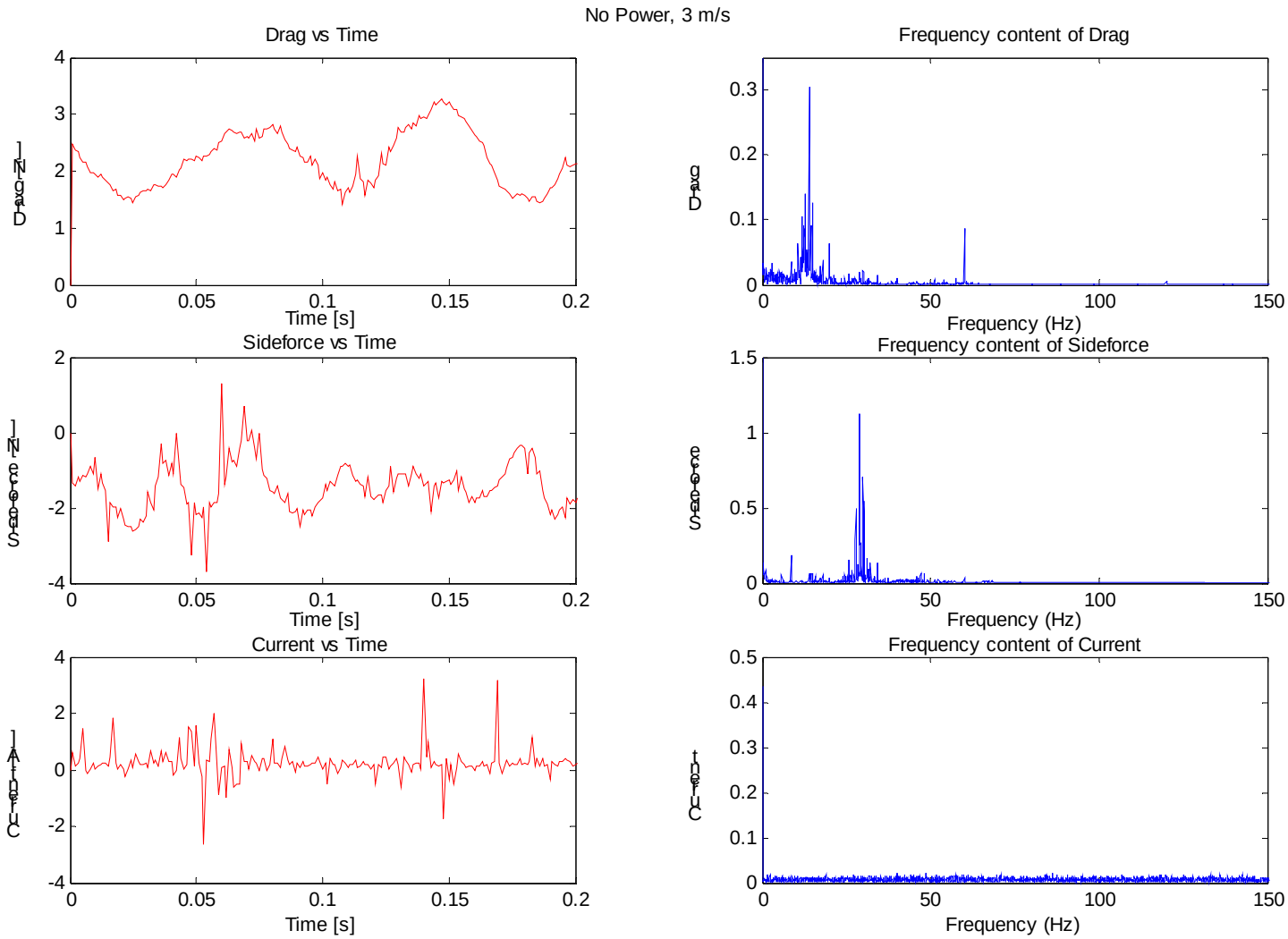
No Power, 3 m/s
Drag vs Time
Drag [N]
Time [s]
Frequency content of Drag
Frequency (Hz)
Sideforce vs Time
Sideforce [N]
Time [s]
Frequency content of Sideforce
Frequency (Hz)
Current vs Time
Current [A]
Time [s]
Frequency content of Current
Frequency (Hz)

Case 1: 0 m/s

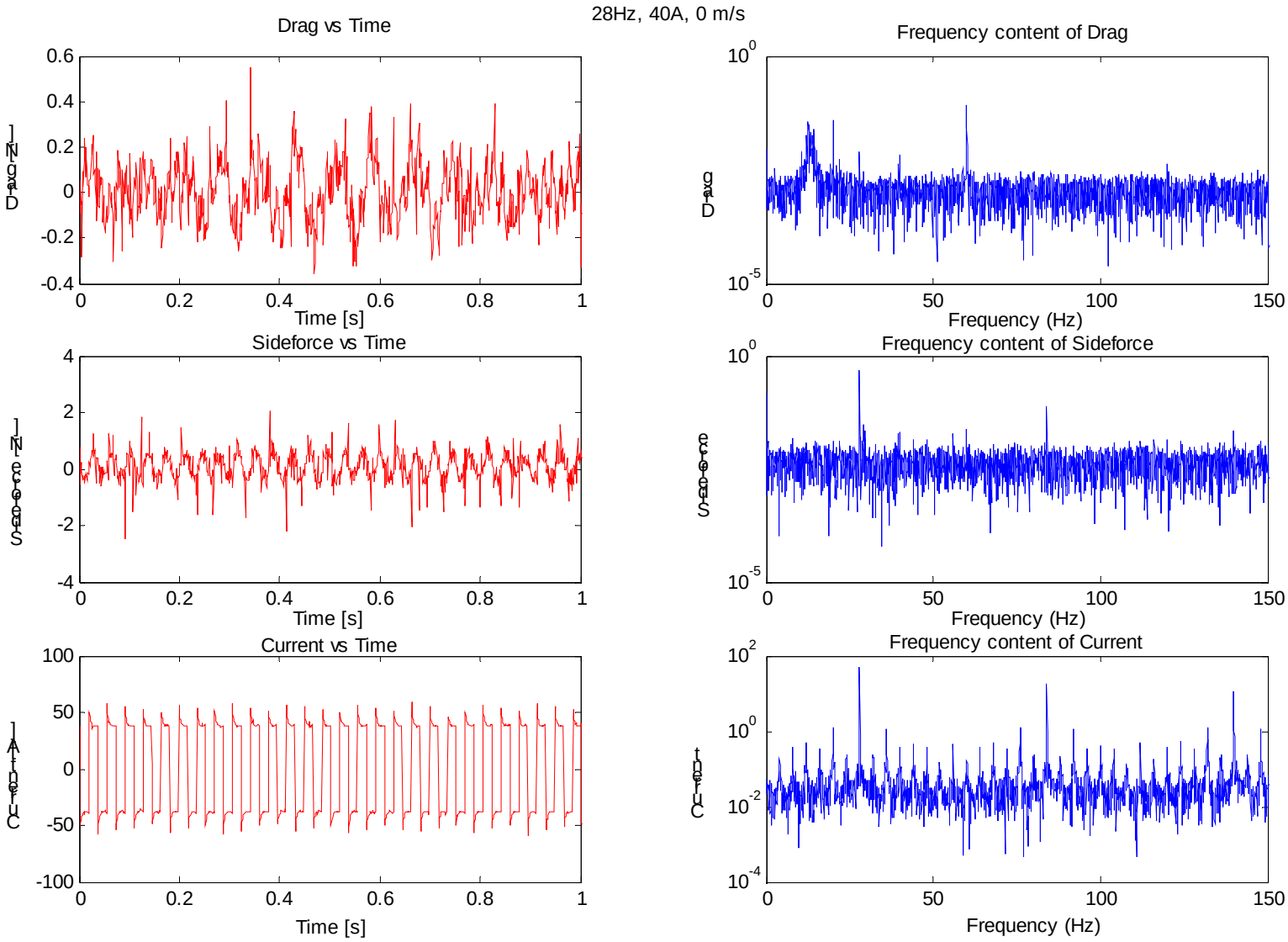
28Hz, 40A, 0 m/s
Drag vs Time
Drag [N]
Time [s]
Frequency content of Drag
Drag [N]
Frequency (Hz)
Sideforce vs Time
Sideforce [N]
Time [s]
Frequency content of Sideforce
Sideforce [N]
Frequency (Hz)
Current vs Time
Current [A]
Time [s]
Frequency content of Current
Current [A]
Frequency (Hz)

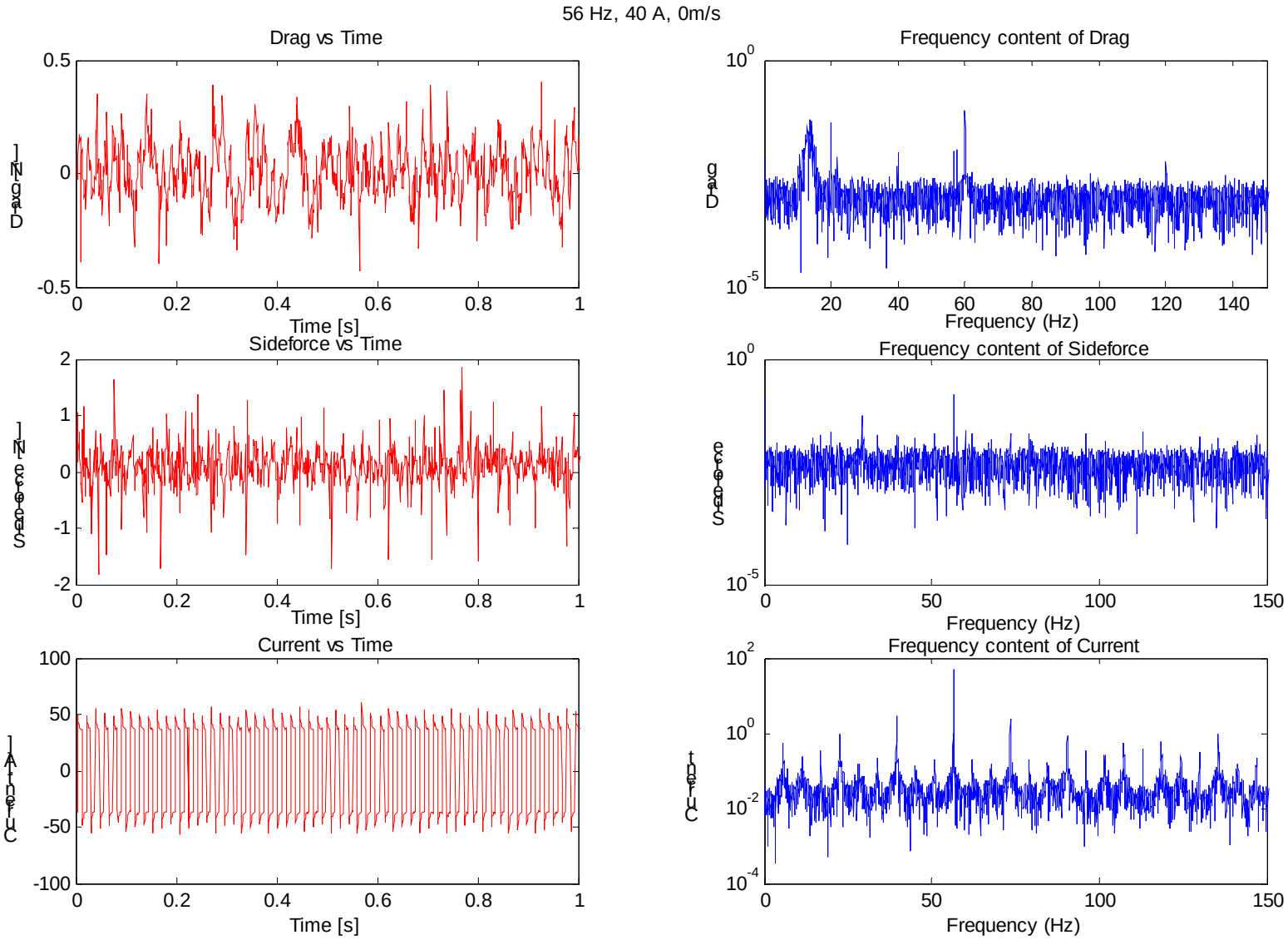
56 Hz, 40 A, 0m/s
Drag vs Time
Drag [N]
Time [s]
Frequency content of Drag
Drag [N]
Frequency (Hz)
Sideforce vs Time
Sideforce [N]
Time [s]
Frequency content of Sideforce
Sideforce [N]
Frequency (Hz)
Current vs Time
Current [A]
Time [s]
Frequency content of Current
Current [A]
Frequency (Hz)

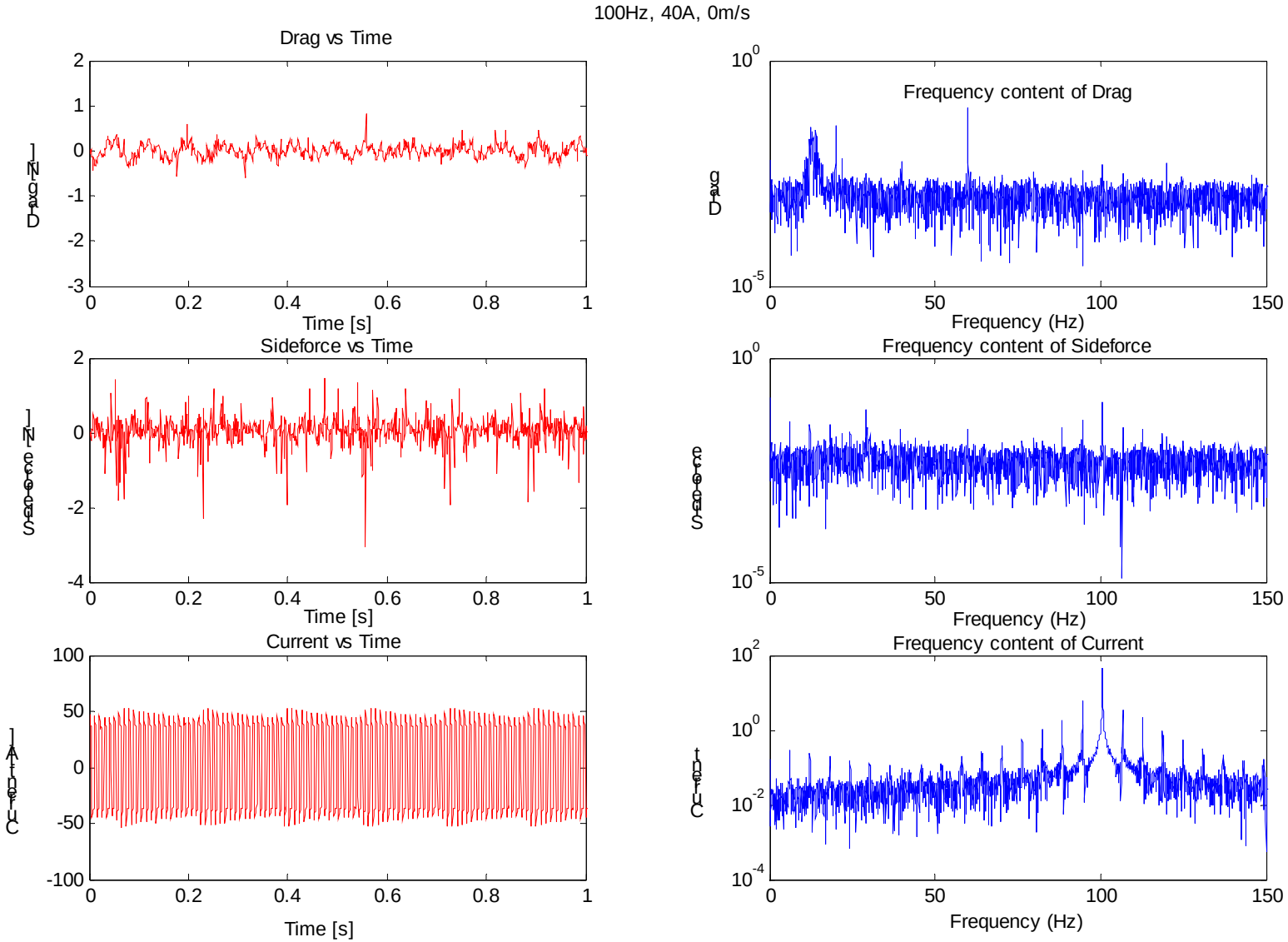
100Hz, 40A, 0m/s
Drag vs Time
Drag [N]
Time [s]
Frequency content of Drag
Drag
Frequency (Hz)
Sideforce vs Time
Sideforce [N]
Time [s]
Frequency content of Sideforce
Sideforce
Frequency (Hz)
Current vs Time
Current [A]
Time [s]
Frequency content of Current
Current
Frequency (Hz)

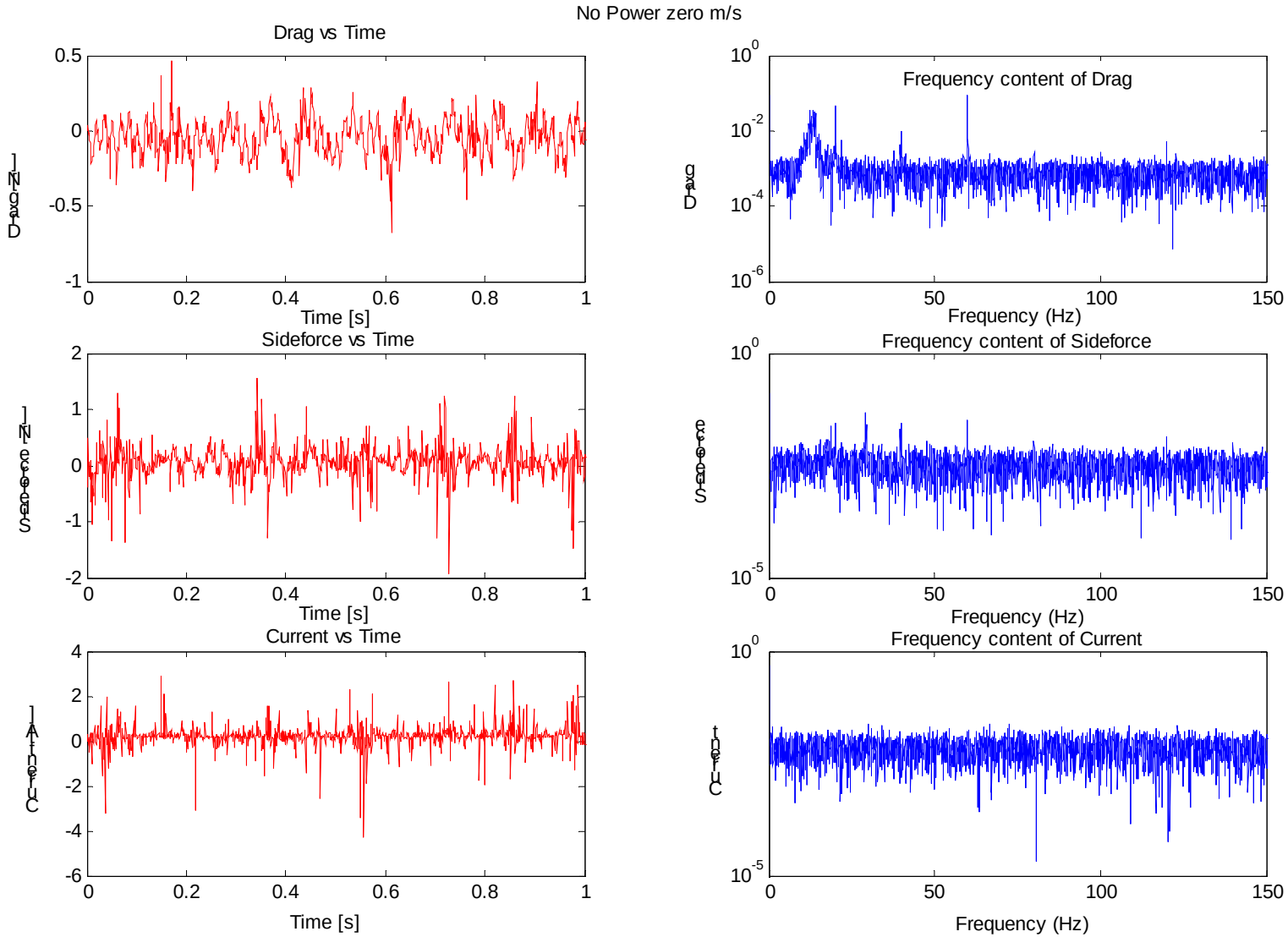
No Power zero m/s
Drag vs Time
Drag [N]
Time [s]
Frequency content of Drag
Frequency (Hz)
Sideforce vs Time
Sideforce [N]
Frequency content of Sideforce
Current vs Time
Current [A]
Frequency content of Current

Case 2: 1.5 m/s

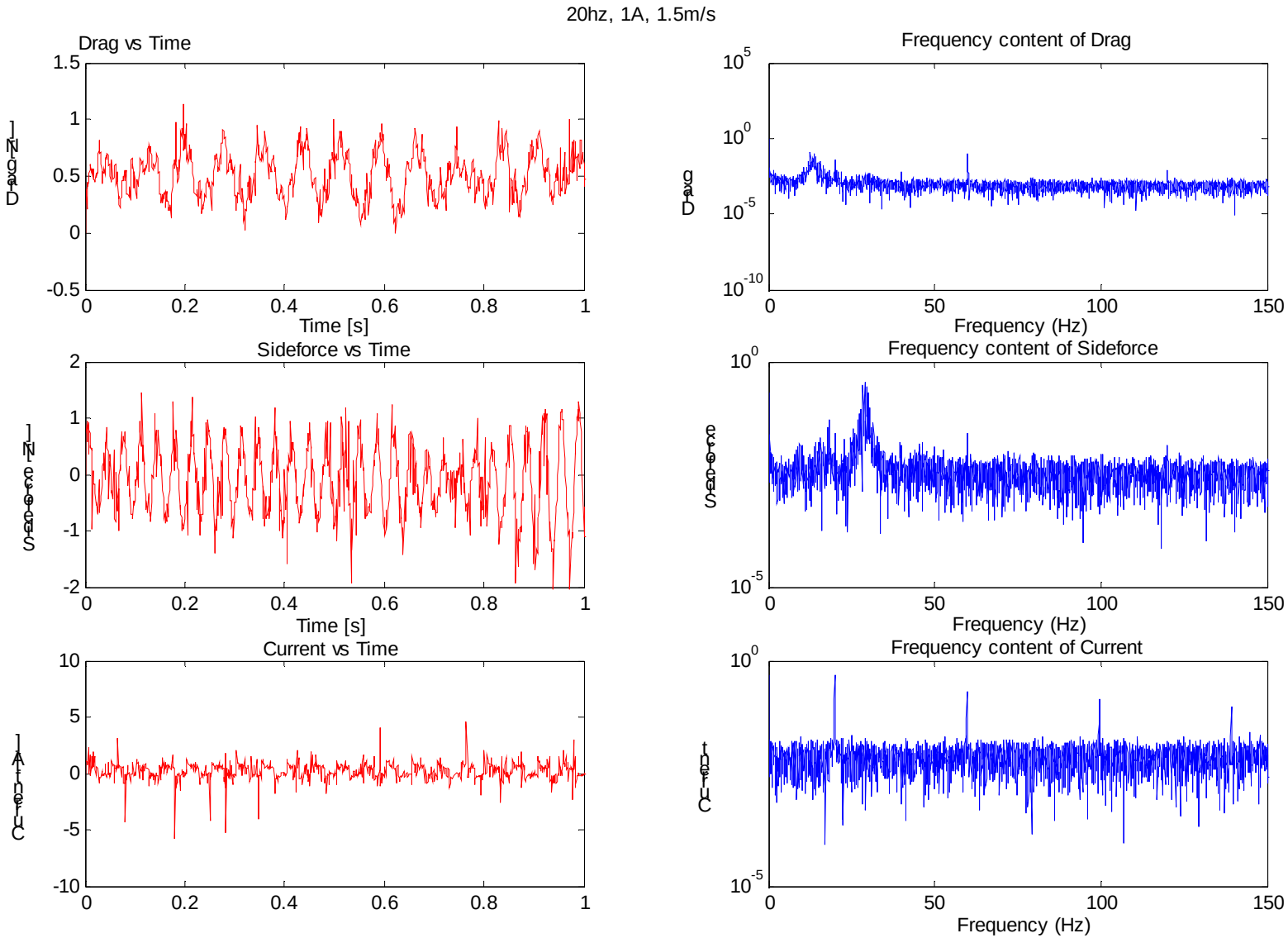
20hz, 1A, 1.5m/s
Drag vs Time
Drag [N]
Time [s]
Sideforce vs Time
Sideforce [N]
Time [s]
Current vs Time
Current [A]
Frequency content of Drag
Drag
Frequency (Hz)
Frequency content of Sideforce
Sideforce
Frequency (Hz)
Frequency content of Current
Current
Frequency (Hz)

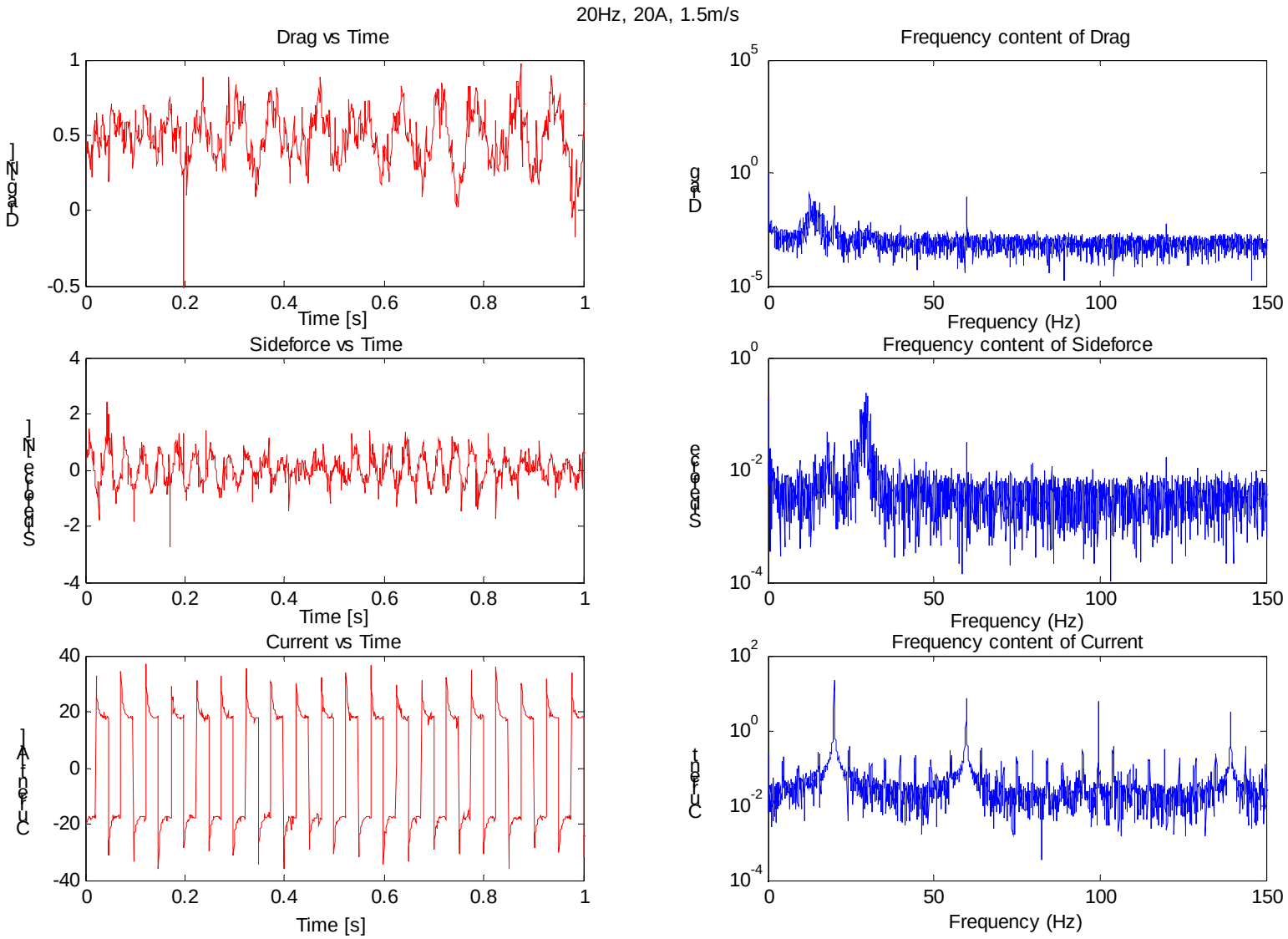
20Hz, 20A, 1.5m/s
Drag vs Time
Drag [N]
Time [s]
Frequency content of Drag
Drag
Frequency (Hz)
Sideforce vs Time
Sideforce [N]
Time [s]
Frequency content of Sideforce
Sideforce
Frequency (Hz)
Current vs Time
Current [A]
Time [s]
Frequency content of Current
Current
Frequency (Hz)

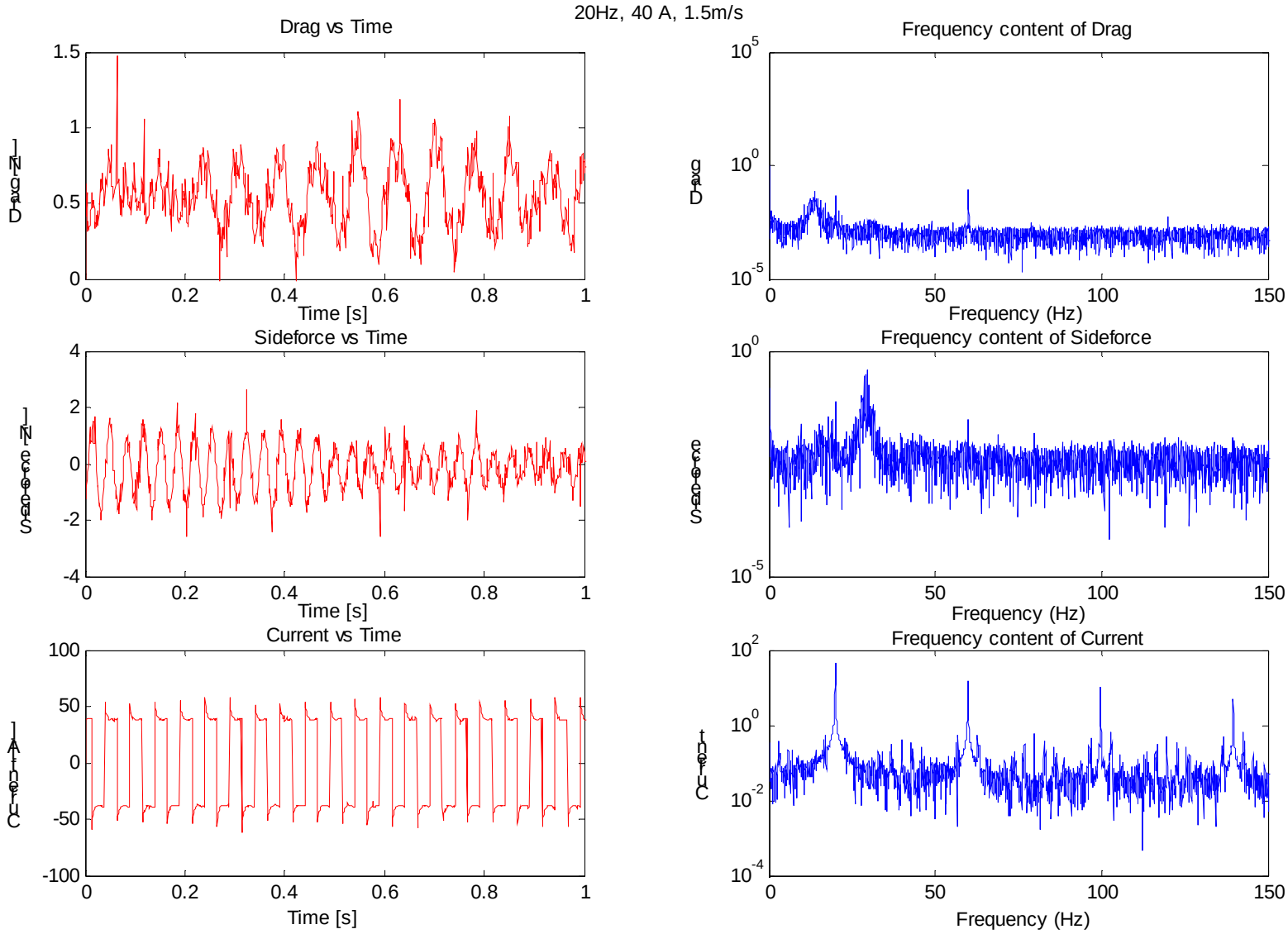
20Hz, 40 A, 1.5m/s
Drag vs Time
Drag [N]
Time [s]
Frequency content of Drag
Drag
Frequency (Hz)
Sideforce vs Time
Sideforce [N]
Time [s]
Frequency content of Sideforce
Sideforce
Frequency (Hz)
Current vs Time
Current [A]
Time [s]
Frequency content of Current
Current
Frequency (Hz)

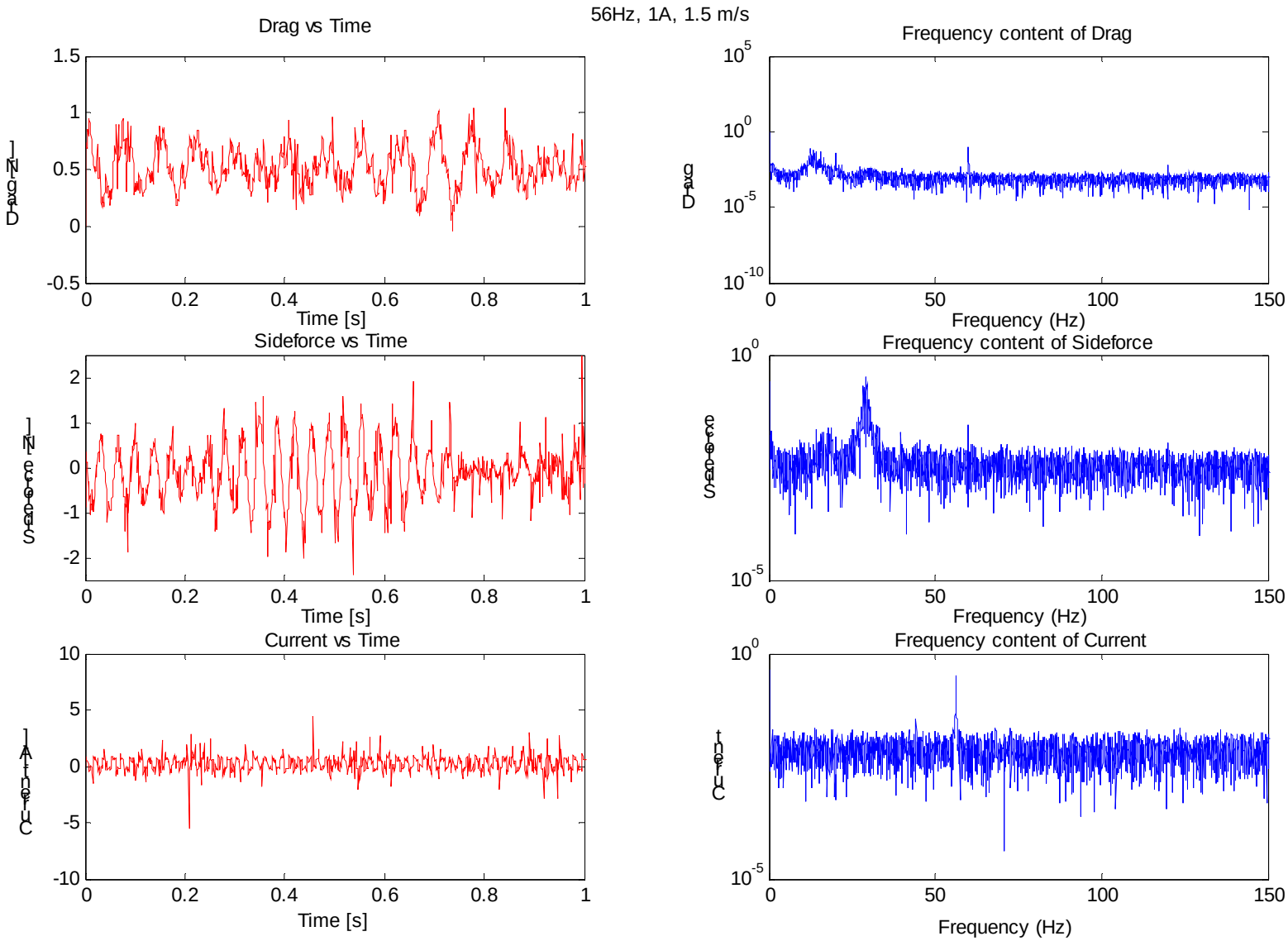
56Hz, 1A, 1.5 m/s
Drag vs Time
Drag [N]
Time [s]
Frequency content of Drag
Drag
Frequency (Hz)
Sideforce vs Time
Sideforce [N]
Time [s]
Frequency content of Sideforce
Sideforce
Frequency (Hz)
Current vs Time
Current [A]
Time [s]
Frequency content of Current
Current
Frequency (Hz)

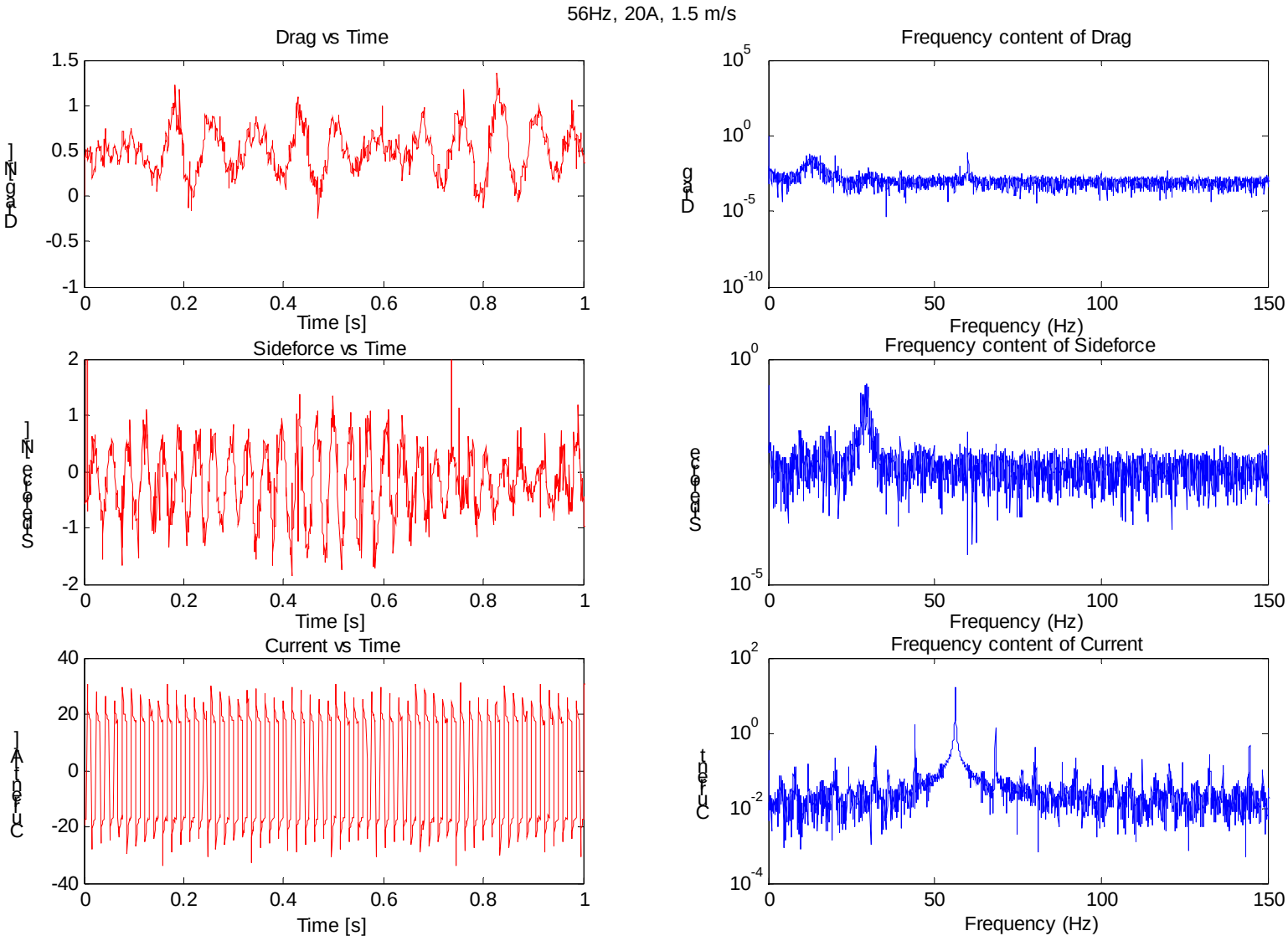
56Hz, 20A, 1.5 m/s
Drag vs Time
Drag [N]
Time [s]
Frequency content of Drag
Drag
Frequency (Hz)
Sideforce vs Time
Sideforce [N]
Time [s]
Frequency content of Sideforce
Sideforce
Frequency (Hz)
Current vs Time
Current [A]
Time [s]
Frequency content of Current
Current
Frequency (Hz)

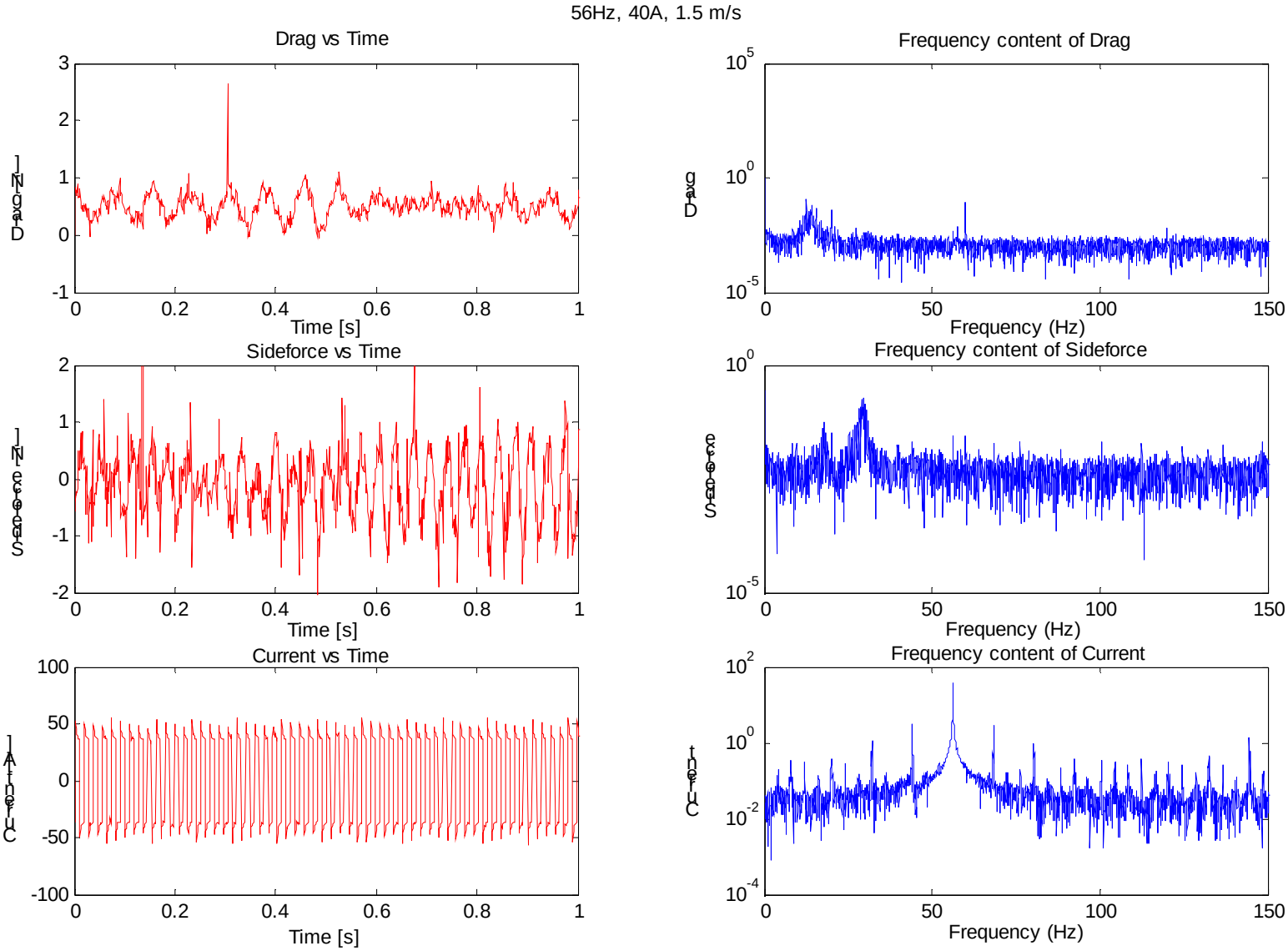
56Hz, 40A, 1.5 m/s
Drag vs Time
Drag [N]
Time [s]
Frequency content of Drag
Drag [N]
Frequency (Hz)
Sideforce vs Time
Sideforce [N]
Time [s]
Frequency content of Sideforce
Sideforce [N]
Frequency (Hz)
Current vs Time
Current [A]
Time [s]
Frequency content of Current
Current [A]
Frequency (Hz)

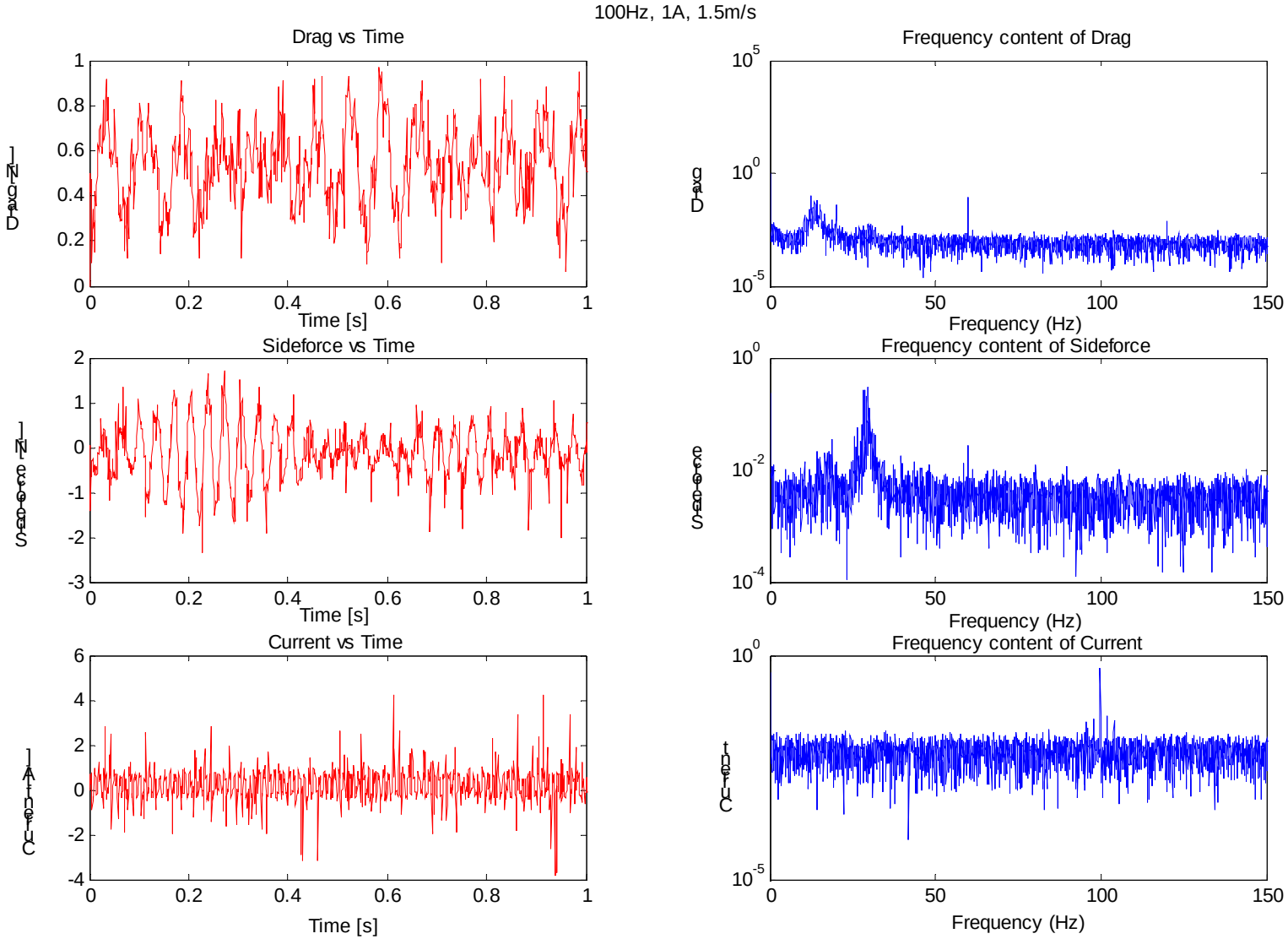
100Hz, 1A, 1.5m/s
Drag vs Time
Drag [N]
Time [s]
Frequency content of Drag
Drag
Frequency (Hz)
Sideforce vs Time
Sideforce [N]
Time [s]
Frequency content of Sideforce
Sideforce
Frequency (Hz)
Current vs Time
Current [A]
Time [s]
Frequency content of Current
Current
Frequency (Hz)

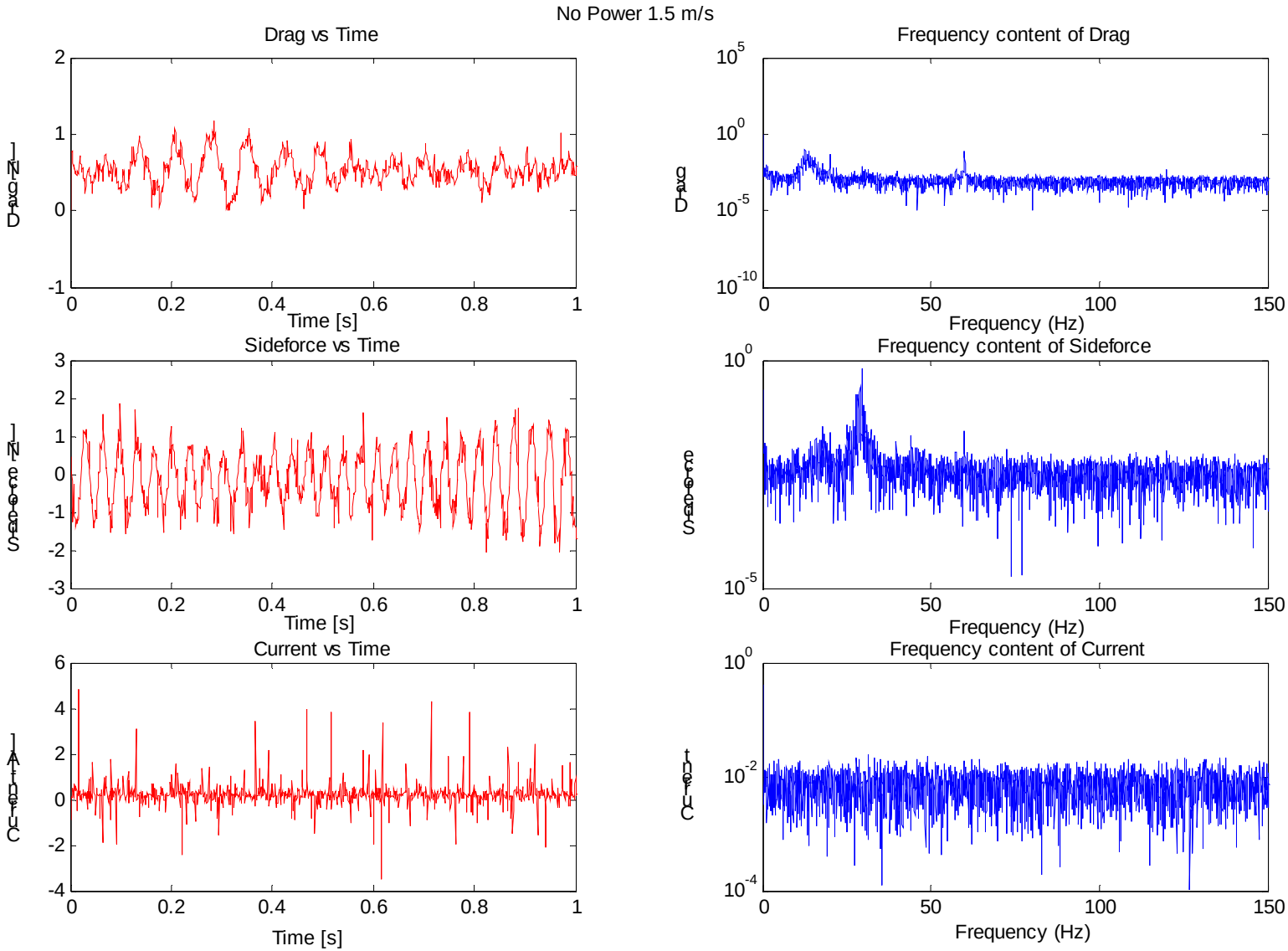
No Power 1.5 m/s
Drag vs Time
Drag [N]
Time [s]
Frequency content of Drag
Drag
Frequency (Hz)
Sideforce vs Time
Sideforce [N]
Time [s]
Frequency content of Sideforce
Sideforce
Frequency (Hz)
Current vs Time
Current [A]
Time [s]
Frequency content of Current
Current
Frequency (Hz)

Case 3: 3.0 m/s

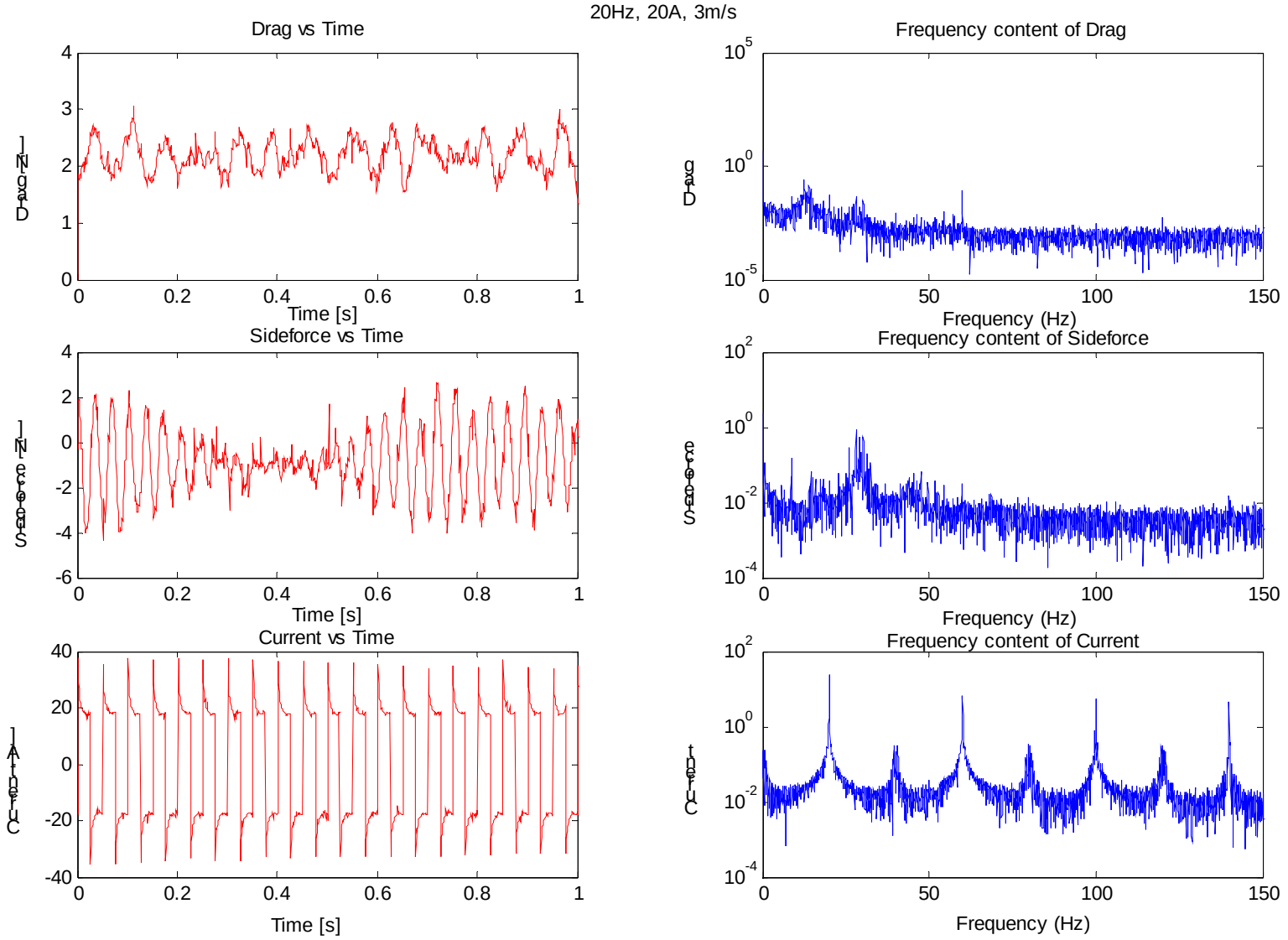
20Hz, 20A, 3m/s
Drag vs Time
Drag [N]
Time [s]
Frequency content of Drag
Drag
Frequency (Hz)
Sideforce vs Time
Sideforce [N]
Time [s]
Frequency content of Sideforce
Sideforce
Frequency (Hz)
Current vs Time
Current [A]
Time [s]
Frequency content of Current
Current
Frequency (Hz)

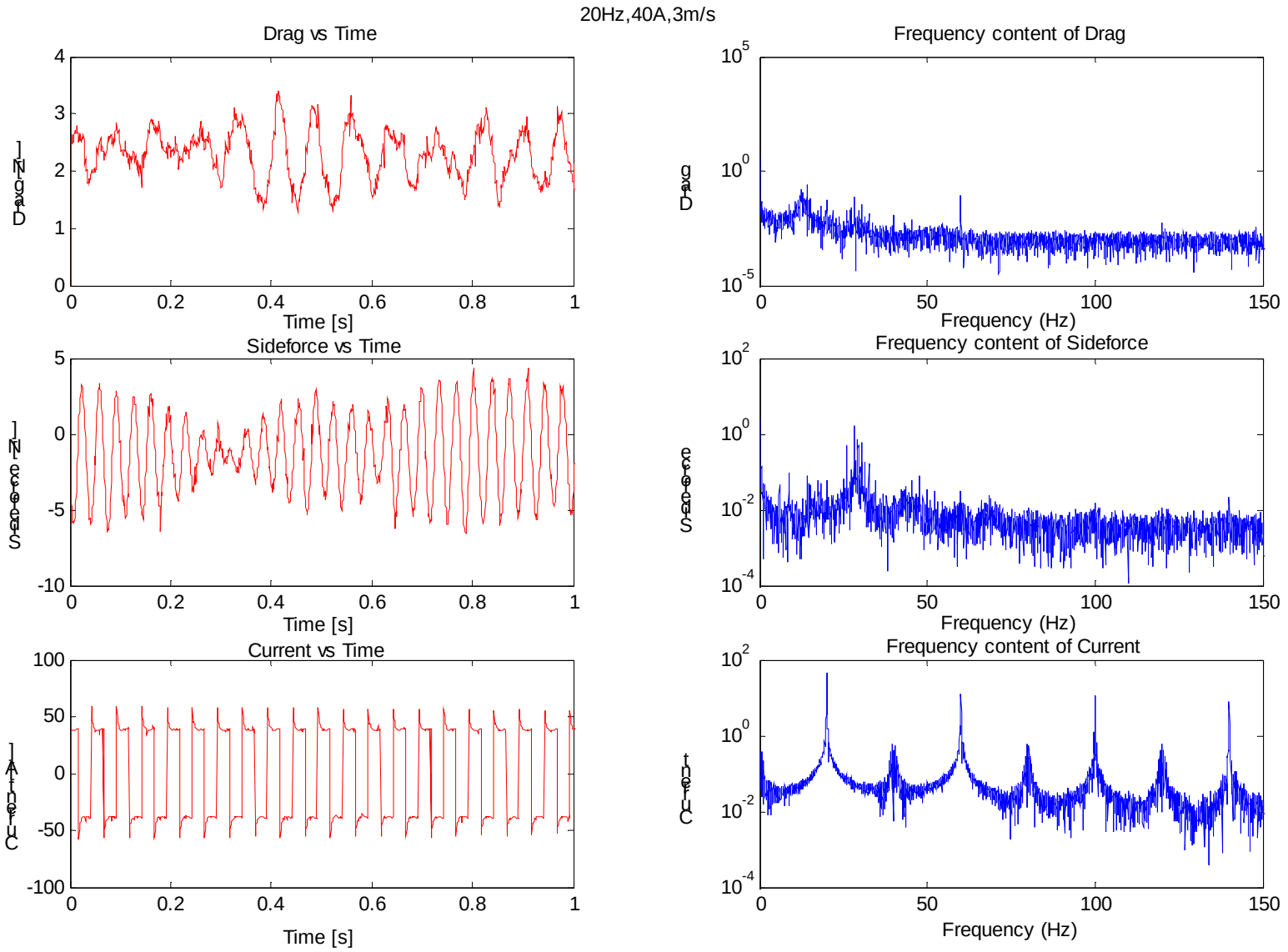
20Hz,40A,3m/s
Drag vs Time
Drag [N]
Time [s]
Frequency content of Drag
Drag
Frequency (Hz)
Sideforce vs Time
Sideforce [N]
Time [s]
Frequency content of Sideforce
Sideforce
Frequency (Hz)
Current vs Time
Current [A]
Time [s]
Frequency content of Current
Current
Frequency (Hz)

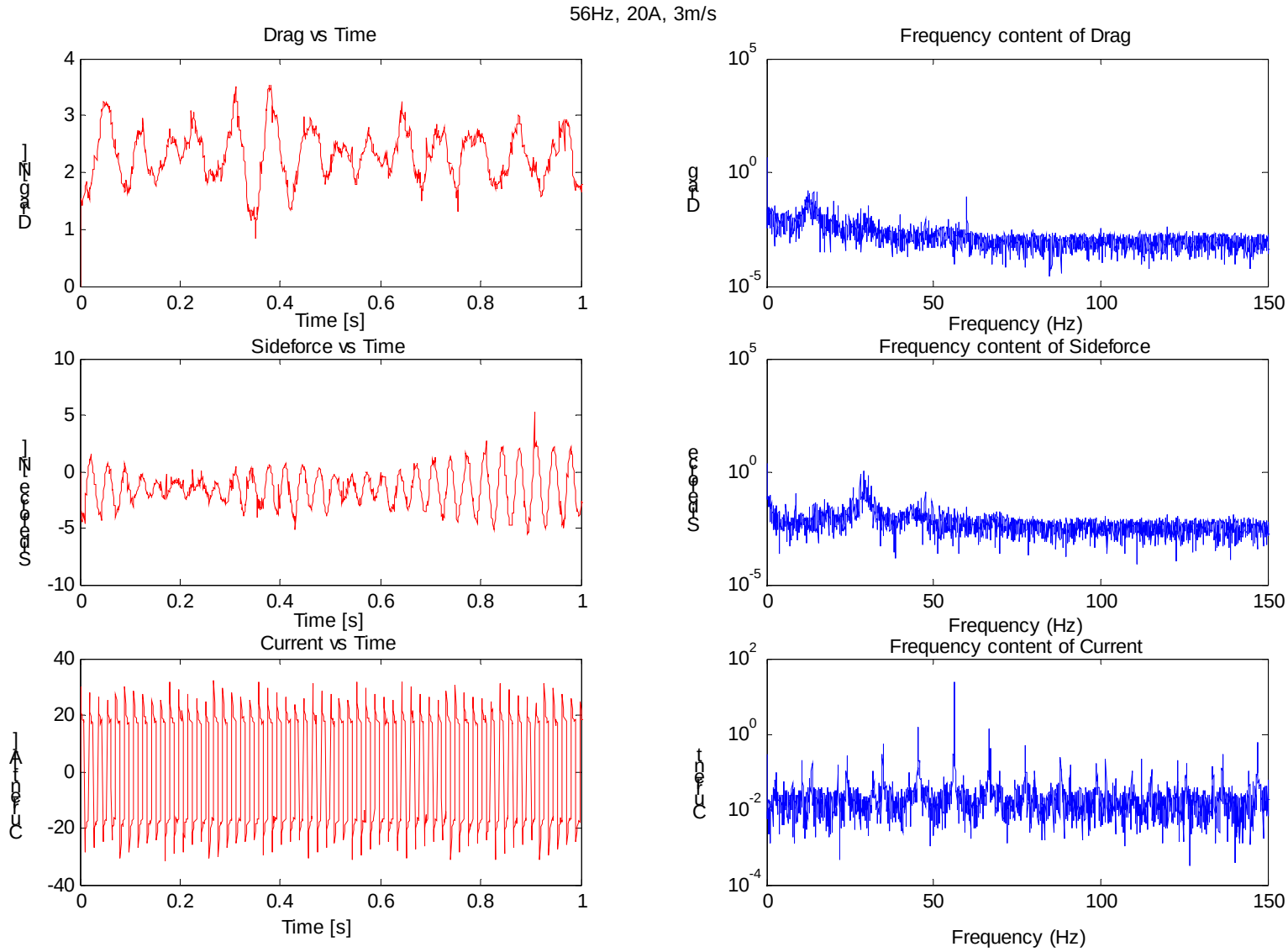
56Hz, 20A, 3m/s
Drag vs Time
Drag [N]
Time [s]
Frequency content of Drag
Drag
Frequency (Hz)
Sideforce vs Time
Sideforce [N]
Time [s]
Frequency content of Sideforce
Sideforce
Frequency (Hz)
Current vs Time
Current [A]
Time [s]
Frequency content of Current
Current
Frequency (Hz)

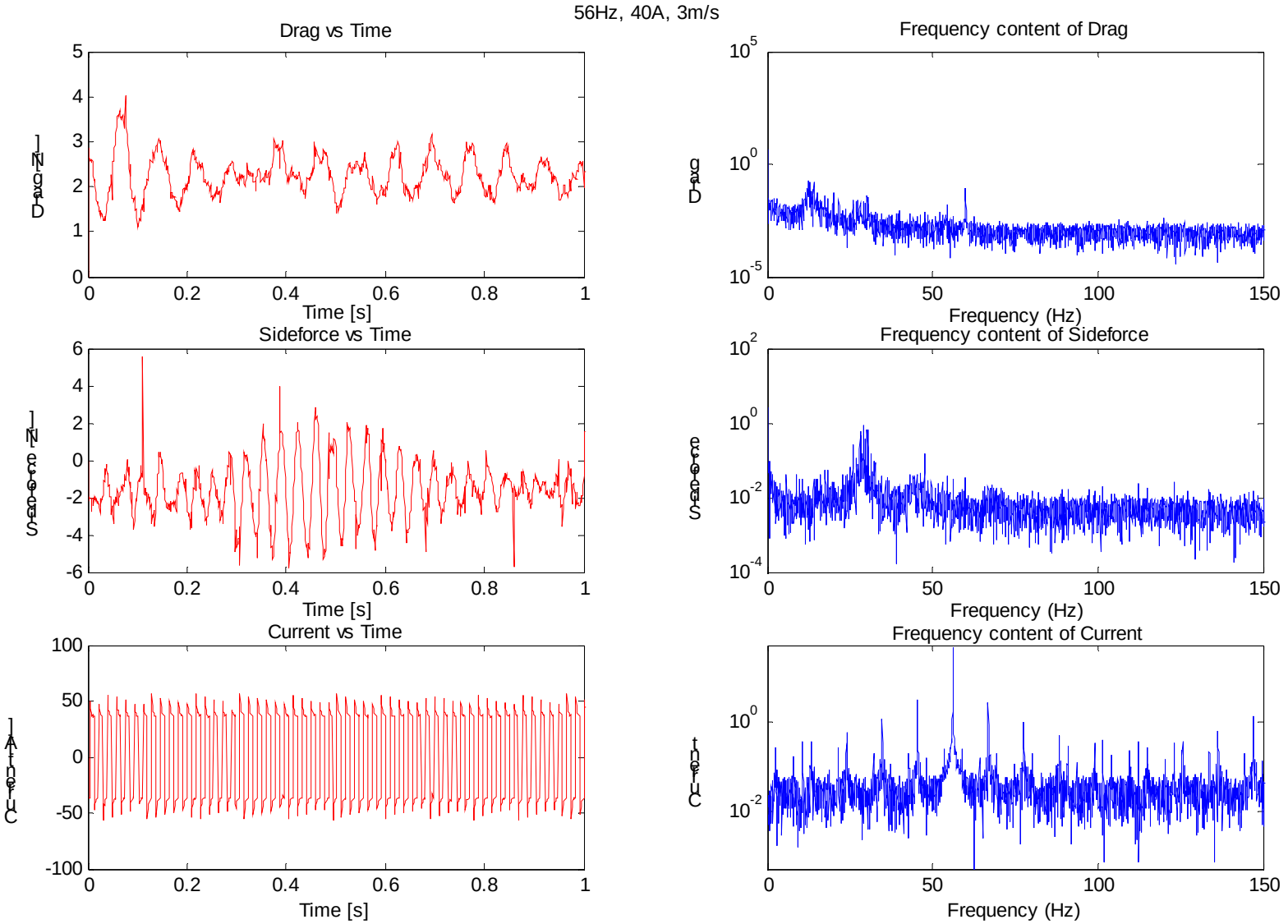
56Hz, 40A, 3m/s
Drag vs Time
Drag [N]
Time [s]
Frequency content of Drag
Drag
Frequency (Hz)
Sideforce vs Time
Sideforce [N]
Time [s]
Frequency content of Sideforce
Sideforce
Frequency (Hz)
Current vs Time
Current [A]
Time [s]
Frequency content of Current
Current
Frequency (Hz)

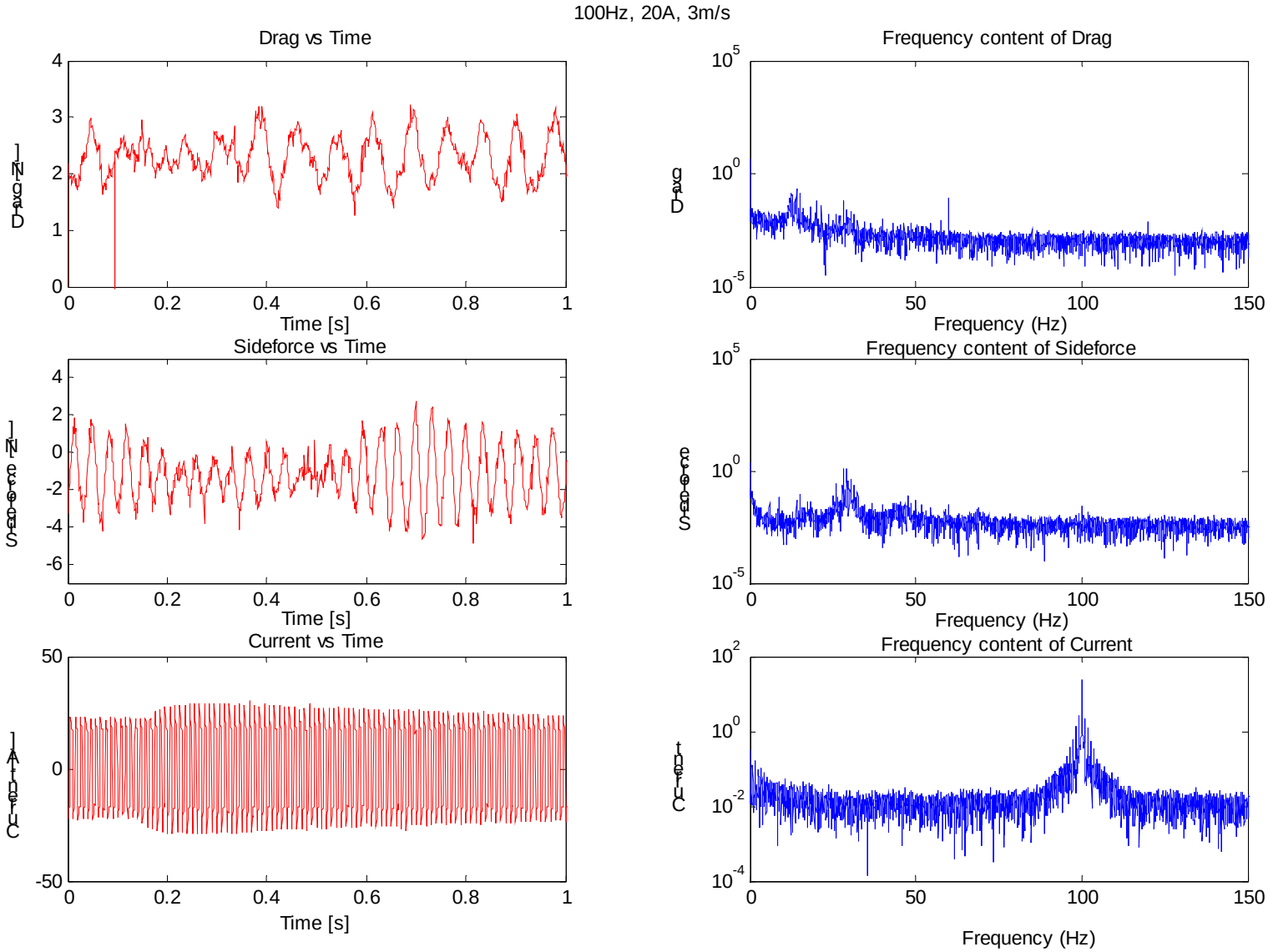
100Hz, 20A, 3m/s
Drag vs Time
Drag [N]
Time [s]
Frequency content of Drag
Drag
Frequency (Hz)
Sideforce vs Time
Sideforce [N]
Time [s]
Frequency content of Sideforce
Sideforce
Frequency (Hz)
Current vs Time
Current [A]
Time [s]
Frequency content of Current
Current
Frequency (Hz)

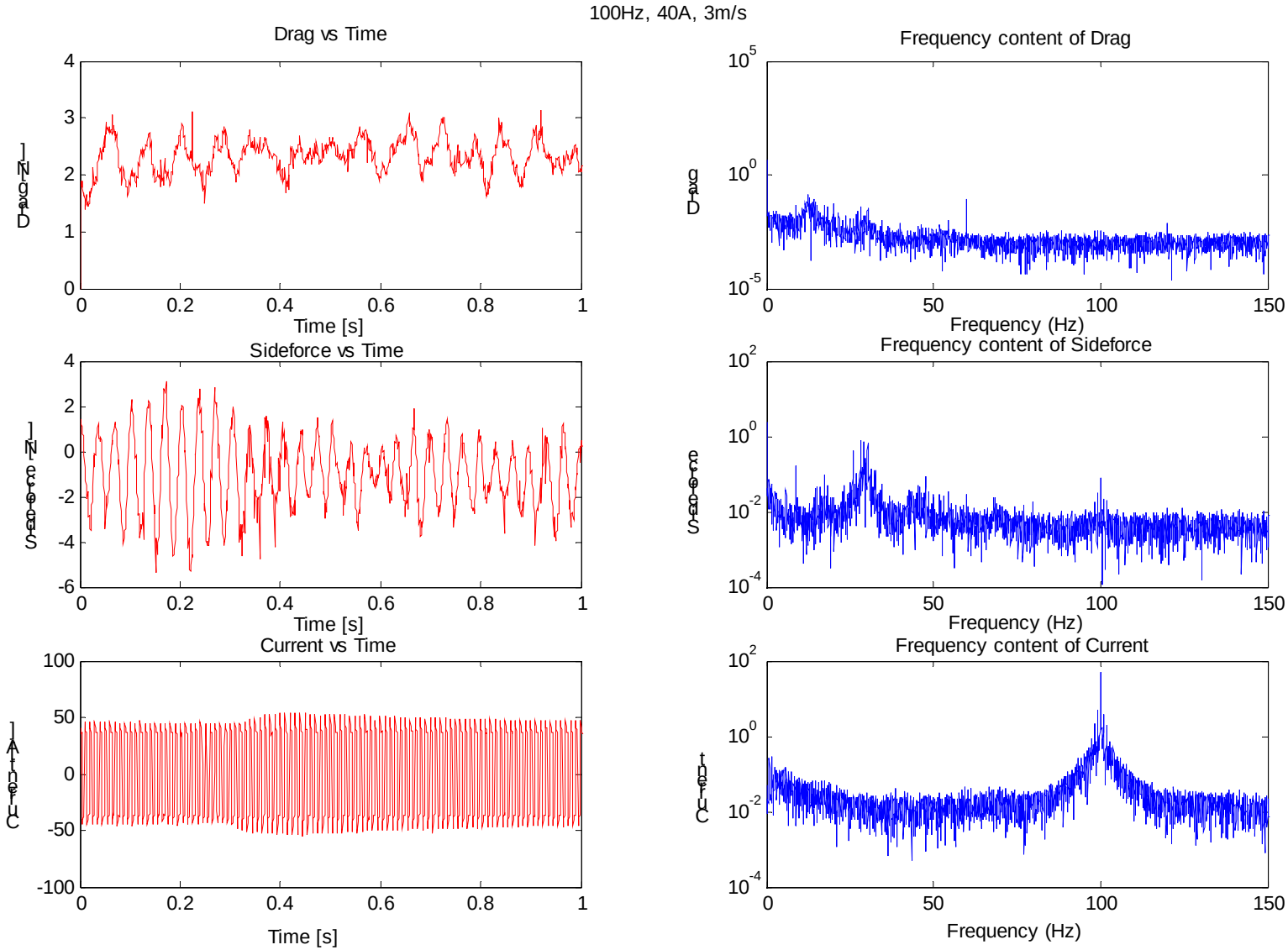
100Hz, 40A, 3m/s
Drag vs Time
Drag [N]
Time [s]
Frequency content of Drag
Drag
Frequency (Hz)
Sideforce vs Time
Sideforce [N]
Time [s]
Frequency content of Sideforce
Sideforce
Frequency (Hz)
Current vs Time
Current [A]
Time [s]
Frequency content of Current
Current
Frequency (Hz)

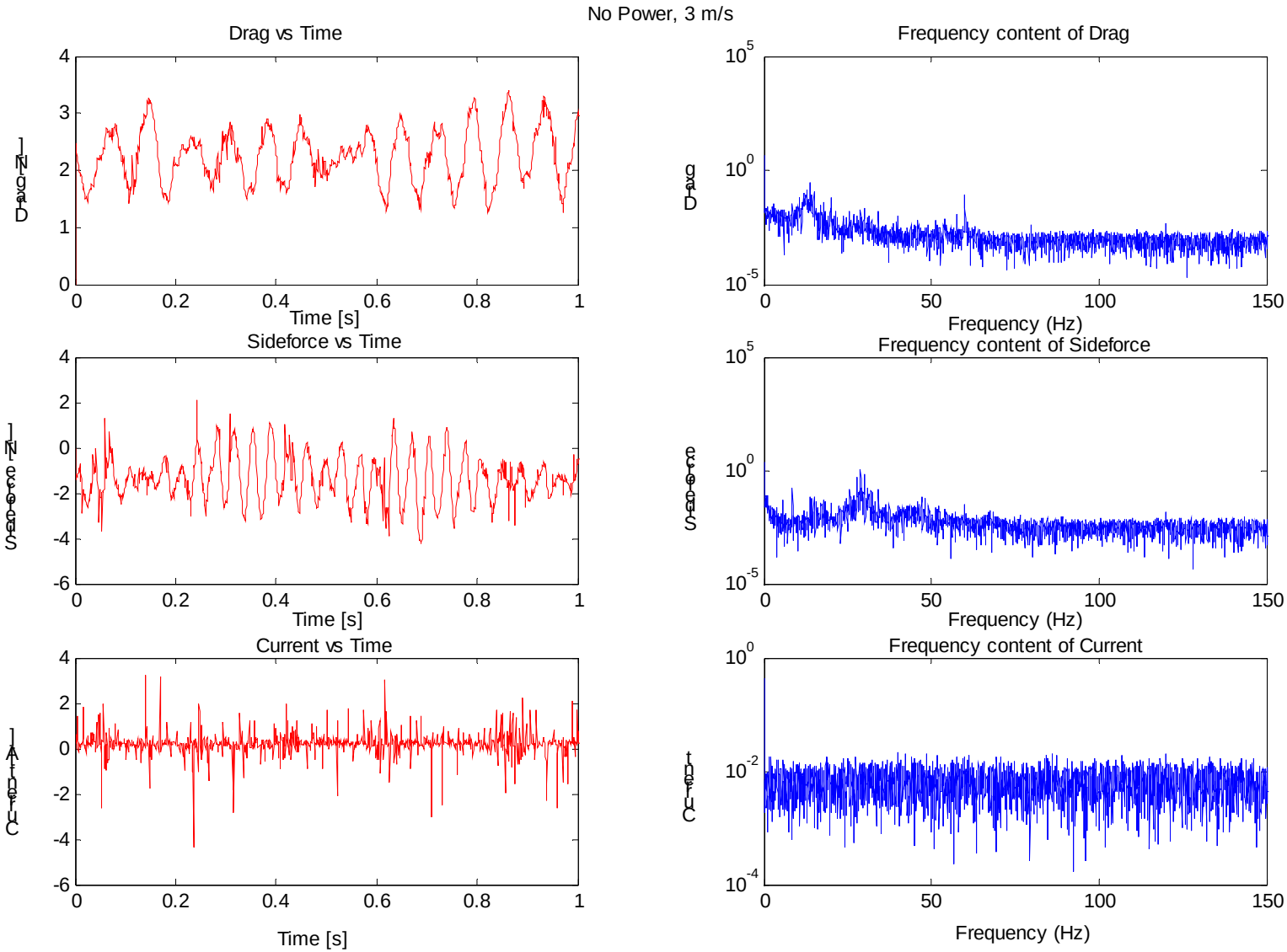
No Power, 3 m/s
Drag vs Time
Drag [N]
Time [s]
Frequency content of Drag
Drag
Frequency (Hz)
Sideforce vs Time
Sideforce [N]
Time [s]
Frequency content of Sideforce
Sideforce
Frequency (Hz)
Current vs Time
Current [A]
Time [s]
Frequency content of Current
Current
Frequency (Hz)

6.2 Electronics Schematics

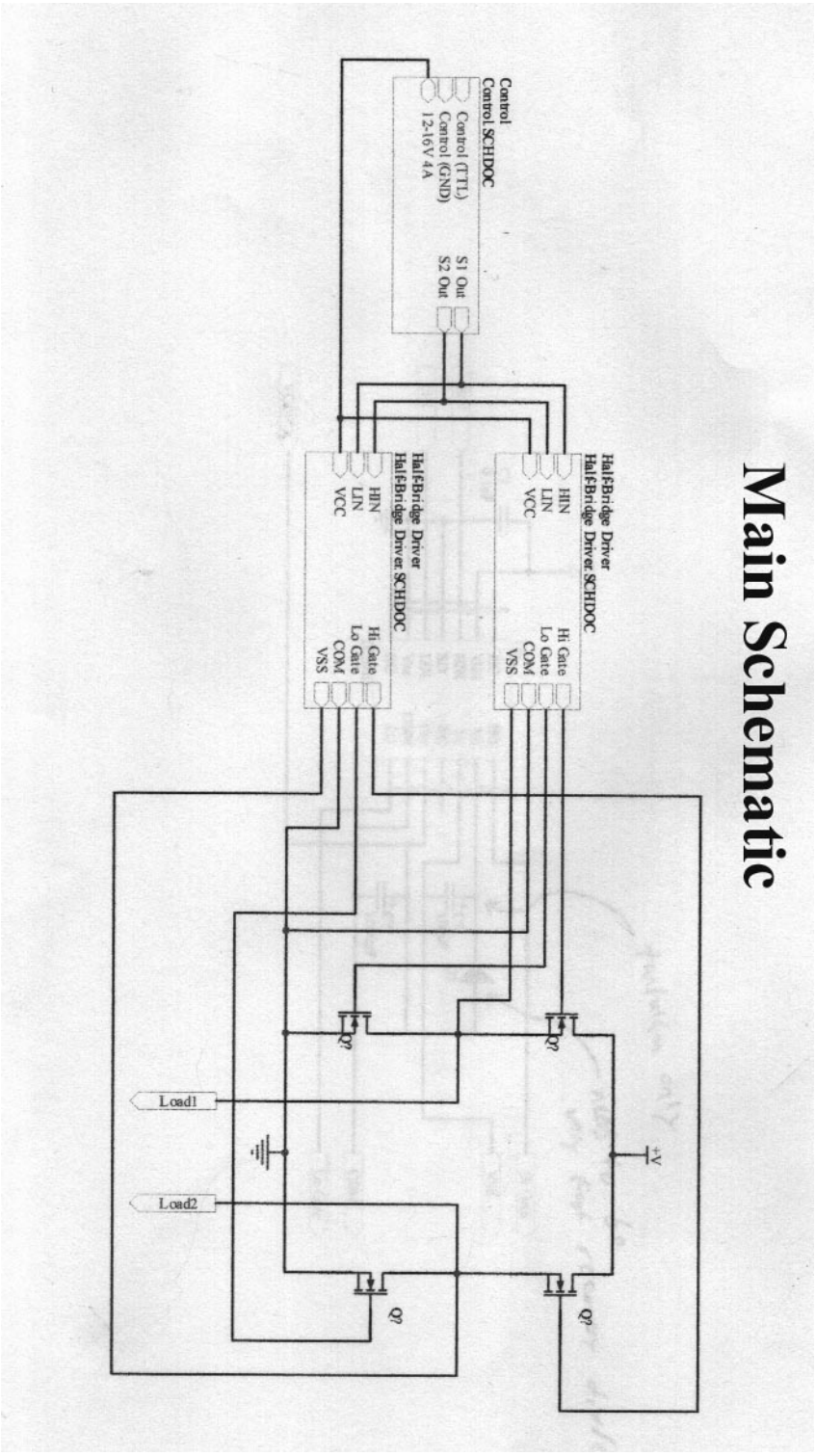

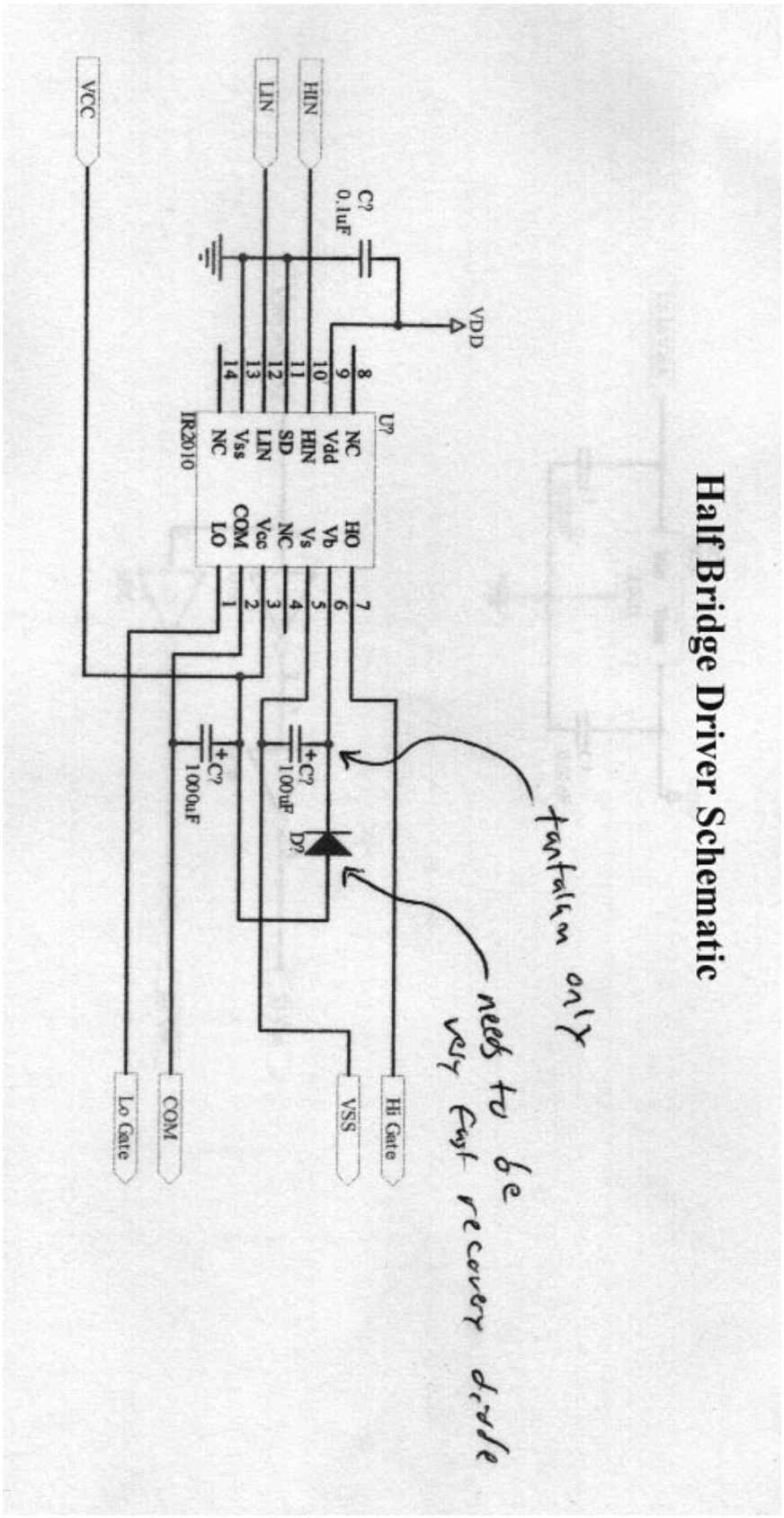
Half Bridge Driver Schematic
tantalum only
needs to be very fast recovery diode
VCC
HIN
LIN
C?
0.1uF
VDD
U?
IR2010
NC
Vdd
HIN
SD
LIN
Vss
NC
HO
Vb
Vs
NC
Vcc
COM
LO
8
9
10
11
12
13
14
7
6
5
4
3
2
1
C?
1000uF
C?
100uF
D?
VSS
Hi Gate
COM
Lo Gate

Control Schematic

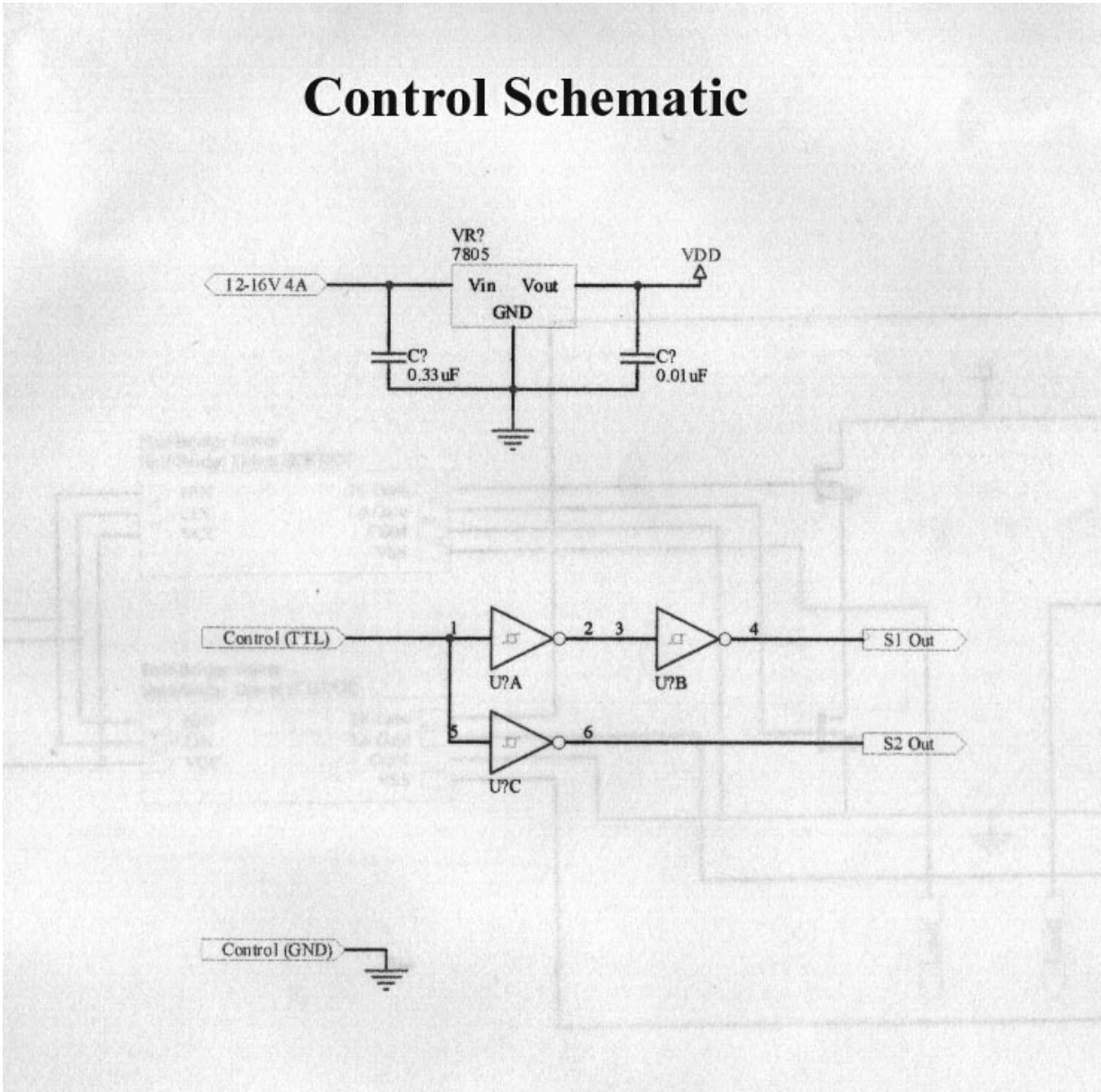

FAIRCHILD SEMICONDUCTOR™

November 1988
Revised December 1999

74AC14 • 74ACT14
Hex Inverter with Schmitt Trigger Input

General Description

The 74AC14 and 74ACT14 contain six inverter gates each with a Schmitt trigger input. They are capable of transforming slowly changing input signals into sharply defined, jitter-free output signals. In addition, they have a greater noise margin than conventional inverters.

The 74AC14 and 74ACT14 have hysteresis between the positive-going and negative-going input thresholds (typically 1.0V) which is determined internally by transistor ratios and is essentially insensitive to temperature and supply voltage variations.

Features

- I_{CC} reduced by 50%
- Outputs source/sink 24 mA
- 74ACT14 has TTL-compatible inputs

Ordering Code:

Order Number	Package Number	Package Description
74AC14SC	M14A	14-Lead Small Outline Integrated Circuit (SOIC), JEDEC MS-012, 0.150" Narrow Body
74AC14SJ	M14D	14-Lead Small Outline Package (SOP), EIAJ TYPE II, 5.3mm Wide
74AC14MTC	MTC14	14-Lead Thin Shrink Small Outline Package (TSSOP), JEDEC MS-153, 4.4mm Wide
74AC14PC	N14A	14-Lead Plastic Dual-In-Line Package (PDIP), JEDEC MS-001, 0.300" Wide
74ACT14SC	M14A	14-Lead Small Outline Integrated Circuit (SOIC), JEDEC MS-012, 0.150" Narrow Body
74ACT14MTC	MTC14	14-Lead Thin Shrink Small Outline Package (TSSOP), JEDEC MS-153, 4.4mm Wide
74ACT14PC	N14A	14-Lead Plastic Dual-In-Line Package (PDIP), JEDEC MS-001, 0.300" Wide

Device also available in Tape and Reel. Specify by appending suffix letter "X" to the ordering code.

Logic Symbol

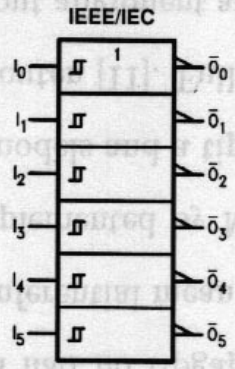

Connection Diagram

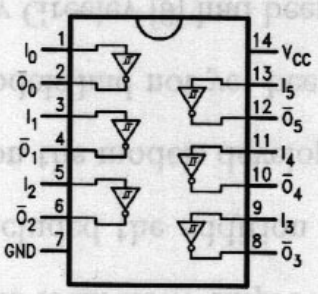

Pin Descriptions

Pin Names	Description
I_n	Inputs
$\overline{O}_n$	Outputs

Function Table

Input	Output
A	$\overline{O}$
L	H
H	L

FACT™ is a trademark of Fairchild Semiconductor Corporation.

 DS009917

International
IOR Rectifier

PD-91651C

FB180SA10

HEXFET® Power MOSFET

- Fully Isolated Package
- Easy to Use and Parallel
- Very Low On-Resistance
- Dynamic dv/dt Rating
- Fully Avalanche Rated
- Simple Drive Requirements
- Low Drain to Case Capacitance
- Low Internal Inductance

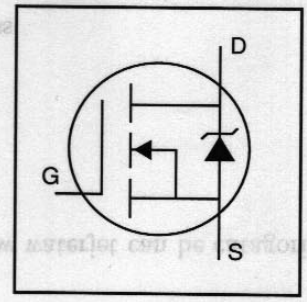

V_{DSS} = 100V

$R_{DS(on)}$ = 0.0065Ω

I_D = 180A

Description

Fifth Generation, high current density HEXFETS are paralled into a compact, high power module providing the best combination of switching, ruggedized design, very low ON resistance and cost effectiveness.

The isolated SOT-227 package is preferred for all commercial - industrial applications at power dissipation levels to approximately 500 watts. The low thermal resistance and easy connection to the SOT-227 package contribute to its universal acceptance throughout the industry.

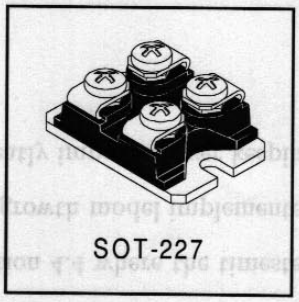

SOT-227

Absolute Maximum Ratings

	Parameter	Max.	Units
I_D @ T_C = 25°C	Continuous Drain Current, V_{GS} @ 10V	180	A
I_D @ T_C = 100°C	Continuous Drain Current, V_{GS} @ 10V	120	
I_{DM}	Pulsed Drain Current ①	720	
P_D @ T_C = 25°C	Power Dissipation	480	W
	Linear Derating Factor	2.7	W/°C
V_{GS}	Gate-to-Source Voltage	± 20	V
E_{AS}	Single Pulse Avalanche Energy②	700	mJ
I_{AR}	Avalanche Current①	180	A
E_{AR}	Repetitive Avalanche Energy①	48	mJ
dv/dt	Peak Diode Recovery dv/dt ③	5.7	V/ns
T_J T_{STG}	Operating Junction and Storage Temperature Range	-55 to + 150	°C
V_{ISO}	Insulation Withstand Voltage (AC-RMS)	2.5	kV
	Mounting torque, M4 srew	1.3	N•m

Thermal Resistance

	Parameter	Typ.	Max.	Units
$R_{\theta JC}$	Junction-to-Case	—	0.26	°C/W
$R_{\theta CS}$	Case-to-Sink, Flat, Greased Surface	0.05	—	